NW Pacific-Eurasia Subduction History and Continental Arc Evolution Along NE Asia Since Cretaceous Times

by
Tsung-Jui Wu

A dissertation submitted to the Department of Earth and Atmospheric Sciences,
College of Natural Sciences and Mathematics
in partial fulfillment of the requirements for the degree of

DOCTOR OF PHILOSOPHY

in GEOLOGY

Chair of Committee: Jonny Wu

Committee Member: John Casey

Committee Member: Kazuaki Okamoto

Committee Member: Thomas Lapen

University of Houston
December 2021

Dedication/Epigraph

To Terri, Ke-Lo,
my dad, mom, sister, grandpa, and grandma.

Thank you for always being there.

Acknowledgments

I appreciate the support and guidance from my advisor Jonny Wu and committee members John Casey, Thomas Lapen, and Kazuaki Okamoto. I'm very grateful for all the support from my collaborators: Dr. Igor Alexandrov and his team that collected rock samples from several challenging field trips in Sikhote-Alin. Lingling Chen and Dr. Mikyoung Jun (UH) developed the statistical analytical method for the time-varying geological dataset using their expertise. The chronological and geochemical analysis in this dissertation was assisted by Terri Tang, Weihang Yang, Weiyao Yan, Minako Righter, Yi-Peng Li, Yi-Ju Hsin, Chieq Hung, Yongjun Gao, and James Maner. My lab members Yi-Wei Chen, Yi-An Lin, Spencer Fuston, Phinphorn Amonpantang, John Boyle, Keaton Denzer, Hasan Burak Ozer, and Sui Jia greatly supported me on technical issues, fruitful discussion, and company. I also like to thank Lorenzo Colli, Yiduo Liu, John Suppe, Kuo-long Wang, Wen-shan Chen, Cin-ty Lee, Yin Liu, Hayato Ueda, Julia Ribeiro, Virginia Sisson, Derek Thorkelson, Lydian Boschman, Gaku Kimura, Christopher Spencer, Larry Lai, Charlie Zheng, Jia-ping Liao, Masako Usuki, Tadashi Usuki, Tsai-wei Chen, Tsai-wei Chen, Kuan-yu Lin, and Yu-hsiang Chien for their valuable discussion and support.

I was supported by the National Science Foundation NSF CAREER grant EAR-1848327 awarded to my advisor Dr. Jonny Wu. I was also supported by GURI Funds that were generously provided by Dr. John Suppe from the State of Texas and the University of Houston.

Abstract

The Eurasian continental margin of NE Asia records abundant Mesozoic to present igneous activity in response to Pacific and Panthalassa (paleo-Pacific) subduction. Plate tectonic studies typically reconstruct long-lived plate convergence involving subduction of the Panthalassa/Pacific plates since 200 Ma. However, many first-order details of NW Panthalassa plate tectonic reconstructions remain controversial, including ridge-trench intersections and intra-oceanic arc accretions along Eurasia since the Early Cretaceous.

In this dissertation, we investigate the Mesozoic to Cenozoic magmatic and plate tectonic history of the 31-52 °N NE Asian continental active margin (Japan, Korea, NE China, and southern Russian Far East). We analyze igneous rock U-Pb geochronology and geochemistry (n=92) of Sikhote-Alin, Russia and add published data (n>800) to create a large regional magmatic database that is compared to published structural geology, stratigraphy, paleomagnetism, and an unpublished fully-kinematic 'tomographic' NE Asian-Pacific plate tectonic reconstruction. I show the following plate tectonic stages along NE Asia since the Cretaceous: (1) subduction of one or more marginal sea plates during the Early Cretaceous; (2) a ~130-100 Ma intra-oceanic arc accretion event that shows magmatism from subducted-slab melting; (3) ~100-50 Ma Izanagi slab subduction correlated to higher magmatic fluxes (up to 1000 km^2 /Myr), high % SiO_2 (mean 66-70 %), and enriched εNd(t) isotopic ratios (-15 to +2), that link to ultrafast subduction (12 to 24 cm/yr); (4) ~50 Ma Pacific-Izanagi spreading ridge subduction based on a 56-46 Ma arc magmatic hiatus; and. (5) ~50-0 Ma slower (2 to 8 cm/yr) Pacific plate subduction correlated to lower magmatic flux (~ 400 km^2 /Myr), SiO_2

(mean 56-63 %), and more depleted εNd(t) isotopic ratios (-5 to +10). Migration of the NE Asian continental arc ~2000 km outboard (eastward) since Jurassic times indicates continental growth within an accretionary orogen that is driven by long-lived ocean-continent subduction.

.

Table of Contents

List of Tables

List of Figures

CHAPTER 1: INTRODUCTION TO THE DISSERTATION

The NE Asian Eurasian margin is an accretionary orogenic belt that has formed in response to the convergence of the Pacific-Panthalassan oceanic plates since at least 200 Ma to present (Müller et al., 2016). The margin exhibits widely-distributed Cretaceous to Cenozoic continental arc magmatism and possible accretion of intra-oceanic arcs, ophiolites, and continental fragments (Isozaki et al., 2010; Khanchuk et al., 2016; Taira et al., 2016; Wakita, 2013; Zharov, 2005). In this dissertation, I investigate the magmatic and plate tectonic history of the northeast Asian continental active margin between Japan, Korea, NE China to Sikhote-Alin (Russian Far East) during Mesozoic to Cenozoic times. My aim is to better constrain the highly controversial regional plate tectonic history (see below) using magmatic constraints from the NE Asian continental arc (e.g. the upper plate). New analyses of igneous rock chronology and geochemistry from the frontier area of Sikhote-Alin, Russian Far East, are combined with a new compilation of published geochronology and geochemistry. My results are compared to published structural geology, stratigraphy, and paleomagnetism, and a fully-kinematic, 'tomographic' GPlates NW Panthalassa/Pacific plate reconstruction developed by our research group, of which I was a co-author (Wu et al., in revision).

Below, I define current scientific questions and outline the four parts of this thesis:

(1) Several late Cretaceous to early Cenozoic plate tectonic reconstructions have suggested that at least one paleo-Pacific plate, probably the Izanagi plate, subducted beneath the northeast Asian margin. Consequently, a mid-ocean ridge between the modern Pacific Plate and the Izanagi Plate could have intersected the East Asia Eurasian continental

margin and subducted. Three competing classes of plate tectonic reconstructions have been proposed for Pacific-Izanagi ridge-trench intersections along East Asia. (i) The high-angle ridge-trench intersection model proposed that an NW-SE trending mid-ocean ridge that separated the Izanagi plate to the north and the Pacific Plate to the south intersected the NE Asian margin at a high angle; the resultant trench-trench-ridge triple junction swept from south to north in the late Cretaceous (Maruyama et al., 1997). (ii) In the low-angle ridge-trench intersection model, an NNE-SSW trending Izanagi-Pacific spreading ridge intersected subparallel to a large swath of the NE Asian margin and was subducted beneath the margin in the early Cenozoic 60 to 50 Ma (Seton et al., 2015; Whittaker et al., 2007). Finally, (iii) the marginal sea closure model involved the closure of now-vanished East Asian marginal seas in the early Cenozoic (Domeier et al., 2017; Itoh et al., 2017). Each plate model class predicts distinct igneous activities along the East Asian margin and is tested in this study. We compile ages and Sr-Nd isotopic values of intermediate to felsic igneous rocks within the continental arc of NE Asia between 110 to 20 Ma and newly analyze magmatic fluxes (i.e. areal addition rates) to search for spatiotemporal constraints on possible ridge subduction. This chapter was published in the journal Geology.

(2) Some models consider that during the Early Cretaceous times, an oceanic plate continuously subducted under the Eurasian continental margin to form an ‘Andean-type’ margin, and a continental arc-trench system was developed (Engebretson, 1985; Li et al., 2019; Matthews et al., 2016; Torsvik et al., 2019). In contrast, others suggest that intra-oceanic arcs formed outboard of the continental margin due to intra-oceanic subduction,

and these arcs accreted along the East Asian margin; we call these 'intra-oceanic arc' models (Arkhipov et al., 2019; Malinovsky and Markevich, 2007; Ueda and Miyashita, 2005). In this study, we review the NE Asian margin geology during Cretaceous times from published igneous activity, stratigraphy, and paleomagnetism of accreted Cretaceous oceanic terranes in northeast Asia. We synthesize an alternative view of NW Pacific basin plate tectonic boundary conditions during the Early Cretaceous that includes accretion of intra-oceanic arcs along the NE Asian margin. In addition, the North China craton had lost a significant (~120 km) thickness of its mantle lithosphere during the early Cretaceous (i.e. North China Craton destruction). Most studies explain North China craton destruction within the context of an Andean-type margin during the Early Cretaceous; intra-oceanic arc models have been less considered. In this study, we discuss the implications for North China craton destruction under an early Cretaceous tectonic setting that includes intra-oceanic subduction. This chapter has been submitted to Earth-Sciences Reviews for peer-review and is in revision.

(3) The igneous geochemistry of the Sikhote-Alin continental arc, Russian Far East, characterizes long-lived subduction along a ~1500 km-wide swath of the northwest Pacific margin since the Mesozoic, but has only been lightly studied due to its remote location and geopolitics. We present new zircon U-Pb chronology and geochemical data (whole-rock major, trace element, and Nd-Hf isotopic compositions) from 94 samples across the entire Sikhote-Alin area. Our results more than doubles the existing published data (n=61). We also provide the first constraints on the ~1000 km-length northern Sikhote-Alin arc, which has no published studies. We combine our new results with

published data to build a comprehensive regional database and discuss the spatiotemporal and geochemical evolution of Sikhote-Alin arc.

(4) Episodic behavior in the production rate and geochemistry of continental magmatic arcs has been long documented in the Cordillera but the mechanisms are debated (e.g. Armstrong et al., 1988; Paterson and Ducea, 2015). Current models argue that arc tempos are primarily driven by some combination of: (1) Internal factors involving crustal thickening, melting, and/or delamination (Ducea 2001; DeCelles et al, 2015); (2) External factors such as the thermal structure of the subduction zone and fluid flux that generally controlled by down-going plate parameters (Zellmer 2008; de Silva et al. 2015; Ardila et al., 2019). In this study, we quantitatively investigate possible external controls on northeast Asian arc tempos along the western Pacific margin since Cretaceous times, which has been less investigated due to data availability. We apply multivariate analysis (i.e. a time-varying coefficient linear regression model TVLM) on a paired geologic/plate tectonic dataset: (1) the large (n>500) NE Asian magmatic database of published and unpublished results assembled in this thesis; and (2) and a fully-kinematic NE Asian-Pacific plate tectonic reconstruction model produced from the relatively independent constraints of tomography (Wu et al., in revision), of which I am a co-author. I specifically investigate the parameters of plate convergence rates vs. silica content and radio-isotope values, and comment on the applicability of this approach for future studies of arc tempos.

CHAPTER 2: IZANAGI-PACIFIC RIDGE SUBDUCTION REVEALED BY A 56 TO 46 MA MAGMATIC GAP ALONG THE NE ASIAN MARGIN

2.1 Introduction

The Eurasian margin along East Asia has been a long-lived convergent margin since early Mesozoic times (e.g. Müller et al., 2016). Several plate tectonic reconstructions have suggested that at least one paleo-Pacific plate, probably the Izanagi plate, subducted beneath the margin during the Mesozoic (Maruyama et al., 1997; Müller et al., 2016). Consequently, a mid-ocean ridge between the modern Pacific Plate and the Izanagi plate could have intersected the East Asia Eurasian continental margin and subducted. Three competing classes of plate tectonic reconstructions have been proposed for Pacific-Izanagi ridge-trench intersections along East Asia (Fig. 2.1) that imply alternative geological histories for the East Asian margin, for NW Pacific Ocean plate reconstructions, and possibly, for a 50 Ma Pacific hemisphere plate-mantle reorganization. The *high-angle ridge-trench intersection model* proposed that a NW-SE trending mid-ocean ridge that separated the Izanagi plate to the north and Pacific plate to the south intersected the NE Asian margin at a high angle; the resultant trench-trench-ridge triple junction swept from south to north in the late Cretaceous (Fig. 2.1b) (Maruyama et al., 1997). In the *low-angle ridge-trench intersection model*, a NNE-SSW trending Izanagi-Pacific spreading ridge intersected subparallel to a large swath of the NE Asian margin and was subducted beneath the margin in the early Cenozoic 60 to 50 Ma (Fig. 2.1c) (Seton et al., 2015; Whittaker et al., 2007). Finally, the *marginal sea closure model*

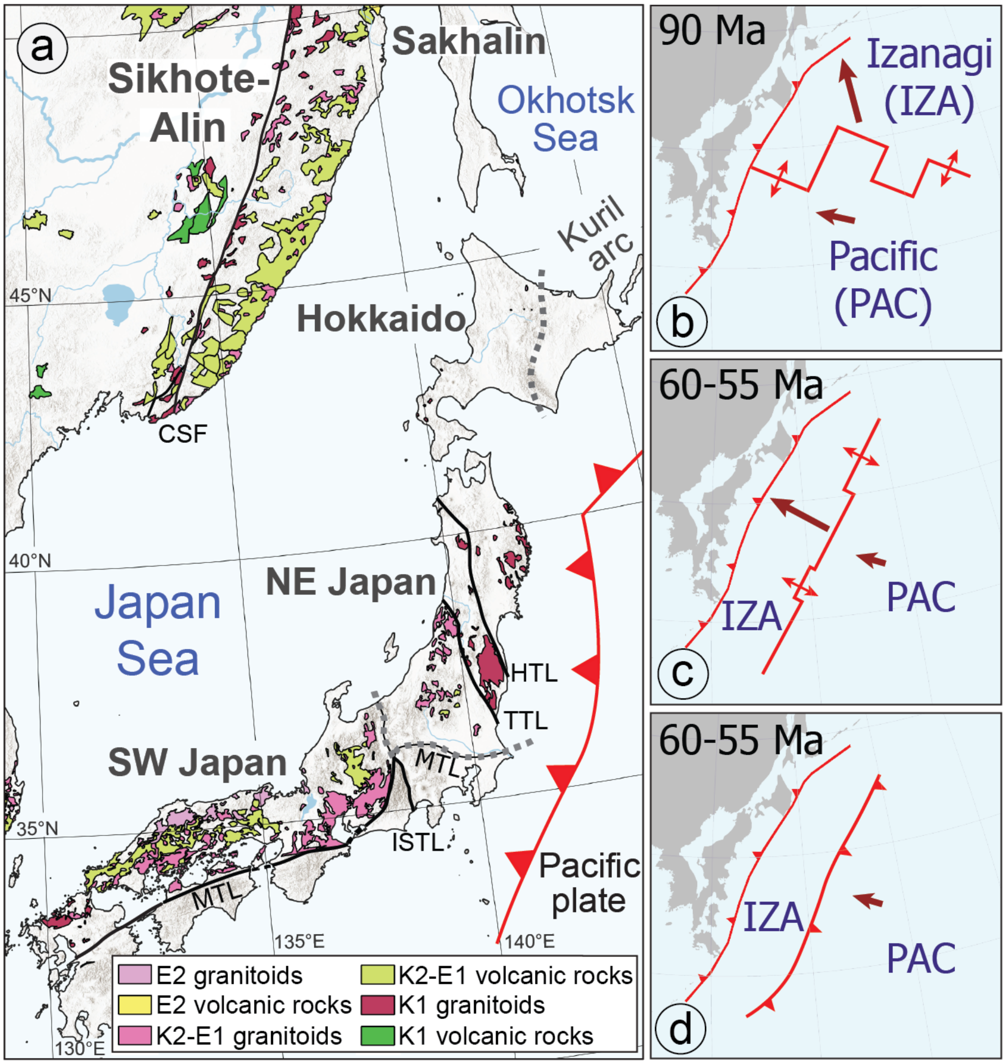

Figure 2. 1 Cretaceous to early Cenozoic NE Asia geology and plate tectonic reconstruction models

(a) Tectonic framework and distribution of Cretaceous to Eocene igneous rocks at the NE Asian margin. The two grey dashed lines show boundaries between SW and NE Japan, and between the Kuril arc system and western Hokkaido. CSF: Central Sikhote-Alin fault, HTL: Hatagawa tectonic line, TTL: Tanakura tectonic line, MTL: Median tectonic line, ISTL: Itoigawa-Shizuoka tectonic line. (b) to (d) show proposed plate tectonic reconstructions of the Izanagi and Pacific plates and the Izanagi-Pacific spreading ridge. b) High-angle ridge-trench intersection model (Maruyama et al., 1997); c) Low-angle ridge-trench intersection model (Whittaker et al., 2007; Seton et al., 2015). The modeled Izanagi-Pacific spreading ridge extends further south into southeast Asia but only the northern portion is shown here for comparative purposes. d) Marginal sea closure model (Domeier et al., 2017).

involved the closure of now-vanished East Asian marginal seas in the early Cenozoic (Fig. 2.1d) (Domeier et al., 2017; Itoh et al., 2017). Each plate model class predicts distinct igneous activities along the East Asian margin and is tested here from magmatic ages, radio-isotopic values, and magmatic flux. We compile ages and Sr-Nd isotopic values of intermediate to felsic igneous rocks within the continental arc of NE Asia (Fig. 2.1) between 110 to 20 Ma to search for spatiotemporal constraints on possible ridge subduction. Published end-member Japan Sea opening plate reconstructions were digitally re-built to palinspastically restore the magmatism prior to the Japan Sea opening.

2.2 Geological setting

The southern Russian Far East and the Japanese Islands along NE Asia have widely distributed Cretaceous to Cenozoic igneous rocks (Fig. 2.1) that provide a sufficient magmatic record of subduction history. In Sikhote-Alin, the continental margin grew from the subduction of oceanic plates and is formed by Mesozoic geological units such as accreted terranes and accretionary prisms (Khanchuk et al., 2016; Zharov, 2005). Likewise, the Japanese Islands are a segmented, subduction-related orogen that grew along the East Asian margin since at least the Jurassic (Taira et al., 2016; Wakita, 2013). During the Japan Sea opening in the early Miocene, NE and SW Japan separated from the continental margin (Otofuji et al., 1985). The pre-rift positions of the Japanese Islands remain debated, but there is a general consensus that Japan was a southern extension of Sikhote-Alin prior to rifting (Van Horne et al., 2017).

2.3 Methods

A 110 to 20 Ma magmatic record for Japan, Sikhote-Alin, and Sakhalin (Fig. 2.2) was compiled from published literature (Imaoka et al., 2011; Jahn et al., 2015; Liao et al., 2018; Morioka et al., 2000; Okamura et al., 2016; Shibata and Ishihara, 1979; Tanaka, 1987; Terakado and Nohda, 1993; Yuhara, 1998; Zhao et al., 2017), and other references in Appendix A). Intermediate to felsic compositions are typically produced within continental arcs (Ducea et al., 2015) and Cretaceous to early Cenozoic subduction in the study area primarily manifested in silicic magmatism (Jahn et al., 2015). Therefore, we compiled ages and whole-rock Sr-Nd isotopic values for igneous rocks with intermediate to felsic compositions into a database of 1291 values. Initial Sr and Nd isotope values were re-calibrated using the same decay constants. Ages from zircon U-Pb analyses were used where possible (173 samples); the remainders were relatively good quality Rb-Sr and K-Ar dates and a small minority (<40) of estimated ages. To roughly estimate magmatic influx across time, we digitized the areal extents of Cretaceous to early Cenozoic igneous rocks from SW Japan to southern Sikhote-Alin area (30°N to 46°N) following the 1:5,000,000 International Geological Map of Asia (Ren et al., 2013) in QGIS software (Team, 2015). The digitized igneous rock polygons were later input into our plate reconstruction within the software Gplates (Boyden et al., 2011). The igneous rocks were palinspastically restored prior to Japan Sea opening by digitally re-creating published end-member Japan Sea opening plate models using the software GPlates

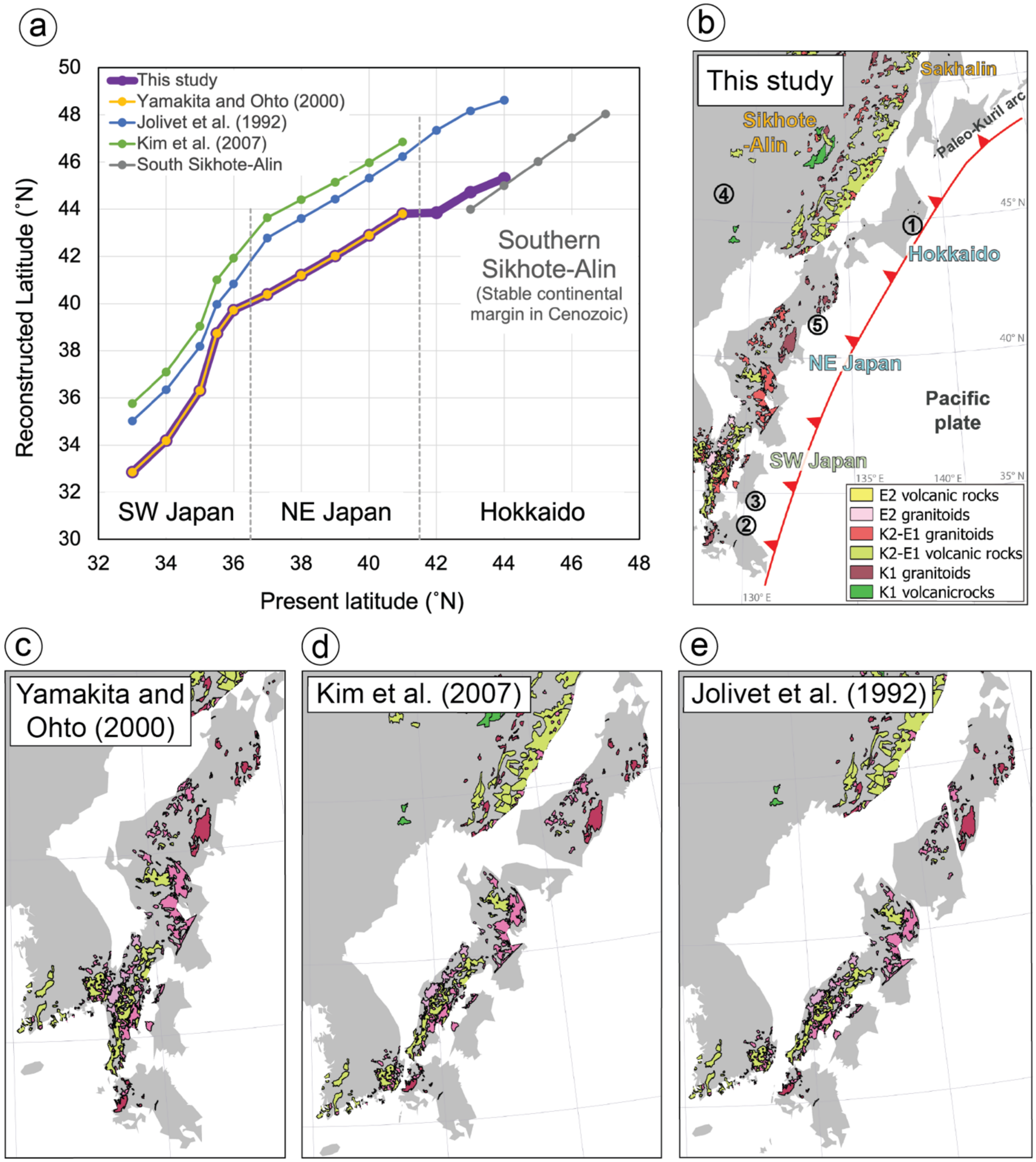

Figure 2. 2 Comparison between alternative Japan Sea reconstruction models at 30 Ma

(a) Present vs. reconstructed latitude of Japan in alternative reconstruction model pririor to the Japan Sea opening. (b) Yamakita and Ohto (2000) model. (c) Kim et al. (2007) model. (d) Jolivet et al. (1992) model.

(Boyden et al., 2011). Here we present our preferred model following (Yamakita and Otoh, 2000); the Kuril arc including eastern Hokkaido was restored closer to the Sakhalin island, and the Kuril basin was closed following (Ueda, 2016). We also show our results are valid within other end-member reconstructions (Fig. 2.3).

2.4 Results

Plots of igneous rock ages against whole-rock εNd(t) and $(^{87}Sr/^{86}Sr)_0$ values show felsic to intermediate rocks of 56 to 46 Ma ages were absent (i.e. a magmatic gap) along the entire study area (Fig. 2.2). Age errors proximal to the magmatic gap were carefully checked to confirm feature integrity. Isotopically, Cretaceous to Paleocene rocks show relatively lower εNd(t) = -15 ~ +2 and higher $(^{87}Sr/^{86}Sr)_0$ between 0.704 to 0.714. In contrast, the Eocene to Oligocene rocks have relatively higher εNd(t) = -2 ~ +6 and lower $(^{87}Sr/^{86}Sr)_0$ between 0.702 to 0.707. Our palinspastic restoration in Fig. 2.4a reveals the 56 to 46 Ma magmatic gap occurred near-synchronously across the NE Asian margin between 38°N to 48°N latitudes, including Sikhote-Alin and Sakhalin (42°~48° N), Hokkaido and NE Japan (38°~46° N), and SW Japan (31°~38° N) (Fig. 2.4b). Comparison to other published Japan Sea reconstructions shifted NE and SW Japan paleolatitudes by 1~3° relative to Sikhote-Alin (Fig. 2.2) but preserved the spatiotemporal trends in Fig. 2.4. Cretaceous to Paleocene arc magmatic fluxes were ~1090 km^2/Ma prior to the 56 to 46 Ma magmatic gap and decreased to ~390 km^2/Ma from the middle to end Eocene (Fig. 2.4c).

Figure 2. 3 110-20 Ma Nd-Sr isotopic composition of felsic to intermediate igneous rocks along the 30°N to 46°N NE Asian margin.

Early Cenozoic tectonic events 1 to 5 (circled numbers) are possibly related to ridge subduction along the NE Asian margin. Location of Events 1 to 5 are shown in Fig. 2.4a. DM: depleted mantle, CHUR: Chrondritic unfractionated reservoir, BSE: Bulk silica earth. The increase in εNd(t) and decrease in $(^{87}Sr/^{86}Sr)_0$ after the 56 to 46 Ma magmatic gap (red area) indicates more depleted mantle component after 46 Ma. References: Event 1 (Maeda and Kagami, 1996; Nanayama et al., in press); Event 2 (Raimbourg et al., 2014); Event 3 (Agar et al., 1989; Hara and Kimura, 2008; Mackenzie et al., 1990; Mukoyoshi et al., 2009); Event 5 (Ando, 2003).

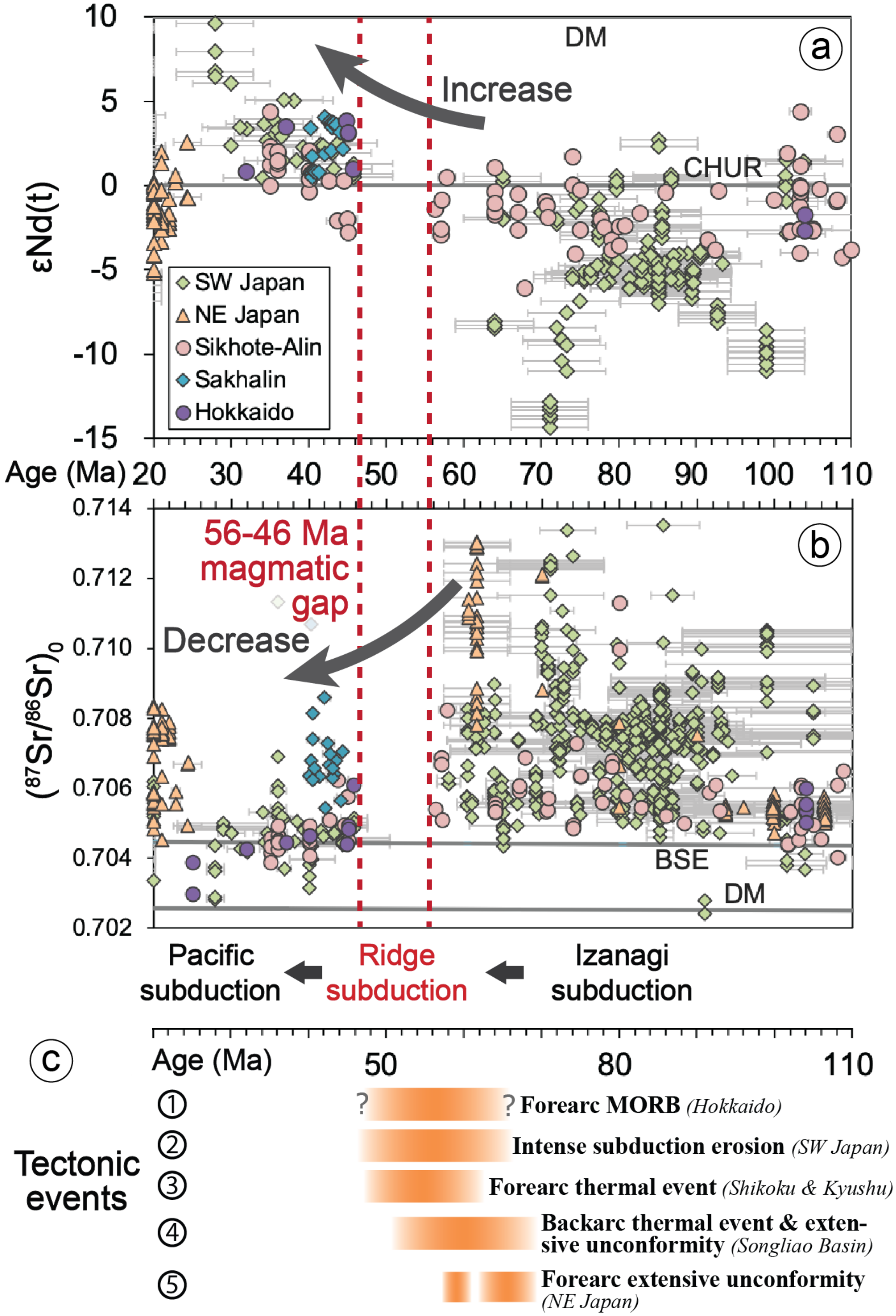

DM
Increase
CHUR
a
εNd(t)
SW Japan
NE Japan
Sikhote-Alin
Sakhalin
Hokkaido
Age (Ma) 20 30 40 50 60 70 80 90 100 110
56-46 Ma
magmatic
gap
Decrease
b
$(^{87}Sr/^{86}Sr)_0$
BSE
DM
Pacific subduction
Ridge subduction
Izanagi subduction
c
Age (Ma) 50 80 110
Tectonic events
① Forearc MORB (Hokkaido)
② Intense subduction erosion (SW Japan)
③ Forearc thermal event (Shikoku & Kyushu)
④ Backarc thermal event & extensive unconformity (Songliao Basin)
⑤ Forearc extensive unconformity (NE Japan)

2.5 Discussion

2.5.1 Implications for East Asia ridge-trench interactions during the early Cenozoic

Ridge subduction events profoundly affect the upper plate but specific processes are non-unique and time-transgressive; therefore, multiple geological constraints must be considered in unison to properly diagnose past ridge subduction (Sisson et al., 2003). Accordingly, we synthesize other geological evidence with our 56 to 46 Ma magmatic gap to discuss proposed Eurasia-NW Pacific ridge-trench intersections (Fig. 2.1). We then discuss our isotopic values and magmatic addition rates relative to our preferred plate model.

Basalts with mid-ocean ridge basalt (MORB) chemical characteristics extruded in the forearc region are considered the most distinctive indicator of ridge-trench intersections (Lagabrielle et al., 1994). Syn-sedimentary pillow basalts with MORB chemical characteristics have been found in the early Cenozoic Hidaka belt in Hokkaido (Event 1 in Fig. 2.4c; Maeda and Kagami, 1996; Miyashita and Katsushima, 1986; Nanayama et al., 2018). Therefore, evidence exists for the ridge-trench intersection at Hokkaido during our observed 56 to 46 Ma near-simultaneous shutdown of subduction magmatism between Japan and southern Sikhote-Alin (Figs. 2.3, 2.4). Ridge subduction has also been linked to the termination of arc magmatism (Dickinson and Snyder, 1979; Sisson et al., 2003; Thorkelson, 1996). These studies proposed ridge subduction would create a slab-free region (i.e. slab window) within the down-going slab beneath the overriding plate, resulting in a temporarily inactive volcanic arc (Fig. 2.5b; Thorkelson, 1996), which is consistent with the 56 to 46 Ma magmatic gap revealed here

Figure 2. 4 56-46 Ma magmatic gap along the NE Asian margin and magma addition rates before-after the gap.

(a) Reconstructed configuration of the NE Asian margin based our preferred Japan Sea plate reconstruction modified from Yamakita and Ohto (2000). Reconstructions following other published models are shown in Fig. 2.2. Locations of early Cenozoic tectonic events from Fig. 2.3 are shown by encircled numbers 1 to 5. (b) Spatiotemporal distribution of igneous rocks across three regions: SW Japan (green box), Hokkaido and NE Japan (blue box), and Sikhote-Alin and Sakhalin (orange box). All regions show a near-simultaneous 56 to 46 Ma magmatic gap. (c) Comparison of areal addition rate of igneous rocks with ages before and after the 56-46 Ma magmatic gap in SW Japan to southern Sikhote-Alin area (30 °N to 46 °N). Relatively higher magmatic addition rates before 56 Ma and lower rates after 46 Ma are consistent with a change from fast Izanagi-Eurasia plate convergence (~20 cm/yr) to slow Pacific-Eurasia convergence (~7 cm/yr) predicted by the low-angle ridge-trench intersection plate model in Fig. 2.1c.

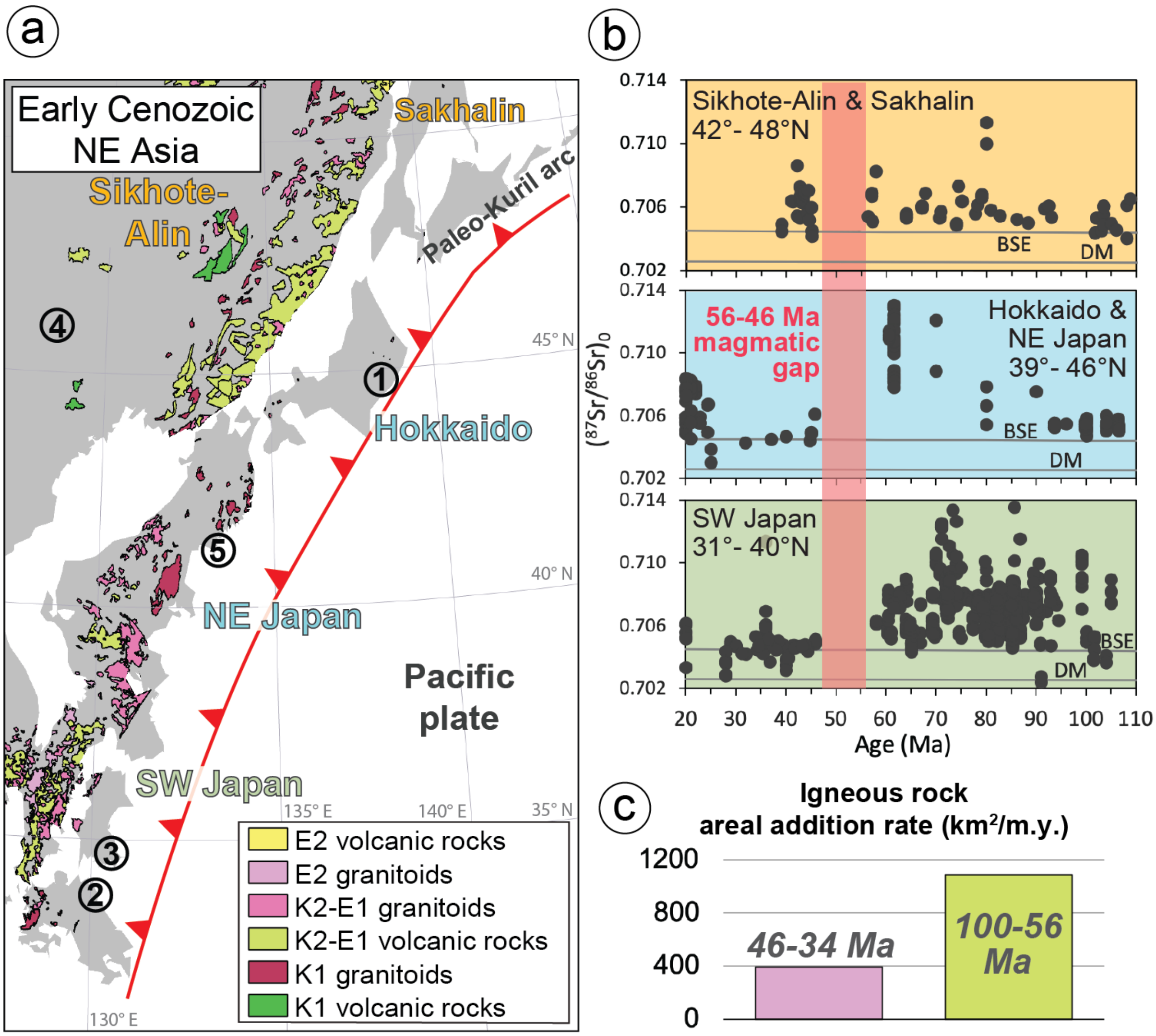

a
Early Cenozoic NE Asia
Sakhalin
Sikhote-Alin
Paleo-Kuril arc
Hokkaido
NE Japan
SW Japan
Pacific plate
45° N
40° N
35° N
130° E
135° E
140° E
E2 volcanic rocks
E2 granitoids
K2-E1 granitoids
K2-E1 volcanic rocks
K1 granitoids
K1 volcanic rocks
b
Sikhote-Alin & Sakhalin 42°- 48°N
Hokkaido & NE Japan 39°- 46°N
SW Japan 31°- 40°N
56-46 Ma magmatic gap
BSE
DM
$(^{87}Sr/^{86}Sr)_0$
Age (Ma)
c
Igneous rock areal addition rate (km²/m.y.)
46-34 Ma
100-56 Ma

(Figs. 2.3, 2.4). Indeed, a magmatic gap and forearc basaltic magmatism have also been observed within the Chile Rise ridge-trench intersection (Gutiérrez et al., 2005; Lagabrielle et al., 1994; Nur, 1981).

Ridge-trench intersections often produce elevated heat flows and topographic uplift (Sisson et al., 2003). These have been observed within the NE Asian margin during the early Cenozoic, near the magmatic gap time interval (Events 2 to 5 in Figs. 2.3, 2.4). At the southern end of the magmatic gap, an early Eocene thermal event was revealed by thermochronology within the Shimanto belt in SW Japan during 58 to 46 Ma (Event 2 and 3 in Figs. 2.3, 2.4; Agar et al., 1989; Hara and Kimura, 2008; Mackenzie et al., 1990; Mukoyoshi et al., 2009; Raimbourg et al., 2014). Extensive early Cenozoic unconformities have also been recorded in NE Japan (Event 5 in Figs. 2.3, 2.4; Ando, 2003). Kimura et al. (2019) showed the Japan islands experienced a general Paleocene to early Eocene interruption in volcanism and trench wedge accretion, unconformities in the forearc basins, followed by shallowing of sedimentary facies that was consistent with ridge subduction. At the northern end of our identified magmatic gap, a strong Paleocene to early Eocene unconformity was identified within the Songliao basin (Song et al., 2014; Wang et al., 2013). Apatite fission track dating suggested intense uplift in the area around 65-50 Ma (Song et al., 2018). Together, these possible ridge subduction signals corroborate with the spatial extent and timing of our magmatic gap, thus strengthening the case that our 56 to 46 Ma magmatic gap is evidence of ridge subduction.

2.5.2 Implications for Izanagi-Pacific plate tectonic reconstructions

Here we consider our results against proposed plate model classes (Figs. 2.1b to d) but other valid solutions exist because the Izanagi plate is conceptual (i.e. fully subducted). The low angle Izanagi-Pacific ridge-trench intersection model (Fig. 2.1c) (Whittaker et al., 2007; Seton et al., 2015) is generally most consistent with the 56 to 46 Ma magmatic gap (Fig. 2.4) but their modeled ridge-trench intersection extended >5000 km into SE China and SE Asia. Magmatism in SE China (Li, 2000; Zhou et al., 2006) and west Borneo (e.g. Hennig et al., 2017) ceased around ~80 Ma and is highly contrasted to our study area (Fig. 2.2). This suggests that Izanagi-Pacific ridge-trench intersections did not extend south of southernmost Japan, in contrast to Seton et al. (2015).

An alternative plate model proposed that marginal seas closed along East Asia in the early Cenozoic and the Izanagi-Pacific spreading ridge never reached Japan (Domeier et al., 2017). Our study shows the Izanagi-Pacific ridge did subduct along East Asia in the early Cenozoic (Fig. 2.2), and likely at a low-angle to the margin (Fig. 2.4b, 2.5). Nonetheless, the presence of now-subducted marginal seas north of the paleo-Kurile trench from Domeier et al. (2017) may explain the early Cenozoic tectonic setting north of 48°N present latitudes. The high-angle ridge-trench intersection model implies that a spatially restricted, amagmatic area migrated along the East Asian margin during the Cretaceous (Maruyama et al., 1997) that is incompatible with our observed synchronous and areally-extensive 56 to 46 Ma magmatic gap (Fig. 2.4b). Finally, given uncertainties, it is possible that a Kula-Pacific ridge-trench

Figure 2. 5 Tectonic evolution of NE Asia during Izanagi-Pacific ridge-trench intersection in the early Cenozoic based on this study.

(a) The mid-Cretaceous to Paleocene arc magmatism was characterized by more enriched isotopic signatures and relatively high (1090 km^2/Ma) magmatic areal addition rates during fast 20 cm/yr Izanagi-Eurasia subduction. (b) Izanagi-Pacific ridge-trench intersection produced a 56 to 46 Ma magmatic gap and a slab window. Influx of asthenosphere into the mantle wedge through the slab window arguably led to relatively depleted isotopic signatures in arc magmatism after 46 Ma. (c) After 46 Ma a less developed igneous arc formed that was characterized by more depleted isotopic signatures and relatively lower (390 km^2/Ma) magmatic area addition rates during slower ~7 cm/yr Pacific subduction.

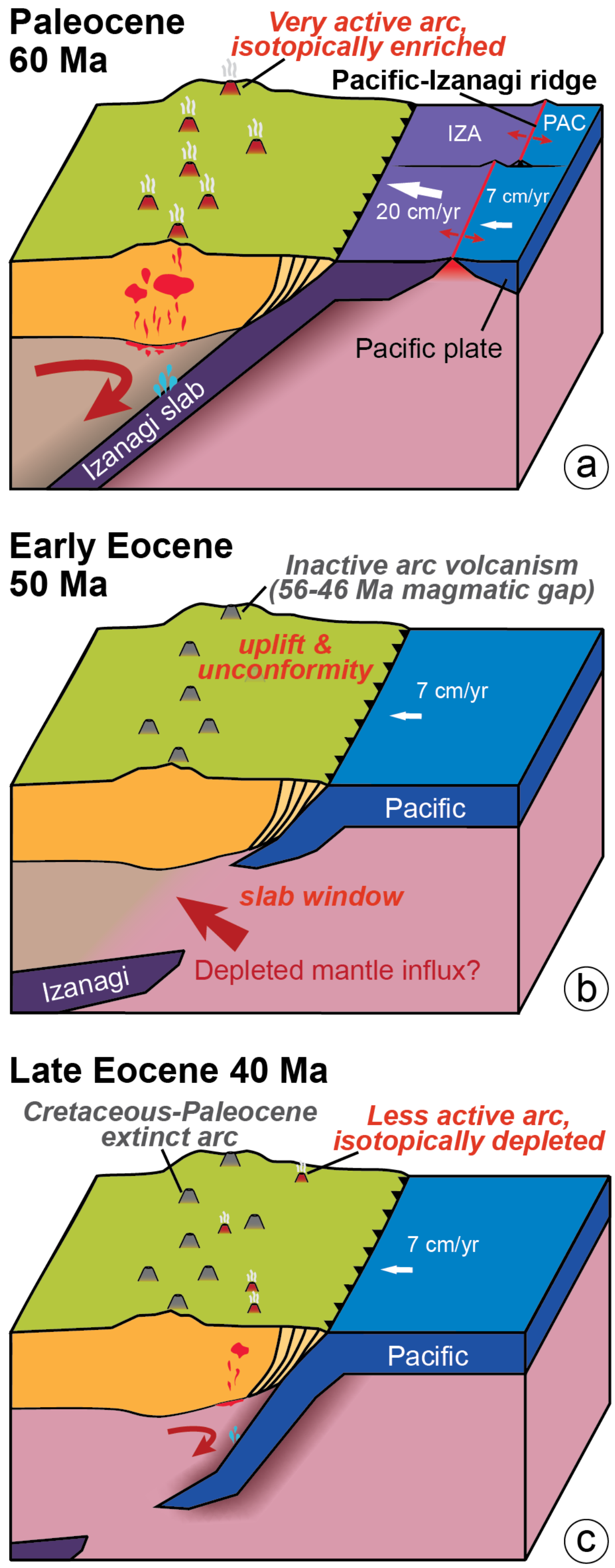
Paleocene
60 Ma
Very active arc,
isotopically enriched
Pacific-Izanagi ridge
IZA
PAC
20 cm/yr
7 cm/yr
Pacific plate
Izanagi slab
a
Early Eocene
50 Ma
Inactive arc volcanism
(56-46 Ma magmatic gap)
uplift &
unconformity
7 cm/yr
Pacific
slab window
Depleted mantle influx?
Izanagi
b
Late Eocene 40 Ma
Cretaceous-Paleocene
extinct arc
Less active arc,
isotopically depleted
7 cm/yr
Pacific
c

intersection with Eurasia in the early Cenozoic could have produced the magmatism shown here; however, a viable plate model has yet to be proposed.

2.5.3 Implications for ~50 Ma Pacific plate reorganization

Seton et al. (2015) suggested sub-parallel arrival of the Pacific-Izanagi ridge along the East Asian margin led to a margin-wide slab detachment that significantly decreased the slab pull force acting on the Pacific Plate at 60 to 50 Ma, possibly leading to the Pacific plate-mantle reorganization at ~53 to 47 Ma (O'Connor et al., 2013; Whittaker et al., 2007). The simultaneous 56 to 46 Ma magmatic gap along the NE Asia margin shown here (Figs. Figs. 2.3, 2.4b) supports the formation of a ~1500 km-long margin-parallel slab window beneath the East Asian margin during this timeframe. However, the apparent lack of magmatic evidence for early Cenozoic Izanagi-Pacific ridge subduction south of Japan (i.e. South China and SE Asia) suggests the modeled >5000 km slab detachment of Seton et al. (2015) may be overestimated by more than a factor of two. The geodynamic viability of a much shorter (i.e. ~1500 km length from this study) Izanagi-Pacific ridge-trench intersection for producing a ~50 Ma Pacific plate reorganization should be re-examined.

2.5.4 Implications for NE Asian margin magmatic evolution

Contrasted areal addition rates (Fig. 2.4c) and isotopic compositions (Fig. 2.2) of igneous rocks astride the 56 to 46 Ma magmatic gap between Japan and Sikhote-Alin are generally consistent with a subduction zone reorganization during low-angle Izanagi-Pacific ridge-trench intersection (Fig. 2.5). Studies have shown positive correlations between magma generation and subduction rates (Cagnioncle et al., 2007; Hughes and Mahood, 2008; Zellmer, 2008). Our preferred low-angle ridge-trench intersection model (Fig. 2.1c, 2.5) indicates the NE Asian continental margin was dominated by fast ~20 cm/yr Izanagi subduction before 55 Ma and slower (65% reduced) Pacific subduction after 50 Ma at ~7 cm/yr (Fig. 2.5) (Whittaker et al., 2007; Seton et al., 2015). Interestingly, our estimated magma addition rates over time show similar a reduction (~65%) in magmatism after the Paleocene, from ~1090 km^2 My^{-1} to ~390 km^2 My^{-1} (Fig. 2.4c). Isotopically, late Eocene igneous rocks show more depleted mantle compositions (i.e. higher εNd(t) and lower $(^{87}Sr/^{86}Sr)_0$) than Cretaceous to Paleocene igneous rocks (Fig. 2.2). This could be consistent with the input of depleted mantle to the mantle wedge through a slab window during the ridge subduction (Fig. 2.5) and/or input of relatively enriched crustal material into the subduction zone during earlier Izanagi subduction.

2.6 Conclusion

Past plate kinematics can be reliably reconstructed from spreading ridge geometries but Eurasia-NW Pacific plate reconstructions remain controversial because the ridges have subducted. Our compiled and palinspastically-restored magmatic record between Sikhote-Alin and SW Japan in the early Cenozoic links fragmentary geological evidence to present new, definitive spatiotemporal constraints on low-angle ridge-trench intersection along ~1500 km of the NE Eurasian margin, clarifying ongoing, first-order plate tectonic controversy. The 56 to 46 Ma magmatic gap shown here coincides with the major Pacific plate reorganization between ~53 to 47 Ma. Although this may support a Pacific Ocean basin plate-mantle reorganization sparked by widespread Izanagi-Pacific ridge subduction, we limit the ridge subduction to the north of SW Japan, which is significantly (>2x) shorter than previously thought. This may require re-evaluation of circum-Pacific geodynamic models.

CHAPTER 3: INTRA-OCEANIC ARC ACCRETION ALONG NORTHEAST ASIA DURING EARLY CRETACEOUS PROVIDES A PLATE TECTONIC CONTEXT FOR NORTH CHINA CRATON DESTRUCTION

3.1 Introduction

The eastern Eurasian continental margin along northeast Asia shows abundant evidence for subduction-related igneous activity during Cretaceous times (Fig. 3.1) (Grebennikov et al., 2016; Isozaki et al., 2010; Khanchuk et al., 2016; Wakita, 2013). Consequently, studies of the eastern Eurasian margin typically reconstruct long-lived plate convergence that involves the subduction of the modern and Paleo-Pacific plates through time (Isozaki et al., 2010; Wilde, 2015). However, many first-order details of NW Paleo-Pacific (Panthalassa) plate tectonic reconstructions remain controversial, including the possibility of intra-oceanic accretion along the continental margin (Fig. 3.2). Some models consider that during the Early Cretaceous times, an oceanic plate continuously subducted under the Eurasian continental margin to form an ‘Andean-type’ margin, and a continental arc-trench system was developed (Fig. 3.2a) (Engebretson, 1985; Li et al., 2019; Matthews et al., 2016; Torsvik et al., 2019). In contrast, others suggest that intra-oceanic arcs formed outboard of the continental margin due to intra-oceanic subduction, and these arcs accreted along the East Asian margin; we call these ‘intra-oceanic arc’ models (Fig. 3.2b) (Arkhipov et al., 2019; Malinovsky and Markevich, 2007; Ueda and Miyashita, 2005). The plate tectonic context for northeast Asia during Early

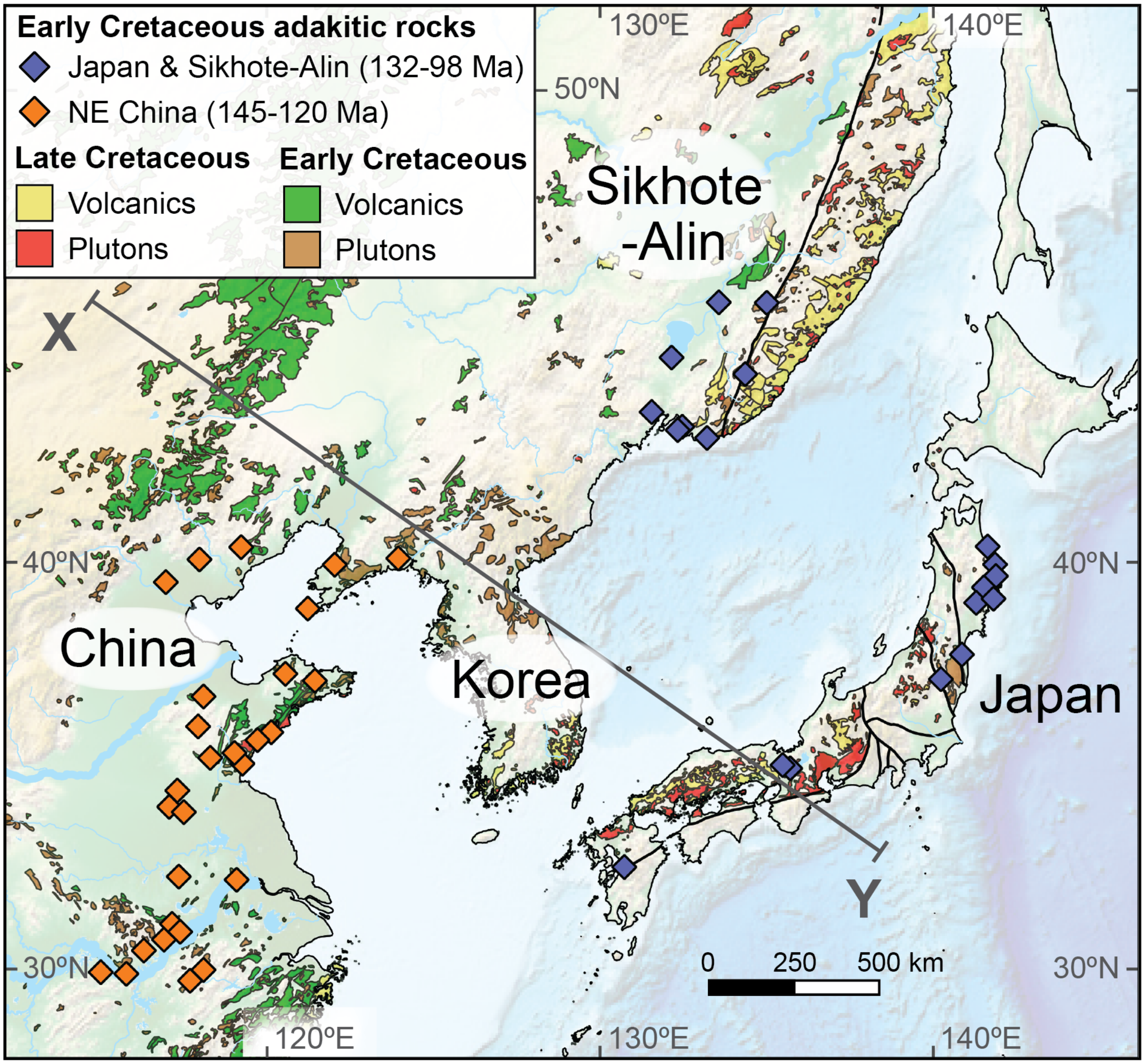

Figure 3. 1 Location map showing Cretaceous igneous rocks in NE Asia.

Transect X-Y shows a line of projection for the spatiotemporal distribution of igneous rocks shown in Figure 3.3a.

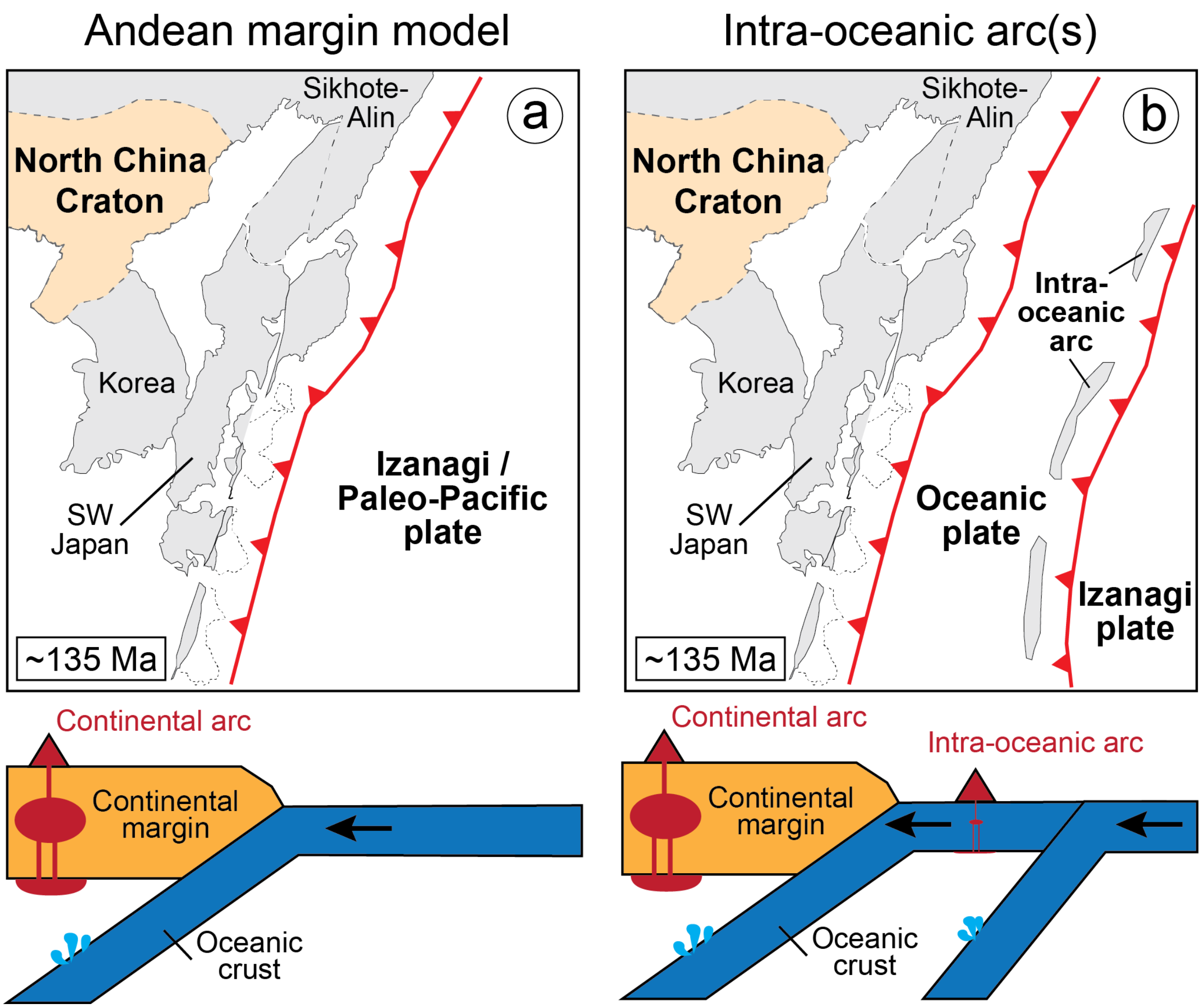

Figure 3. 2 Proposed NW Pacific basin plate tectonic reconstructions during the Early Cretaceous and associated schematic cross-sections.

(a) Andean margin type models show continuous westward subduction of a large Izanagi /paleo-Pacific plate under NE Asia (e.g. Matthews et al., 2016). (b) Intra-oceanic arc models show intra-oceanic subduction zone(s) developed outboard of NE Asia, which results in multiple subduction zones (e.g. Ueda and Miyashita, 2005). In (b), the large Izanagi /paleo-Pacific plate subduct offshore are precluded from subducting under NE Asia by the intra-oceanic subduction zone.

Cretaceous times has important implications for the following significant events: biogeographic realms of the Jehol biota, one of the best-preserved terrestrial fossil assemblages in Earth history (Pan et al., 2013); the origin of economic mineral deposits in the region (e.g Li et al., 2019); voluminous magmatism (Fig. 3.1, 3.3); an abrupt change from contractional to extensional stresses that induced sedimentary basin formation and metamorphic core complexes within continental NE China (e.g. Li et al., 2019); and, thinning and loss of a significant (~120 km) thickness of mantle lithosphere from the North China craton (i.e. North China craton destruction) (Dai et al., 2016; Liu et al., 2019; Ma et al., 2016a; Zheng et al., 2018), which is the focus of this paper.

Most studies explain North China craton destruction within the context of an Andean-type margin during the Early Cretaceous, specifically, continuous Izanagi /paleo-Pacific plate subduction under Eurasia (e.g. Fig. 3.2a) (Liu et al., 2019; Wu et al., 2019; Zheng et al., 2018). However, the alternative possibility that North China craton destruction occurred during intra-oceanic arc accretion (Fig. 3.2b) has been proposed (e.g. Ueda and Miyashita, 2005) but not fully examined. In this study, we review NE Asian margin geology during Cretaceous times from published igneous activity, stratigraphy, and paleomagnetism of accreted Cretaceous oceanic terranes in Japan, Korea, North China, and the southern Russian Far East (Sikhote-Alin and Sakhalin). We give particular attention to Early Cretaceous-aged adakitic rock suites within NE Asia because the adakites occur between now-separated parts of the continental arc (Wu et al., 2017) and may have tectonic significance (Castillo, 2012). We synthesize an alternative view of NW Pacific basin plate tectonic boundary conditions during Early Cretaceous that includes accretion of intra-oceanic arcs along the NE Asian margin, and discuss their implications for North China craton destruction models.

3.2 A brief review of Eurasian margin geology along NE Asia during Cretaceous times

3.2.1 Published plate tectonic reconstructions of the NW Pacific basin

The geology of the NE Asian margin is typically interpreted in the context of westward subduction of Pacific and paleo-Pacific plates beneath the Eurasian margin since at least ~200 Ma (Guan et al., 2020; Kusky et al., 2007; Wilde, 2015; Zhou et al., 2009). In reality, plate reconstruction constraints are extremely sparse due to consumption of >8000 km of oceanic lithosphere since the Cretaceous by subduction (e.g. Matthews et al., 2016). Consequently, numerous plate tectonic reconstruction models for the NW Pacific basin during Cretaceous times have been proposed. The most popular class of proposed plate models are Andean-type models (Fig. 3.2a) that show a continental arc-trench system and continuous subduction of oceanic plate(s) along the NE Asian margin. Recent global plate reconstructions and other plate models constrained by NE China geology consider Andean-type subduction of a large Izanagi /paleo-Pacific plate that occupied the NW Pacific basin from late Triassic to Cretaceous (Li et al., 2019; Matthews et al., 2016; Torsvik et al., 2019). Other Andean-type models show mid-oceanic ridges between the Izanagi and Pacific plates that intersected the Eurasian margin and swept northwards during the Cretaceous (Engebretson, 1985; Isozaki et al., 2010; Maruyama et al., 1997). A variant suggests that during the Early Cretaceous, a northward-sweeping Izanagi-Farallon ridge-trench intersection produced the adakitic Kitakami granitic plutons, NE Japan (Osozawa et al., 2019).

An alternative, less-considered class of models involves the accretion of intra-oceanic arc(s) and multiple plates (Fig. 3.2b). These models suggest one or more intra-oceanic arc system(s) formed outboard of Eurasia along an intra-oceanic subduction zone between the Izanagi plate and other oceanic plate(s), and these arcs were later accreted during the Early Cretaceous to mid-Cretaceous (Arkhipov et al., 2019; Malinovsky et al., 2008; Ueda and Miyashita, 2005; Utsunomiya et al., 2011). Models in this category imply that at least one additional oceanic arc-trench existed outboard and co-eval to the NE Asian continental arc-trench system. One model that included global seismic tomographic constraints implied a long-lived and very wide (>3000 km width in early Jurassic) oceanic plate named Pontus existed between Eurasia and the Izanagi plate since at least early Triassic to the Early Cretaceous (Van der Meer et al., 2012). Other models propose intra-oceanic arcs formed along the eastern boundary of narrower (3000-1000 km during Early Cretaceous) marginal seas that were located near the East Asia continental margin during late Jurassic to Early Cretaceous (Arkhipov et al., 2019; Malinovsky and Markevich, 2007; Ueda and Miyashita, 2005). These models suggest the intra-oceanic arcs were located sufficiently close to the Eurasian continental margin to receive continent-derived sediments based on geological constraints from Early Cretaceous accretionary terranes in Japan and Sikhote-Alin (Russian Far East).

3.2.2 North China Craton destruction

Cratons are old and stable regions of stable continental lithosphere that often have thick lithospheric roots to ~200 km (Boyd, 1989; Lee et al., 2011; Pearson, 1999). However, xenoliths show that lithospheric thicknesses along the eastern part of the North China Craton decreased from ~200 km in the Paleozoic to less than 80 km in the Cenozoic, implying lithospheric thinning and destruction of the lowermost NCC between these periods (Griffin et al., 1998; Menzies et al., 1993). Some suggest the initiation of NCC destruction occurred ~145 Ma based on a 145 to 120 Ma episode of adakitic magmatism that was likely generated from partial melting of the lower crust of the eastern NCC (Gu et al., 2013; Ma et al., 2016b; Wang et al., 2007). The ancient NCC sub-continental lithospheric mantle (SCLM) was then replaced by a juvenile one at 120 to 110 Ma, based on an abrupt change in mafic magmatism from isotopically-enriched and arc-like to an isotopically-depleted (i.e. juvenile) and intraplate-like signature (Dai et al., 2016; Liu et al., 2019; Ma et al., 2016a; Zheng et al., 2018).

Continuous westward subduction of Izanagi /paleo-Pacific plate (i.e Andean-type models in Fig. 3.2a) have been considered as the first-order geodynamic mechanism for NCC thinning, destruction, and development of juvenile lithospheric mantle (Liu et al., 2019; Wu et al., 2019; Zheng et al., 2018). A subduction origin for NCC thinning is supported by very high water contents (>1000 ppm) within lithospheric mantle-sourced basalts of Early Cretaceous age within the NCC (Xia et al., 2019; Xia et al., 2013). Within the context of Andean-style models (Fig. 3.2a), the following mechanisms have been proposed: (1) Back-arc extension in

NE China corresponding to the roll-back of the Izanagi plate during Early Cretaceous (Zheng and Dai, 2018; Zhu et al., 2012a; Zhu and Xu, 2019; Zhu et al., 2012b); (2) mantle wedge suction forces induced by the subduction of the paleo-Pacific plate (Niu, 2005); (3) convective erosion or asthenosphere upwelling within a big mantle wedge that sat between a stagnant slab and the overriding NCC lithosphere (He, 2014; Li and Wang, 2018; Liu et al., 2019); or, (4) a spreading ridge on the paleo-Pacific plate subducted beneath the NCC, triggered the destruction of the cratonic lithosphere (Ling et al., 2013). We do not find many models that relate possible intra-oceanic arc accretion along the NE Asian margin (Fig. 3.2b) to NCC destruction, which has motivated this paper, since the accretion of an intra-oceanic arc along East Asia would change the first-order plate tectonic boundary conditions and possibly introduce slab breakoff, subduction polarity changes, or other complexities. Furthermore, if an intra-oceanic subduction zone existed, it would preclude Izanagi subduction under the Eurasian continental margin (Fig. 3.2b). This would mean that NW Pacific basin plate tectonic models are much less insightful for interpreting eastern Eurasian continental magmatism.

3.3 Cretaceous igneous activity along the Eurasian margin, northeast Asia

3.3.1 General observations

We provide a broader picture of Eurasian continental margin magmatism during the Mesozoic by newly synthesizing the spatial-temporal distribution of igneous rocks from Wu et al. (2019) with newly compiled data (N= 616) for Japan, Korean and Sikhote-Alin (Belyansky et al., 2011; Cheong and Jo, 2017; Iida et al., 2015; Ito et al., 2010; Jahn et al., 2014; Jahn et al., 2015; Khanchuk et al., 2008; Kim et al., 2003; Kim et al., 2016; Koike and Tsutsumi, 2018; Kon et al., 2015; Kon and Takagi, 2012; Nakajima et al., 2004; Osozawa et al., 2019; Sagong et al., 2005; Sakashima et al., 2003; Sato et al., 2016; Skrzypek et al., 2016; Sueoka et al., 2018; Suzuki and Adachi, 1998; Takahashi et al., 2010; Takahashi et al., 2012; Takahashi et al., 2016; Tang et al., 2016; Tani et al., 2016; Watanabe et al., 2000; Wu et al., 2007; Wu et al., 2017b; Zhai et al., 2016; Zhang et al., 2012; Zhao et al., 2017). The compiled igneous ages are primarily U-Pb zircon ages, with smaller numbers of U-Pb monazite ages (N=59), U-Pb sphene ages (N=9), and Rb-Sr whole-rock ages (N= 14). The igneous rock ages and distributions are projected along a transect across NE Asia (Fig. 3.3a). Precise positioning of Japanese igneous rocks (labeled 'paleo-Japan' in Fig. 3.3a) is not critical to our analysis, but for added realism, these rocks were palinspastically-restored to the first-order by applying a ~500 km westward shift from their present location following the previous Japan Sea plate reconstructions (e.g. van Horne et al., 2017; Wu and Wu, 2019). We also created a statistics histogram with the complied U-Pb zircon ages of igneous rocks from NE China, Japan, Korea, and Sikhote-Alin separately, to reveal the spatiotemporal evolution and intensity of the late Jurassic to Cretaceous magmatic activity in NE Asia (Fig. 3.3b). We herein call the areas of Sikhote-Alin, Japan, and Korea as 'easternmost NE Asia'. We will contrast these areas to 'NE China', which includes the areas within the North China craton.

Mesozoic igneous activity along NE China migrated >1000 km inboard (i.e. westwards) during the Jurassic followed by a >1000 km migration outboard (i.e. eastward) during the

Figure 3. 3 Spatiotemporal distribution of igneous rock in NE China, Japan, Korea and south Sikhote-Alin (Russian far east) and their geochemistry

a) Spatiotemporal distribution of igneous rocks in NE Asia projected along the X-Y section in Fig. 1, modified from Wu et al. (2019) with newly compiled data for Japan, Korea, and Sikhote-Alin (See Appendix 1 for references). The location of igneous rocks in "Paleo-Japan" are shifted ~500 km west from their present location along the X-Y section to provide a first-order restoration of Japan Sea opening (~500 km is the average opening distance of the Japan islands during Japan Sea opening in the Miocene). We note the easternmost NE Asian area (Japan, Korea, and Sikhote-Alin) shows a 160-140 Ma magmatic quiescence that is supported by the detrital zircon age spectrum of sedimentary rocks within Japan and Korea (Lee et al., 2018; Pastor-Galán et al., 2021). b) Histogram of zircon U-Pb ages of late Jurassic to Cretaceous igneous rocks in NE Asia. At ~110 Ma, igneous activity moved eastwards from NE China towards easternmost NE Asia. c) Age vs CI chondrite value normalized La/Yb ratios plot highlighting adakitic signatures of some Cretaceous igneous rocks. d) K_2O vs SiO_2 plot of Early Cretaceous igneous rocks within easternmost NE Asia. Points are color-coded to show rocks with and without adakitic signatures.

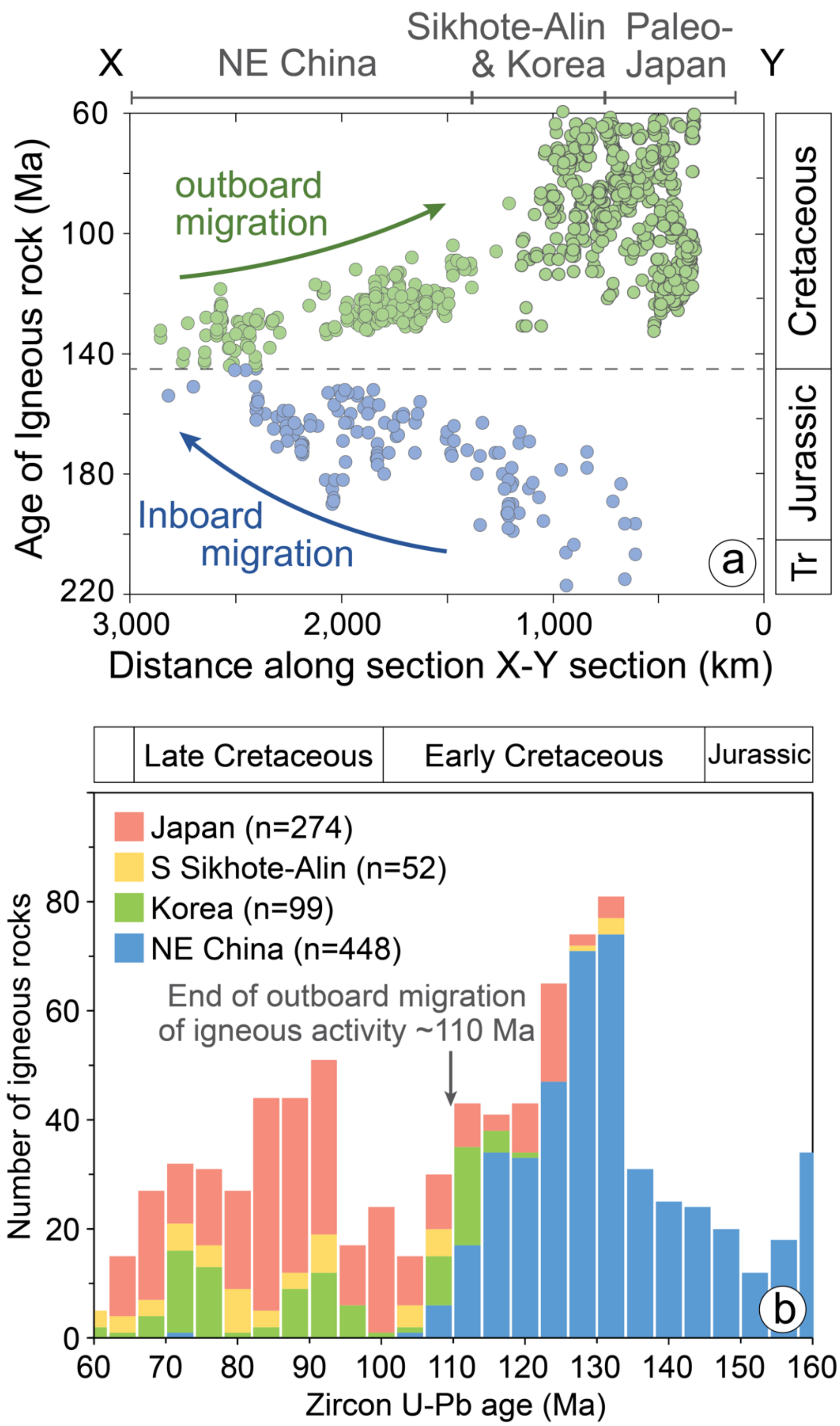
X
NE China
Sikhote-Alin & Korea
Paleo-Japan
Y
Age of Igneous rock (Ma)
outboard migration
Inboard migration
Cretaceous
Jurassic
Tr
a
Distance along section X-Y section (km)
Late Cretaceous
Early Cretaceous
Jurassic
Japan (n=274)
S Sikhote-Alin (n=52)
Korea (n=99)
NE China (n=448)
End of outboard migration of igneous activity ~110 Ma
Number of igneous rocks
b
Zircon U-Pb age (Ma)

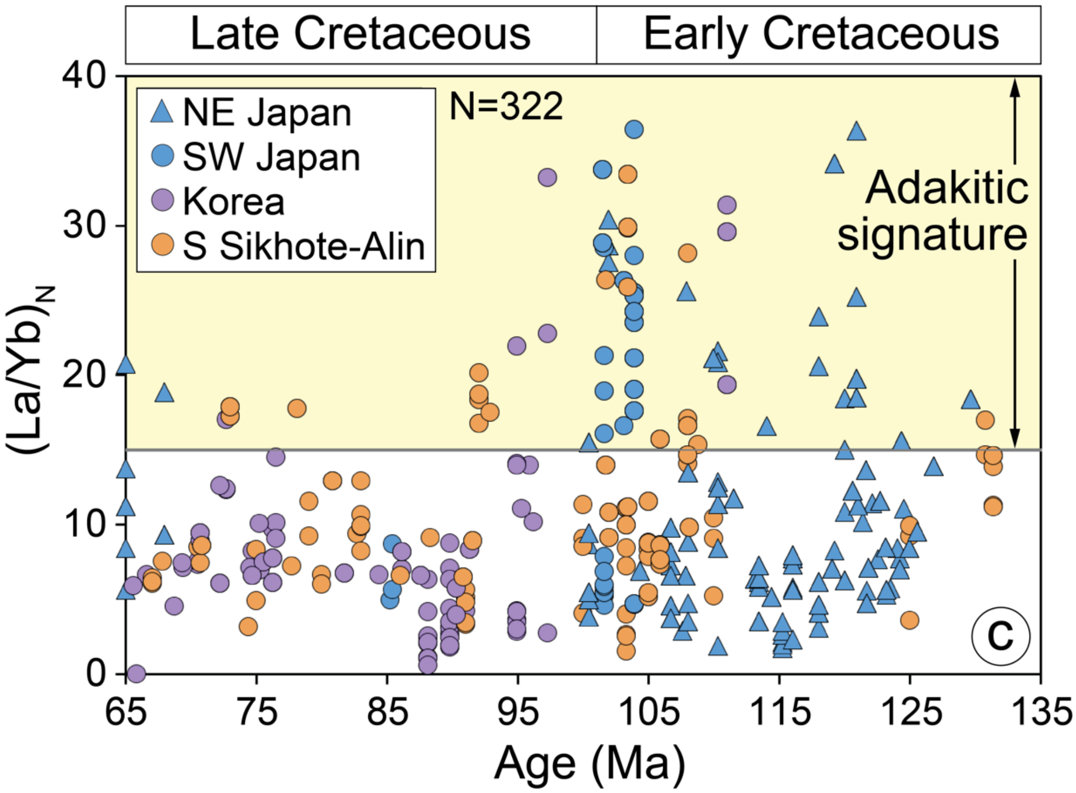
Late Cretaceous
Early Cretaceous
NE Japan
SW Japan
Korea
S Sikhote-Alin
N=322
Adakitic signature
c
(La/Yb)N
Age (Ma)

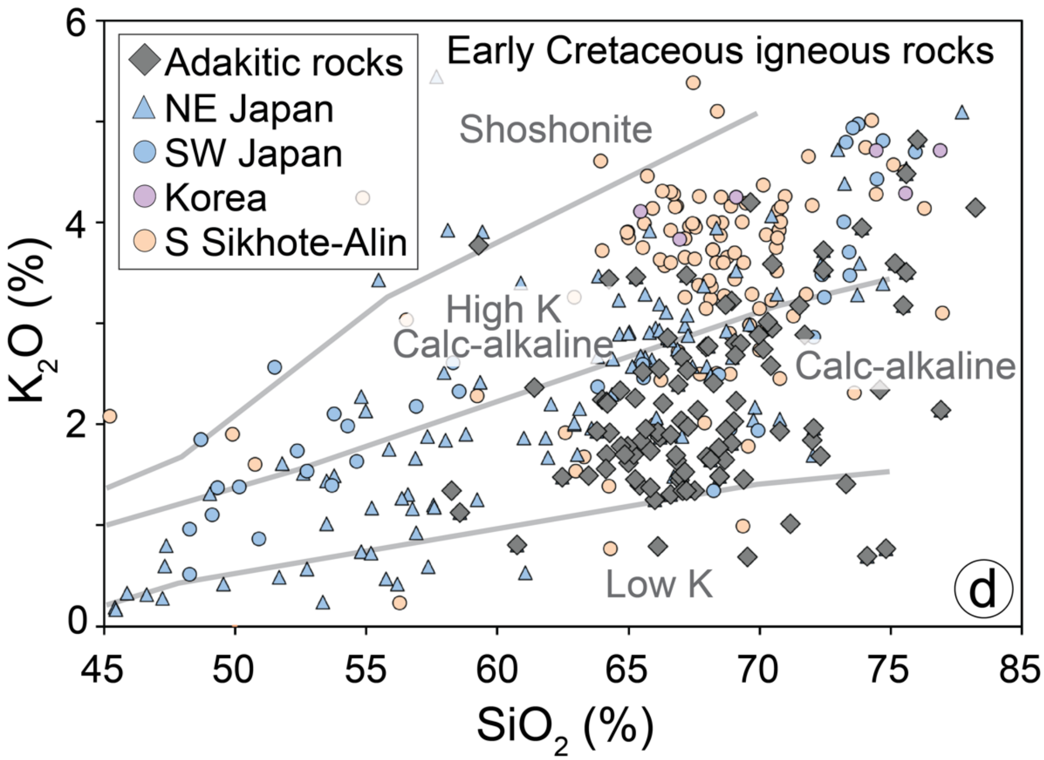
Adakitic rocks
NE Japan
SW Japan
Korea
S Sikhote-Alin
Early Cretaceous igneous rocks
Shoshonite
High K Calc-alkaline
Calc-alkaline
Low K
d
K2O (%)
SiO2 (%)

Early Cretaceous (Fig. 3.3a) (Liu et al., 2019; Wang et al., 2006; Wu et al., 2019). This was followed by a 132 to 120 Ma magmatic flare-up (Fig. 3.3b) (Liu et al., 2019; Wu et al., 2005; Zhang et al., 2014). We newly show that the NE China outboard migration of magmatism during the Early Cretaceous occurred co-eval to extensive magmatism along easternmost NE Asia (i.e. Sikhote-Alin, Japan, and Korea) (Fig. 3.3a, b). The outboard migration ended ~110 Ma when the majority of igneous activity moved eastward from NE China to easternmost NE Asia (Fig. 3.3b). Before the 160 to 140 Ma outboard migration, NE China magmatism was continuous, whereas the easternmost NE Asian margin shows a clear 160 to 140 Ma gap in igneous activity (Fig. 3.3a). The 160 to 140 Ma magmatic quiescence has been noted in previous studies (Zhai et al., 2016), and is further supported by a hiatus in U-Pb detrital zircon ages in Japan and Korea sedimentary basins that confirm very limited igneous activity during this time (Lee et al., 2018; Pastor-Galán et al., 2021). After the 160 to 140 Ma magmatic quiescence, Early Cretaceous magmatism within easternmost NE Asia shows dominant high-K calc-alkaline and calc-alkaline signatures (Fig. 3.3d). Some of the Early Cretaceous-aged magmatism in NE Asia show typical arc-related chemical signatures (i.e. derived from slab-fluid saturated mantle source with crustal contamination) (Chen et al., 2004; Jahn et al., 2015; Osozawa et al., 2019). In contrast, other igneous rocks with adakitic signatures formed within both NE China and easternmost NE Asia (Fig. 3.3c, 3.4a). These adakites can be sub-divided into two adakite suites that show contrasting isotopic signatures (e.g. Fig. 3.4d, e), and are discussed in more detail in the following section.

Figure 3. 4 Early Cretaceous adakitic rocks in NE Asia.

a) Locations of adakitic rocks in Sikhote-Alin, Japan and NE China. b) CI chondrite value normalized La vs La/Yb diagram that distinguishes adakites and typical arc magmatic rock. c) K_2O vs Na_2O plot showing adakitic rocks in NE China are more enriched in K_2O than those in Japan and Sikhote-Alin. d) Nd-Sr isotope diagram for Early Cretaceous-aged adakitic rocks in NE China, Japan, and Sikhote-Alin. The plot differentiates two contrasting adakitic suites within NE Asia that are located within NE China, and within Japan and Sikhote-Alin. e) Igneous rock age vs whole-rock Nd isotope diagram. The 132 to 99 Ma adakites in Japan and Sikhote-Alin are more depleted in Nd isotopic composition compared to 143 to 120 Ma adakites in NE China. See Appendix B for the database and references for early Cretaceous NE Aisa adakitic rocks

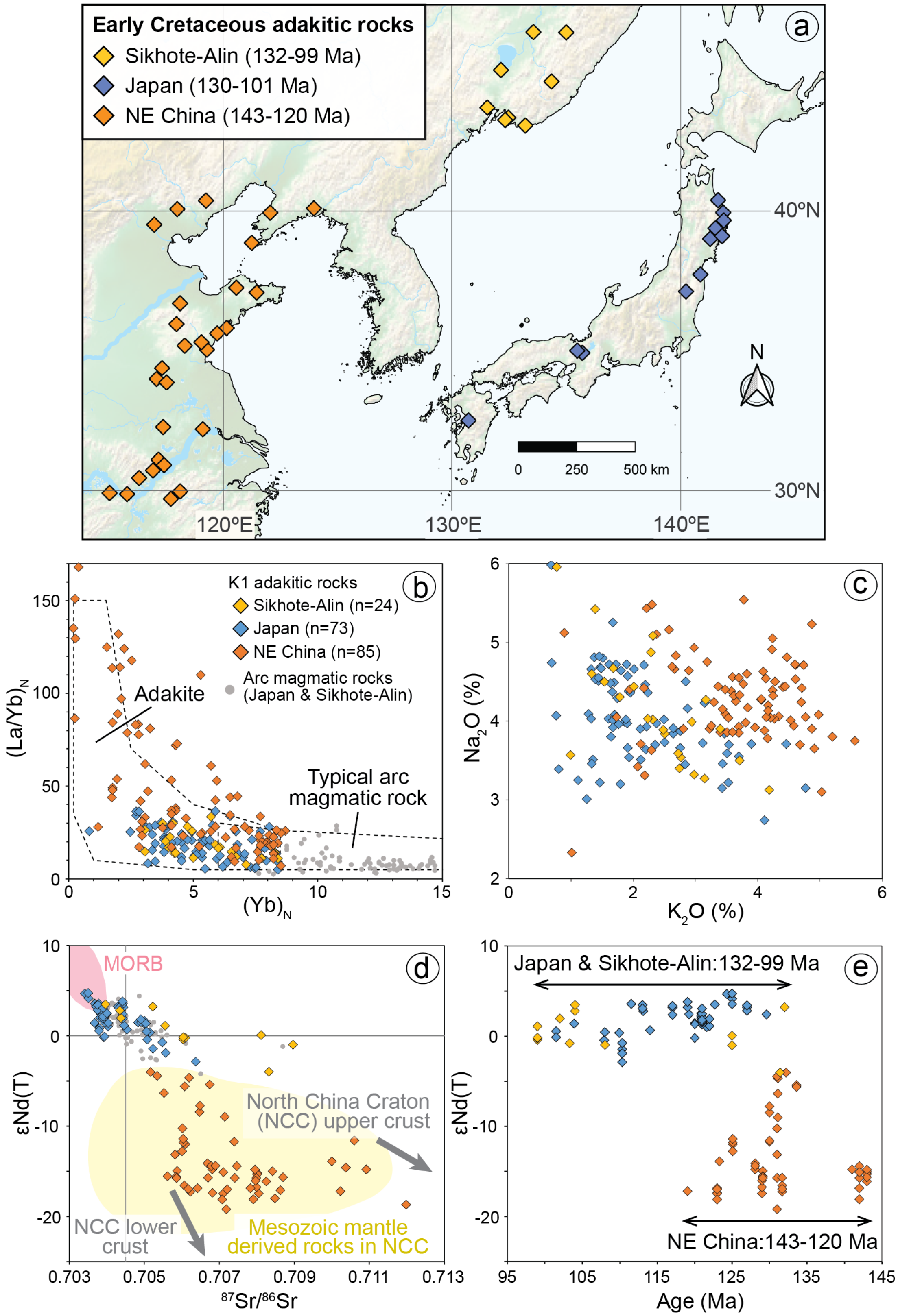

Early Cretaceous adakitic rocks
Sikhote-Alin (132-99 Ma)
Japan (130-101 Ma)
NE China (143-120 Ma)
a
40ºN
30ºN
120ºE
130ºE
140ºE
N
0
250
500 km
b
K1 adakitic rocks
Sikhote-Alin (n=24)
Japan (n=73)
NE China (n=85)
Arc magmatic rocks
(Japan & Sikhote-Alin)
Adakite
Typical arc
magmatic rock
(La/Yb)N
(Yb)N
c
Na2O (%)
K2O (%)
d
MORB
North China Craton
(NCC) upper crust
NCC lower
crust
Mesozoic mantle
derived rocks in NCC
εNd(T)
87Sr/86Sr
e
Japan & Sikhote-Alin:132-99 Ma
NE China:143-120 Ma
εNd(T)
Age (Ma)

3.3.2 Adakitic magmatism

Adakitic rocks are intermediate to felsic igneous rocks that are geochemically defined by high Sr/Y and La/Yb ratios, low Y and Yb (Defant and Drummond, 1990) and thought to be generated by partial melting of garnet-bearing basaltic rock or garnet-involved fractional crystallization. Previous studies have interpreted adakite petrogenesis to be meta-basic rock melting in a subduction zone (i.e. partial melting of a subducted oceanic lithosphere), melting of thickened, mafic-composition lower crust at depths greater than 10-12 kbar, or fractional crystallization of amphibole/garnet from a basaltic magma at about 5-6 kbar (Castillo, 2012; Moyen, 2009). Since this is the case, the interpretation that adakites signify melted oceanic crust (i.e. slabs) has been viewed with increasing caution (e.g. Castillo, 2012; Moyen, 2009; Ribeiro et al., 2016). Nonetheless, some adakites could be generated during specific tectonic events, including arc collision, ridge subduction, and slab break-off, if the ocean crust is melting within the garnet stability field (Castillo, 2012). Here we discuss the petrogenesis of adakitic rocks along the Eurasian margin in detail, since at least two adakitic suites have been previously identified and shown to have possible plate tectonic significance (e.g. Gu et al., 2013; Wu et al., 2017).

A group of easternmost NE Asian igneous rocks (i.e. Japan and Sikhote-Alin, Russian Far East) with ages 132 to 99 Ma show adakitic signatures (purple and yellow diamonds in Fig. 3.4) (Imaoka et al., 2014; Kamei, 2004; Kamei and Takagi, 2003; Osozawa et al., 2019; Tsuchiya and Kanisawa, 1994; Tsuchiya et al., 2007; Tsuchiya et al., 2012; Wu et al., 2017b). A second suite of 143 to 120 Ma adakitic rocks are widespread in NE China, far to the west of the 132 to 99 Ma easternmost NE Asian adakites (orange diamonds in Fig. 3.4) (Gu et al., 2013; Liu et al., 2010; Ma et al., 2016b; Wang et al., 2007; Xu et al., 2006). The two Early Cretaceous adakitic magmatism episodes show contrasting geochemistry (Fig. 3.4): the 132 to 99 Ma adakitic rocks in Japan and Sikhote-Alin show lower potassium concentrations and more depleted Nd-Sr isotopic compositions (Average K_2O= 2.9 wt.% ; εNd(t)= -4.0 to 4.7; $(^{87}Sr/^{86}Sr)_0$= 0.7034 to 0.7090), compared to the 145 to 120 Ma adakitic rocks in NE China, which have high potassium and enriched isotopic composition (Average K_2O = 3.8 wt.% ; εNd(t)= -20 to -4; $(^{87}Sr/^{86}Sr)_0$= 0.7052 to 0.7120) (Fig. 3.4c-e).

The K-rich adakitic rocks in NE China with ages 143 to 120 Ma are generally thought to be derived from the partial melting of the lower crust of the NCC during the destruction of the craton lithosphere (Gu et al., 2013; Liu et al., 2012; Ma et al., 2016b). In contrast, the origin of the 132 to 99 Ma adakites in easternmost NE Asia (Japan and Sikhote-Alin) is less clear. Some adakites can be explained by differentiation within the garnet stability field (Macpherson et al., 2006) where rocks with typical adakitic signatures (high La/Yb, Sr/Y) evolve from a basaltic precursor generated from a fluid-modified mantle. In such a case, the adakites would have a strong positive correlation between SiO_2 and the adakitic signatures, and lower Na_2O, higher K_2O, and similar or more enriched Nd isotopic composition than the basaltic precursor. The easternmost NE Asia 132 to 99 Ma adakitic rocks, however, have more depleted Nd isotopic compositions and higher Na_2O than the contemporaneous mafic rocks (Tsuchiya and Kanisawa, 1994; Wu et al., 2017b). Moreover, there is no significant correlation between the SiO_2 and adakitic signature of the rocks (Wu et al., 2017b). Thus, it seems the 132 to 99 Ma adakitic rocks were probably not differentiated from mantle-derived mafic magmas.

The easternmost NE Asia overriding plate had an insufficient crustal thickness to produce depths and pressures to stabilize a significant amount of garnet in the lower crust; therefore, lower crustal melting is also an unlikely mechanism to explain the adakites. The present Moho depth in the NE Asian margin is 30 ~ 35 km in north Japan and 30 ~ 40 km in Sikhote-Alin, (Matsubara et al., 2017; Nevstruyev and Kozlova, 2018). During the Early Cretaceous times, the accretionary complex would have been younger and thinner than the present (30 to 40 km). This thin, juvenile crust would be inadequate to generate adakitic magma through its garnet stability field, even if the lower crust was partially melted (Tsuchiya et al., 2007). As well, previous studies have noted the trace element composition of the adakitic rocks shows a fit when modeled as a mixed source by MORB and minor subduction sediments with mantle contamination (Tsuchiya et al., 2007; Tsuchiya et al., 2005). Thus, we prefer to interpret the source region of the adakites to be a subducting oceanic slab. This interpretation also fits with their spatial extent along a former subduction zone at the outer Eurasian continental margin (Fig. 3.4a). We will further discuss the thermal mechanism that induced oceanic slab melting resulting in the 132 to 99 Ma adakitic magmatism in easternmost NE Asia (see section 4.4).

3.4 Evidence for Early Cretaceous intra-oceanic arc accretion along the NE Asian continental margin from sedimentary records and paleomagnetism

3.4.1 SW Japan

In SW Japan, subduction-accretion processes during the Cretaceous are mainly recorded within the Sambagawa metamorphic belt and the Northern Shimanto belt (Fig. 3.5) (Aoki et al., 2019; Taira, 1988). The Sambagawa belt is an early to middle Cretaceous accretionary complex that experienced metamorphic conditions up to eclogite facies (Aoki et al., 2009; Okamoto et al., 2000). According to Aoki et al. (2019), three eclogite-facies units with different accretion ages have been identified in the Sambagawa belt (Fig. 3.5): The Besshi unit with accretion ages of ~130 Ma (Okamoto et al., 2000; Okamoto et al., 2004), the Asemi-gawa unit with accretion ages 100 to 90 Ma (Aoki et al., 2019), and the Oboke unit that has protolith accreted after 95 to 90 Ma (Endo et al., 2018).

Strong deformation of mafic metamorphic rocks like those in the Sambagawa belt can obliterate the original mineralogy and texture of the rocks, creating challenges for determining their petrogenesis. To resolve the difficulty, previous studies have looked into the age and geochemistry of the core and rim domains of zircons in the Besshi unit. Aoki and others considered the 120 to 90 Ma zircon rim domain with metamorphic origin as a record of strong metamorphism, and the 200 to 180 Ma zircon core domain were from an igneous rock-origin protolith that showed oceanic arc-like zircon geochemistry (Aoki et al., 2020a; Aoki et al., 2020b). The protolith of the Besshi unit accreted to the margin around 130-120 Ma,

Figure 3. 5 Cretaceous geological framework of SW Japan.

(a) Surface geological map of SW Japan. (b) Geological units in the Sambagawa metamorphic belt. (c) Geological units in the North Shimanto belt. The Besshi unit in the Sambagawa belt is interpreted as an ocean island arc that accreted to the continental margin at ~130 Ma.

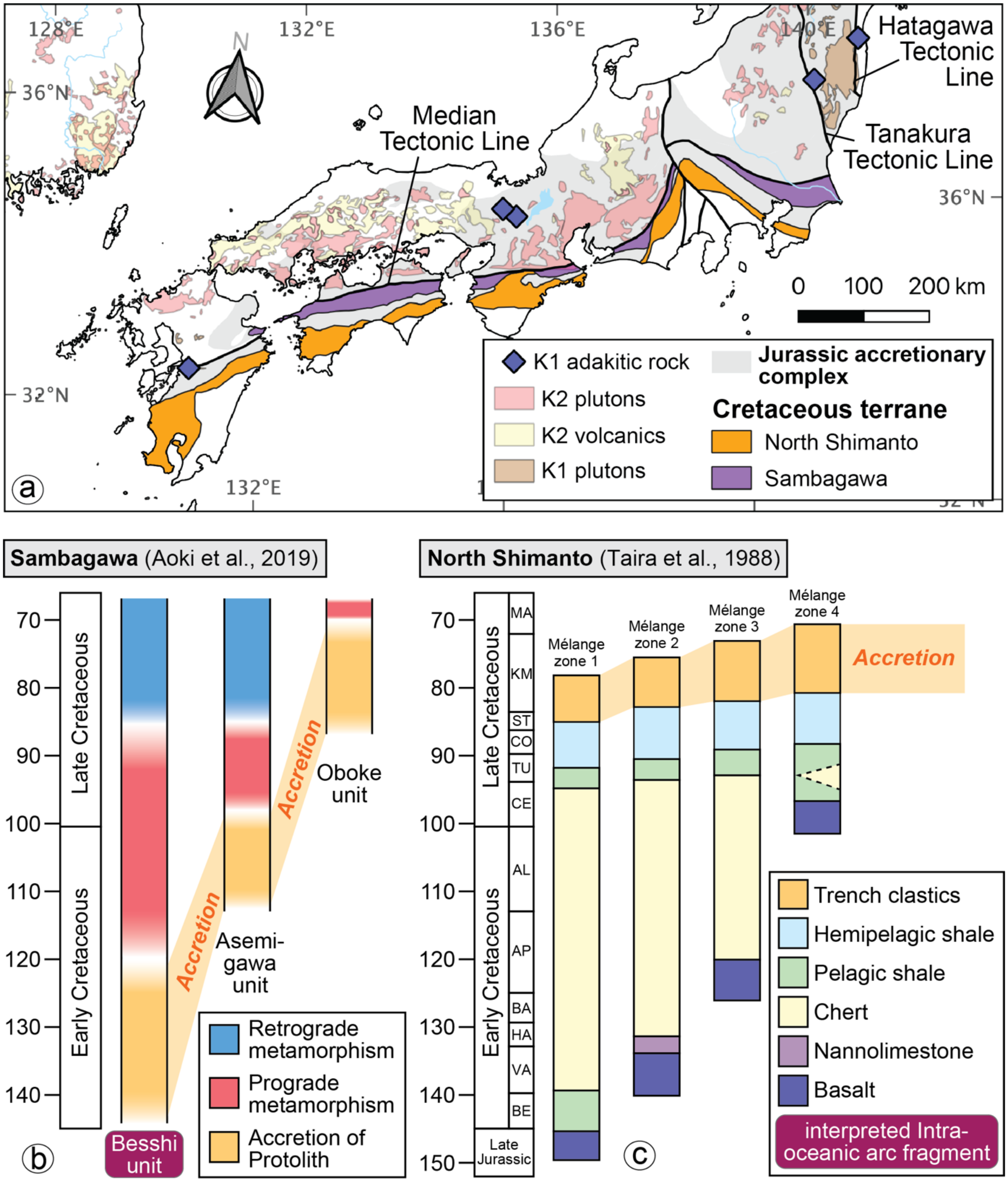

128°E
132°E
136°E
140°E
36°N
32°N
N
Median Tectonic Line
Hatagawa Tectonic Line
Tanakura Tectonic Line
0 100 200 km
K1 adakitic rock
K2 plutons
K2 volcanics
K1 plutons
Jurassic accretionary complex
Cretaceous terrane
North Shimanto
Sambagawa
a
Sambagawa (Aoki et al., 2019)
Late Cretaceous
Early Cretaceous
Besshi unit
Asemi-gawa unit
Oboke unit
Accretion
Retrograde metamorphism
Prograde metamorphism
Accretion of Protolith
b
North Shimanto (Taira et al., 1988)
MA
KM
ST
CO
TU
CE
AL
AP
BA
HA
VA
BE
Late Jurassic
Mélange zone 1
Mélange zone 2
Mélange zone 3
Mélange zone 4
Accretion
Trench clastics
Hemipelagic shale
Pelagic shale
Chert
Nannolimestone
Basalt
interpreted Intra-oceanic arc fragment
c

constrained by 120 to 110 Ma peak metamorphic U-Pb ages in the zircon rim domain, and by late Jurassic to Early Cretaceous protolith ages determined by fossil ages and 148 to 134 Ma U-Pb ages from the core domain of zircons in quartz-rich rocks (Isozaki and Itaya, 1990; Okamoto et al., 2004).

The eclogites and garnet amphibolites of the Besshi unit may be the lower crustal portion of an oceanic island arc, based on evidence for crystallization under oxygen-enriched and hydrous conditions (Utsunomiya et al., 2011). In contrast, the Asemi-gawa and Oboke units show MORB-origin chemical compositions (Fig. 3.6) (Endo et al., 2018; Nozaki et al., 2006) and have been interpreted to be fragments of typical subducted oceanic crust that accreted at ~100 to 80 Ma (Fig. 3.5b). Therefore, the geology of the Sambagawa belt in SW Japan shows an ocean island arc accretion along SW Japan at ~130 Ma, followed by accretion of typical oceanic crustal fragments at 100 to 90 Ma.

3.4.2 NE Japan

The Cretaceous accretionary complex of the Japan arc-trench system extends northwards into western Hokkaido, and includes the Idonnappu, Sorachi-Yenzo, and Rebun-Kabato belts (Fig. 3.7) (Ueda, 2016). The Oku-Niikappu complex within the Idonnappu belt is a mid-Cretaceous accretionary complex (Fig. 3.7) (Kiyokawa, 1992). Here, late Jurassic volcanic rocks show island arc geochemical characteristics (Fig. 3.6b) (Ueda and Miyashita, 2005). These are interpreted to be a fragment of an island arc that accreted during the mid-Cretaceous

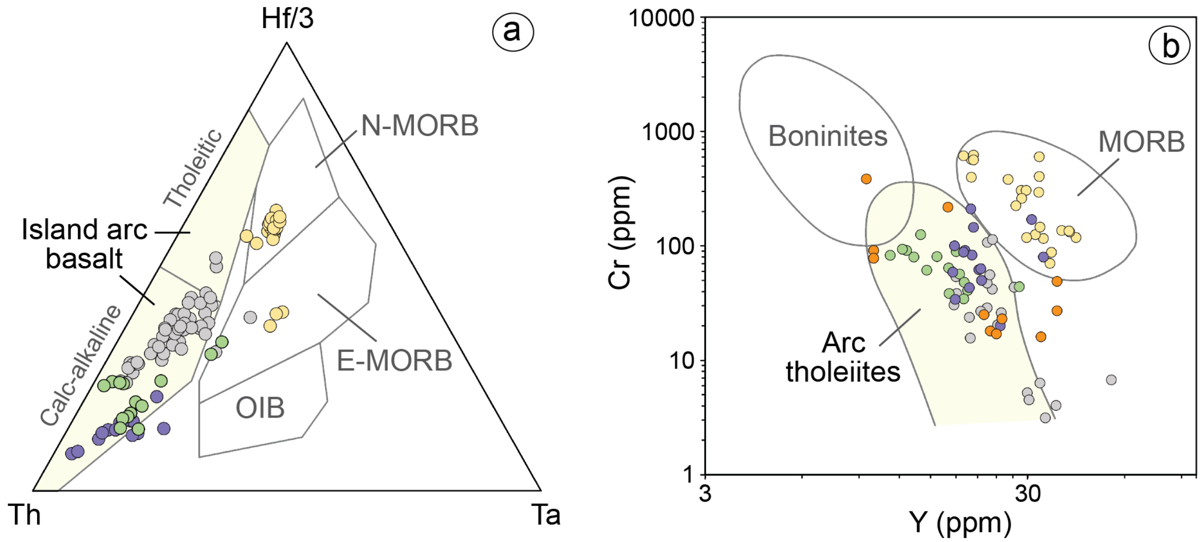

(c) **Mafic rocks within Early Cretaceous terranes**

Geological unit	Accretion time	Geochemistry	Reference
Kiselevka-Manoma	~110 Ma	Island arc	Arkhipov et al. (2019)
Kema	~110 Ma	Island arc	Malinovsky et al. (2008)
Rebun-Kabato	~110 Ma	Island arc	Simanenko et al. (2011)
Oku-Niikappu complex / Idonnappu	~100 Ma	Island arc	Ueda et al. (2005)
Besshi unit / Sambagawa	~130 Ma	Island arc (zircon chem.)	Aoki et al. (2019, 2020)
Asemi-gawa unit / Sambagawa	~90 Ma	MORB	Nozaki et al. (2006)

Figure 3. 6 Mafic rocks with arc affinities in Early Cretaceous-aged accretionary terranes along NE Asia, and their accretion times.

(a) Whole-rock Hf-Th-Ta ternary diagram (Wood, 1980). (b) Whole-rock Y vs Cr diagram (Pearce et al., 1981). (c) shows a legend for the color-coded data points in Fig. 3.6a, b and timing of intra-oceanic arc accretion. The island arc origin of the eclogites from the Besshi unit in the Sambagawa belt was determined by zircon geochemistry (Aoki et al., 2020a; Aoki et al., 2020b). Accretion time for the Besshi unit is constrained by peak metamorphic U-Pb ages and protolith U-Pb ages from zircon rim and core domains, respectively. For the rest of the geological units, the accretion time was constrained using the age of continental-derived clastics that were identified as trench-filled sediments overlying the pelagic sediments (Arkhipov et al., 2019; Ueda and Miyashita, 2005). In general, the ocean island arc terranes accreted to the Eurasian continental margin along NE Asia during the Early Cretaceous 130 to 100 Ma.

(Ueda and Miyashita, 2005). Contemporaneous volcanic breccia of Hachimoriyama Tuff Member in the adjacent Sorachi-Yenzo belt also shows arc-related geochemical signatures (Takashima et al., 2002, 2006), further supporting an island arc origin. The mid-Cretaceous (~100 Ma) accretion time of the island arc was constrained by ages of the siliciclastic trench-filled turbidites that sit stratigraphically above the island-arc volcanic unit (Ueda and Miyashita, 2005). The subduction polarity of the island arc system was probably west-dipping, since the accretionary complexes in the Idonnappu belt display an overall eastwards-younging arrangement (Fig. 3.7) (Ueda, 2001). In summary, NE Japan ophiolite sequences are incompatible with Andean-style subduction models (Fig. 3.2a), and instead, show a record of island arc accretion during mid-Cretaceous times around ~100 Ma that is more consistent with intra-oceanic subduction models (Fig. 3.2b).

3.4.3 Sikhote-Alin (Russian Far East)

In the southernmost of the Russian Far East, the Sikhote-Alin orogenic belt consists of several Mesozoic-aged, accreted oceanic terranes, with the last stage of amalgamation involving accretion of an Early Cretaceous island arc during the mid-Cretaceous (i.e. late Albian) (Khanchuk et al., 2016). The island arc system, sometimes known as the Moneron-Samarga island arc, includes the Early Cretaceous Kema and Kesilevka-Manoma terranes in the Sikhote-Alin (Fig. 3.7); these are considered to be the back-arc basin and accretionary prism, respectively (Malinovsky, 2010; Malinovsky et al., 2006; Simanenko et al., 2011). Some also considered the Rebun-Kabato belt as the volcanic arc of the Moneron-Samarga island arc

Figure 3. 7 Cretaceous geological framework of NE Japan, Sakhalin, and Sikhote-Alin (Russian Far East).

(a) Surface geological map. (b) Geological units in Sikhote-Alin & Sakhalin. (c) Geological units in Hokkaido, NE Japan. In general, the geology of these areas shows accretion of oceanic arcs between ~115 to 100 Ma.

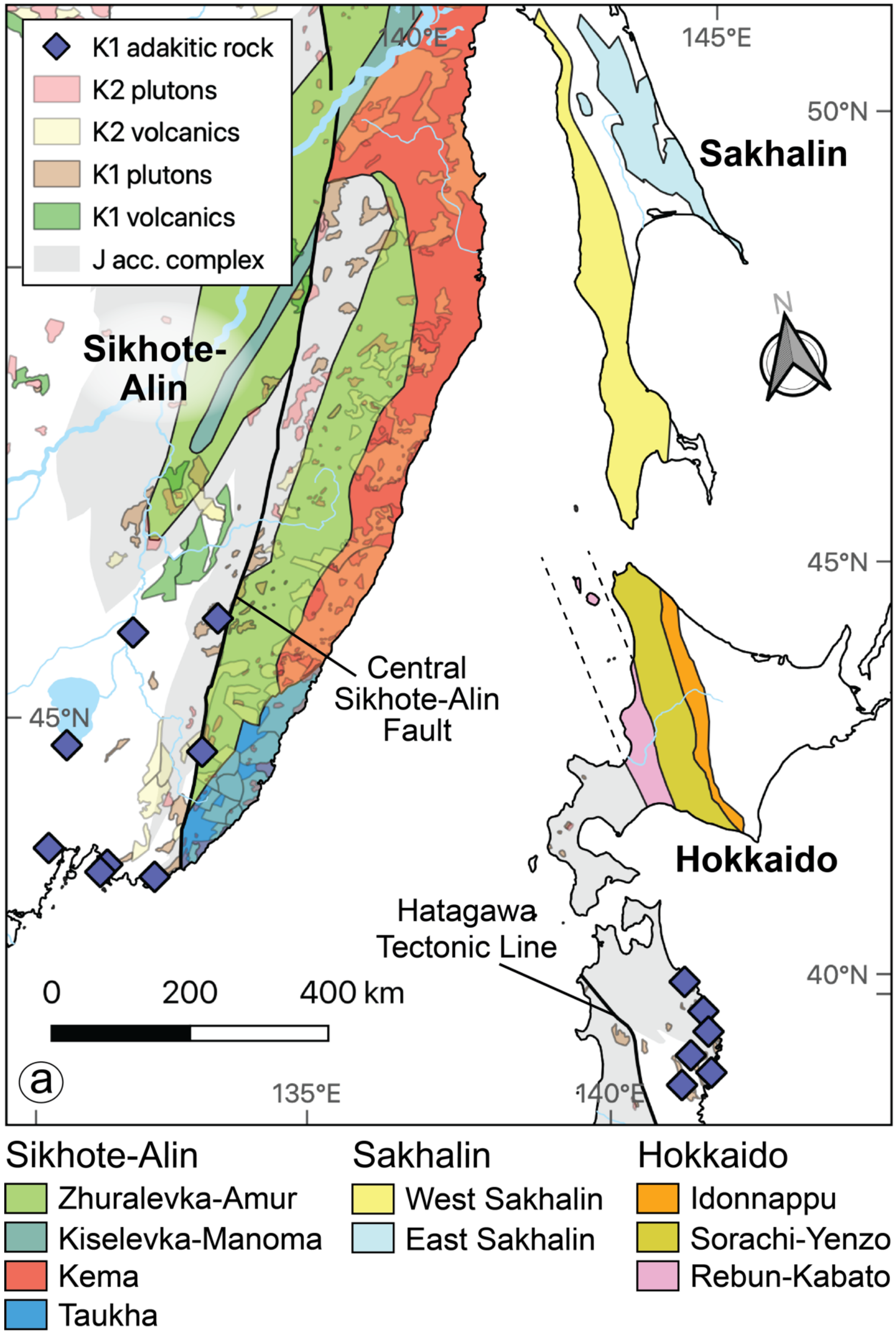
K1 adakitic rock
K2 plutons
K2 volcanics
K1 plutons
K1 volcanics
J acc. complex
140°E
145°E
50°N
Sakhalin
Sikhote-
Alin
N
45°N
Central
Sikhote-Alin
Fault
45°N
Hokkaido
Hatagawa
Tectonic Line
40°N
0
200
400 km
a
135°E
140°E
Sikhote-Alin
Zhuralevka-Amur
Kiselevka-Manoma
Kema
Taukha
Sakhalin
West Sakhalin
East Sakhalin
Hokkaido
Idonnappu
Sorachi-Yenzo
Rebun-Kabato

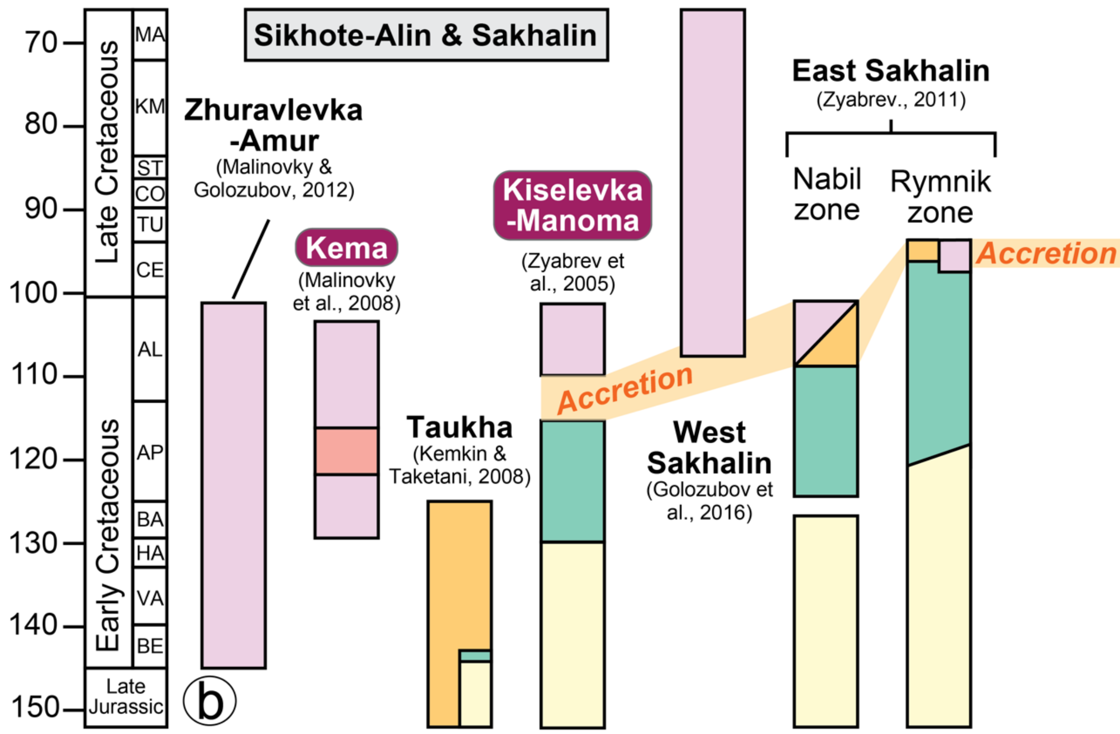

Sikhote-Alin & Sakhalin
Zhuravlevka -Amur
(Malinovky & Golozubov, 2012)
Kema
(Malinovky et al., 2008)
Taukha
(Kemkin & Taketani, 2008)
Kiselevka -Manoma
(Zyabrev et al., 2005)
West Sakhalin
(Golozubov et al., 2016)
East Sakhalin
(Zyabrev., 2011)
Nabil zone
Rymnik zone
Accretion
Accretion
Late Cretaceous
Early Cretaceous
Late Jurassic
MA
KM
ST
CO
TU
CE
AL
AP
BA
HA
VA
BE
70
80
90
100
110
120
130
140
150
b

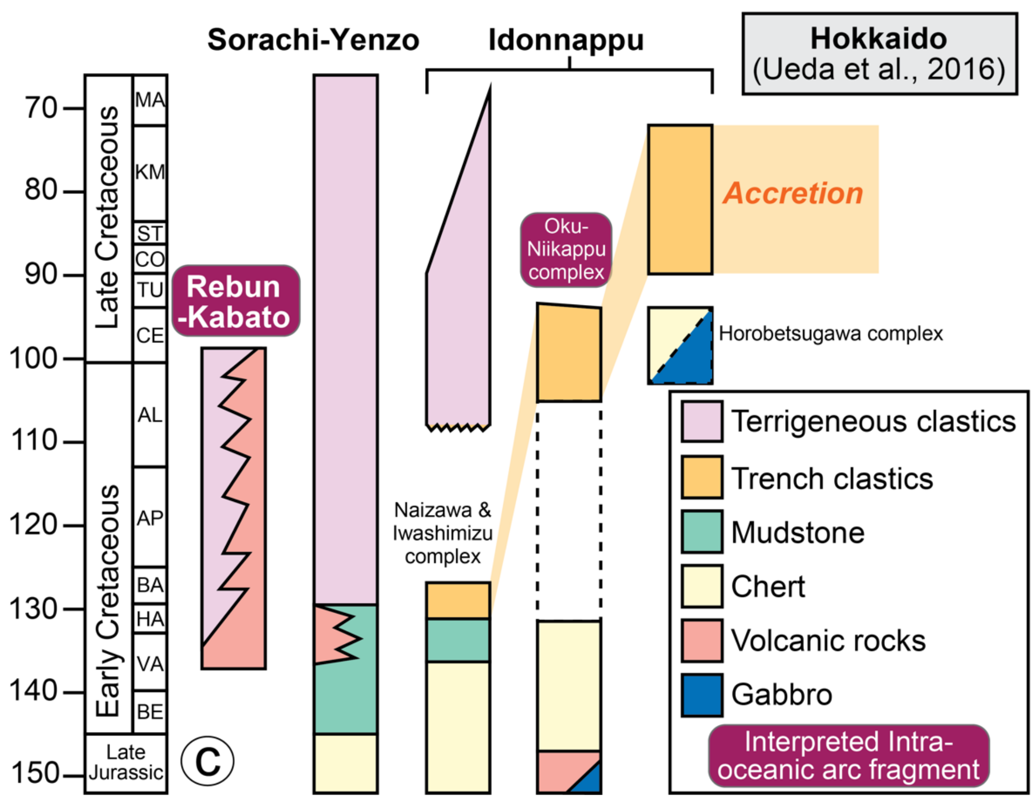

Sorachi-Yenzo
Idonnappu
Hokkaido
(Ueda et al., 2016)
Rebun -Kabato
Oku-Niikappu complex
Naizawa & Iwashimizu complex
Horobetsugawa complex
Accretion
Terrigeneous clastics
Trench clastics
Mudstone
Chert
Volcanic rocks
Gabbro
Interpreted Intra-oceanic arc fragment
Late Cretaceous
Early Cretaceous
Late Jurassic
MA
KM
ST
CO
TU
CE
AL
AP
BA
HA
VA
BE
70
80
90
100
110
120
130
140
150
c

(Simanenko et al., 2011), while others suggested the belt was the arc volcanics erupted on the accretionary complex of continental margin (Kiminami, 1986; Taira et al., 2016). Other models suggest the Kiselevka-Manoma and Kema terranes represent different oceanic arc systems (Arkhipov et al., 2019). Regardless, the island arc origin of these terranes is supported by Early Cretaceous volcanic rock chemical compositions that show arc-related signatures (Fig. 3.6a) (Arkhipov et al., 2019; Malinovsky et al., 2008; Simanenko et al., 2011). It is considered that the Kiselevka-Manoma terranes accreted during the late Aptian to middle Albian (~110 Ma) based on the age of trench fill sediments within the terrane (Fig. 3.7b) (Zyabrev, 2011). Clastic rocks in the Kema terrane have heterogeneous sources including volcanic island arc and minor continental crust material, which suggest a back-arc basin setting for the terrane (Malinovsky and Markevich, 2007). Importantly, this implies the Kema island arc was not very far offshore from the continental margin, perhaps within 1000 km of the continent, consistent with typical turbidite fan transport distances (Shanmugam, 2016). In summary, Sikhote-Alin geology is incompatible with straightforward Andean-style subduction (Fig. 3.2b) and instead requires accretion of active island arcs (Kiselevka-Manoma and Kema terranes) to eastern Eurasia around the mid-Cretaceous ~100 Ma or slightly earlier. There is some evidence that the island arcs were not far removed from the eastern Eurasian margin (e.g. intra-oceanic model shown in Fig. 3.2b) based on continent-derived clastics within the Kema terrane.

3.4.4 Timing of intra-oceanic arc accretions and potential link to adakitic magmatism

The Kiselevka-Manoma and Oku-Niikappu island arcs likely accreted at ~110 Ma and ~100 Ma, respectively, based on the ages of continental-derived clastics identified as trench fill sediments that overlie pelagic sediments within the accretionary units (Matsuda and Isozaki, 1991; Arkhipov et al., 2019; Ueda and Miyashita, 2005). The accretion time for island arc-origin Besshi unit in the Sambagawa belt is 130 to 120 Ma, constrained by peak metamorphic U-Pb ages and protolith U-Pb ages from zircon rims and cores, respectively (Okamoto et al., 2004). Thus, Early Cretaceous geological records in Japan and Sikhote-Alin area reveal a relatively widespread accretion of late Jurassic to Early Cretaceous-aged intra-oceanic arcs to the East Asian continental margin within the period 130 to100 Ma (Fig. 3.5).

As previously mentioned, there are multiple sources of Early Cretaceous igneous activity along the NE Asian margin including 132 to 99 Ma adakitic magmatism derived from subducting oceanic slab (Fig. 3.3c-d and Fig. 3.4). This adakitic magmatism has been formerly linked to the ridge-trench intersection of a mid-ocean with the continental margin (Tsuchiya and Kanisawa, 1994), or slab rollback after flat subduction (Yan et al., 2015). Indeed, oceanic slab-derived adakitic melt can be generated during subduction rollback (Kincaid and Griffiths, 2003). However, considering the 140 to110 Ma period of slab rollback does not precisely overlap with the 132 to 99 Ma adakitic magmatism at easternmost NE Asia (event 1 and 5 in Fig. 3.5), some of the younger adakites (<110 Ma) are unlikely to be generated by slab rollback. We also do not prefer a scenario where the 132 to 99 Ma adakites were generated from the ridge-trench intersection (Osozawa et al., 2019; Tsuchiya and

Kanisawa, 1994). A previous study indicated the subducting oceanic crustal ages in the Hokkaido area during the Jurassic to Early Cretaceous was 150 to 200 Myrs old (Ueda and Miyashita, 2005). These very old ages seem to exclude the possibility of an active mid-ocean ridge offshore of the East Asian margin during the Early Cretaceous, since an active ridge near the trench would generate a much younger oceanic crust.

Instead, we observe that the 132 to 99 Ma adakitic magmatism was relatively coeval with the 130 to 100 Ma intra-oceanic arc accretion (Event 5 in Fig. 3.8). We therefore link the 132 to 99 Ma adakites to slab melting induced by enhanced mantle flow within the wedge, under a tectonic setting that includes both intra-oceanic arc accretion and slab rollback in the Early Cretaceous. Adakites have been found in other arc accretion/collision settings in Tibet, Philippine, and the Solomon Islands (Gao et al., 2007; König et al., 2007; Sajona et al., 1996) and have been linked to a sinking oceanic slab after it was fully consumed following arc accretion. Although the detailed mantle thermal evolution under an arc accretion setting has not been fully explored, some suggest the detachment of a sinking slab may lead to partial melting of the slab surface (Gao et al., 2007).

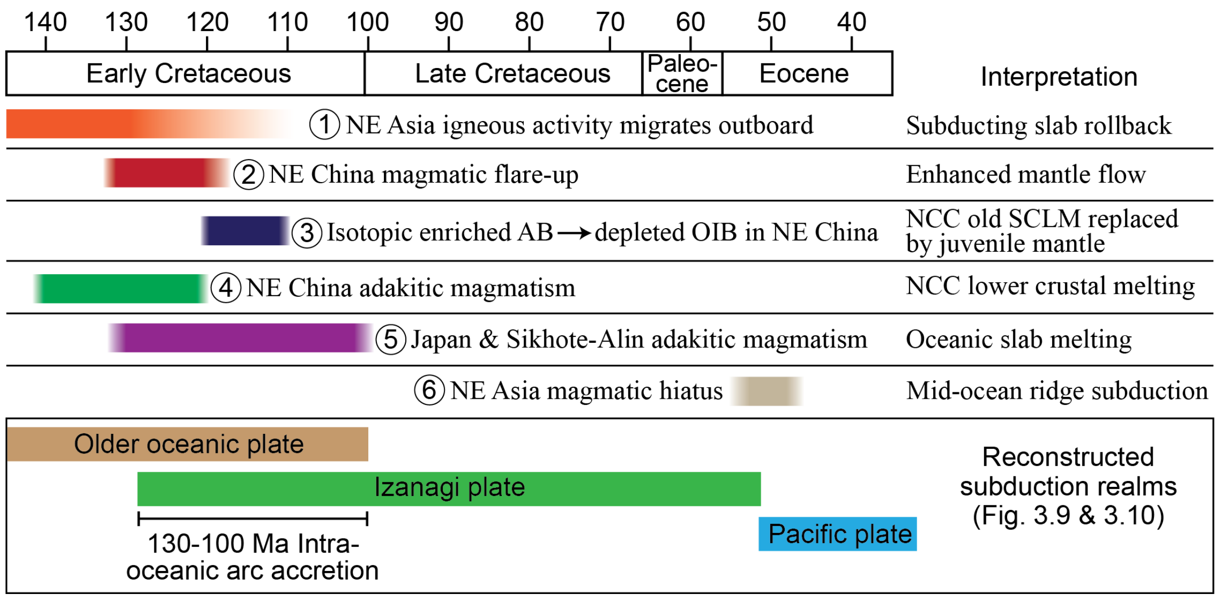

Figure 3. 8 Cretaceous to early Cenozoic igneous activity and tectonics within the NE Asian active margin and reconstructed subduction realms from our reconstruction model.

See Figs. 3.9 and 3.10 for details in our model. AB: arc basalt, OIB: ocean island basalt (intra-plate basalt), NCC: North China craton, SCLM: sub-continental lithospheric mantle. References for the igneous events and tectonic interpretation: Event 1 (Jing et al., 2021; Wu et al., 2019; Zhang et al., 2014); see also Figs. 3a, b); Event 2 (Liu et al., 2019; Wu et al., 2005; Zhang et al., 2014)); Event 3 (Dai et al., 2016; Liu et al., 2019; Zheng et al., 2018)); Event 4 (Gu et al., 2013; Liu et al., 2010; Ma et al., 2016b; Wang et al., 2007; Xu et al., 2006); see also Fig. 4); Event 5 (Kamei, 2004; Kamei and Takagi, 2003; Osozawa et al., 2019; Tsuchiya and Kanisawa, 1994; Tsuchiya et al., 2007; Tsuchiya et al., 2012; Wu et al., 2017b); see also Fig. 4); Event 6 (Kimura et al., 2019; Wu and Wu, 2019).

3.5 Discussion

We synthesize an alternative, intra-oceanic subduction-style plate tectonic setting of the NE Asian margin that spans NE China, Japan, Korea, and southern Sikhote-Alin. We do not attempt to build a fully-kinematic plate tectonic reconstruction due to the considerable challenge of spatiotemporally restoring Eurasian continental deformation; thousands of kilometers of subducted oceanic plates; ancient intra-oceanic subduction zone positionings; and, plate kinematics without seafloor or paleomagnetic constraints. Instead, we reconstruct the NE Asian margin during three key time windows in the mid-Cretaceous (Fig. 3.9, 3.10), building from a composite of published models (described next). We then reconstruct the timing of possible intra-oceanic arc accretion events and their associated plate tectonics, taking an approach of implementing the most straightforward solution (i.e. Occam's razor). Finally, we discuss the implications of our newly synthesized plate tectonic setting against current models of North China craton destruction.

3.5.1 Plate tectonic reconstruction of the NE Asian margin during the Early Cretaceous: a synthesis

3.5.1.1 Restoring the Eurasian continental margin

Reconstructions of the NE Asia Eurasian continental margin are controversial, especially before the Japan Sea opening (Jolivet et al., 1994; Kim et al., 2007; Otofuji, 1996; Otsuki, 1990; Van Horne et al., 2017; Yamakita and Otoh, 2000). We close the Japan Sea and

Figure 3. 9 Plate tectonic reconstructions of NE Asia during the Cretaceous synthesized from this study.

Our NE Asia plate tectonic reconstruction for the time periods: a) 135 Ma, b) 115 Ma, and c) 95 Ma. The Eurasian margin was reconstructed by building a composite from various published studies (Kemkin, 2008; Wu et al., 2018; Yamakita and Otoh, 2000; Zhu et al., 2012). Following an approach to produce the most straightforward reconstruction for the oceanic realm based on our synthesis, we show a single, curved intra-oceanic arc-trench system between a marginal sea plate and the Izanagi plate. The oceanic arc diachronouslly accreted to Eurasia between 130 and 100 Ma. However, more complex reconstructions are possible that could include multiple intra-oceanic arcs and oceanic plates. Regardless, it is important to note the 130 to 100 Ma arc accretion timings along NE Asia and their overlap with the outboard adakites (purple and yellow diamonds), which could have formed from ocean slab melting. CSF: Central Sikhote-Alin fault; HTL: Hatagawa tectonic line; KFZ: Kurosegawa fault zone; MTL: Median tectonic line; TTL: Tanakura tectonic line.

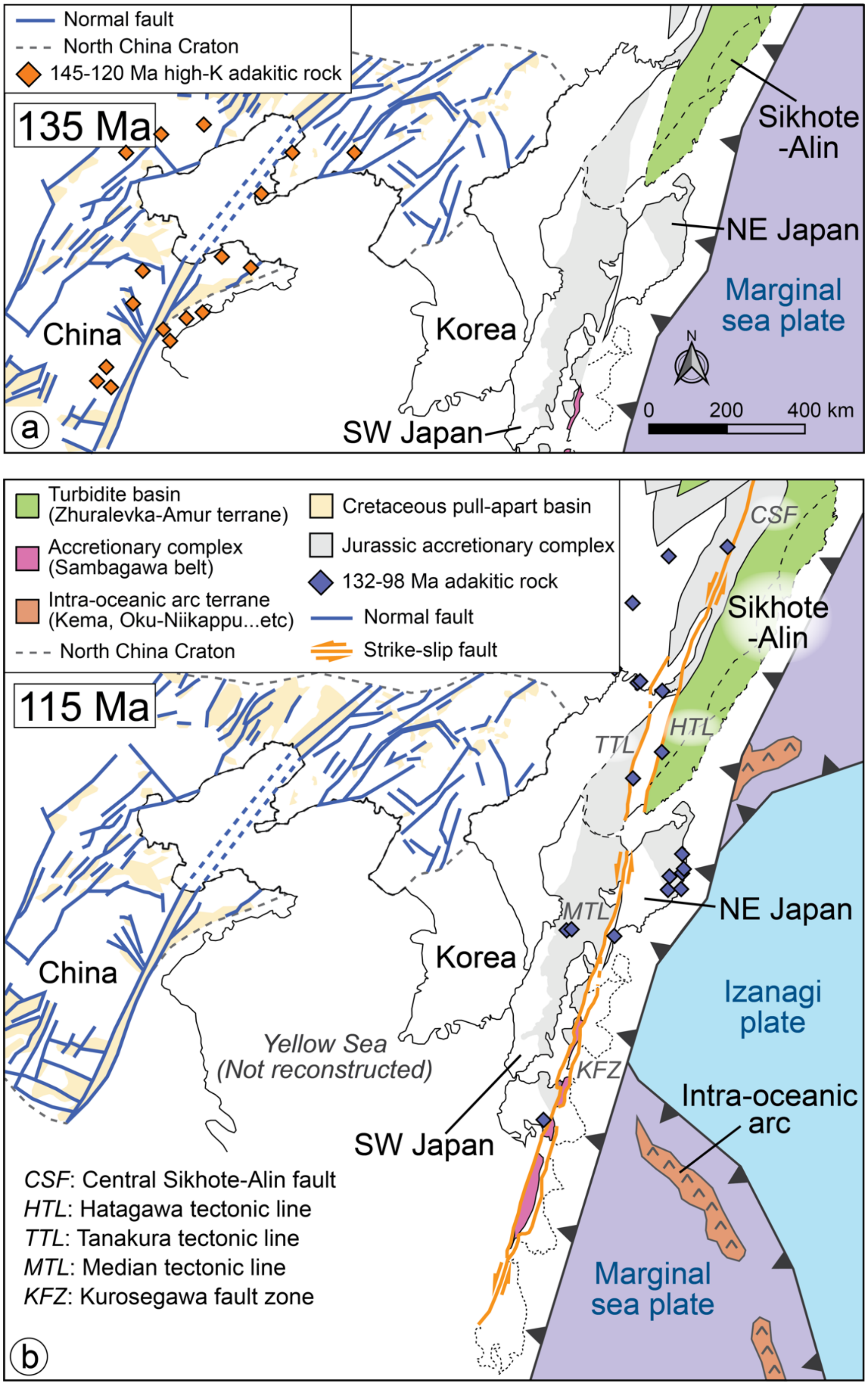

Normal fault
North China Craton
145-120 Ma high-K adakitic rock
135 Ma
Sikhote
-Alin
NE Japan
Marginal
sea plate
China
Korea
SW Japan
N
0 200 400 km
a
Turbidite basin
(Zhuralevka-Amur terrane)
Accretionary complex
(Sambagawa belt)
Intra-oceanic arc terrane
(Kema, Oku-Niikappu...etc)
North China Craton
Cretaceous pull-apart basin
Jurassic accretionary complex
132-98 Ma adakitic rock
Normal fault
Strike-slip fault
115 Ma
CSF
Sikhote
-Alin
HTL
TTL
MTL
NE Japan
Izanagi
plate
KFZ
Intra-oceanic
arc
Marginal
sea plate
China
Korea
Yellow Sea
(Not reconstructed)
SW Japan
CSF: Central Sikhote-Alin fault
HTL: Hatagawa tectonic line
TTL: Tanakura tectonic line
MTL: Median tectonic line
KFZ: Kurosegawa fault zone
b

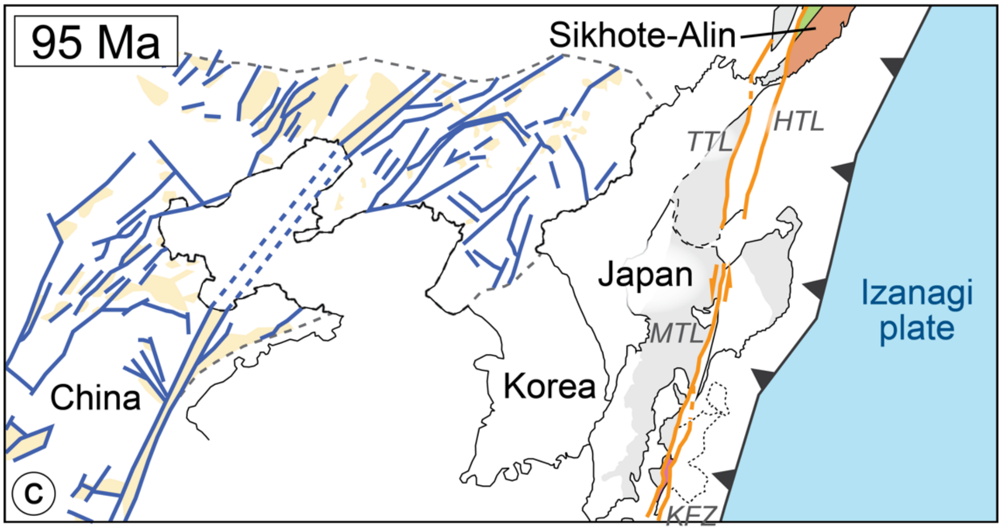

Figure 3. 10 Schematic tectonic evolution of NE Asia during the Early Cretaceous.

The NE Asia tectonic evolution model based on our Figure 3.9 plate reconstruction at: a) 150 Ma, b) 125 Ma, and c) 100 Ma. In a), we reconstruct the subduction of a marginal sea plate. The continental arc has migrated inboard due to flat-slab subduction, following Wu et al. (2019). In b), the peak of North China craton lithospheric thinning occurred ~130 Ma, after the continental arc migrated outboard due to rollback of the marginal sea slab between ~150 to 135 Ma. An intra-oceanic arc approaches the Eurasian margin and accretes diachronouslly until 100 Ma, producing a plate boundary reorganization that involves Eurasia, the marginal sea, and the Izanagi plate. c) shows the final stages of intra-oceanic arc accretion. The Izanagi plate is now subducting along Eurasia. The former accretionary prism is metamorphosed and forms the Sambagawa belt, Japan. A possible slab gap formed during the plate reorganization allows new flow of juvenile mantle into the mantle wedge, which was formerly enriched. Granitoid magmatic intrusions are color-coded by age.

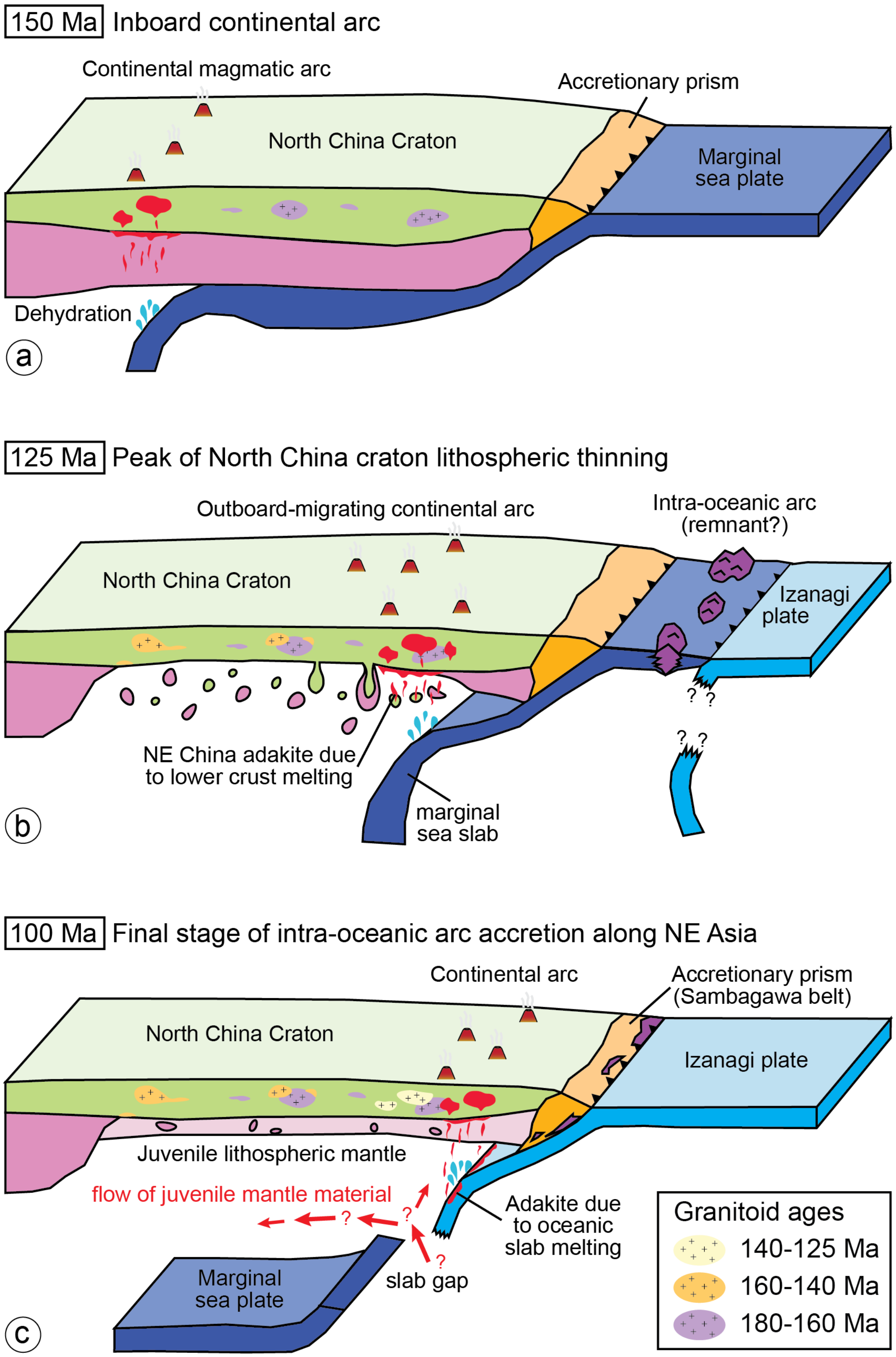

150 Ma
Inboard continental arc
Continental magmatic arc
Accretionary prism
North China Craton
Marginal sea plate
Dehydration
a
125 Ma
Peak of North China craton lithospheric thinning
Outboard-migrating continental arc
Intra-oceanic arc (remnant?)
North China Craton
Izanagi plate
NE China adakite due to lower crust melting
marginal sea slab
b
100 Ma
Final stage of intra-oceanic arc accretion along NE Asia
Continental arc
Accretionary prism (Sambagawa belt)
North China Craton
Izanagi plate
Juvenile lithospheric mantle
flow of juvenile mantle material
Adakite due to oceanic slab melting
Marginal sea plate
slab gap
c
Granitoid ages
140-125 Ma
160-140 Ma
180-160 Ma

reconstruct left-lateral strike-slip faulting along the Eurasian margin by creating a composite of two published models (Fig. 3.9b): a model for Sikhote-Alin (Kemkin, 2008), and the Yamakita and Otoh (2000) model for Japan. Our reconstruction of Cretaceous geology in NE China follows Wu et al. (2018) and Zhu et al. (2012a). During the Cretaceous, NE China was under crustal extension, as shown by the blue faults in Figures 3.9a and b (Zhu et al., 2012a). Our synthesized plate model reconstructs a throughgoing, left-lateral strike-slip fault system along the East Asian margin that connects the Median Tectonic Line in Japan (Fig. 3.5) with the Central Sikhote-Alin fault to the north (Fig. 3.7). In our model, left-lateral strike-slip motions produce a limited northward translation of some geological units along the outboard Eurasian margin during the Cretaceous, including the Sambagawa belt (SW Japan), the north and south Kitakami terrane (NE Japan), and the Zhuravlevka terrane (Sikhote-Alin). These limited northward motions may explain some of the paleolatitudes of SW Kyushu, Kiselevka-Manoma, Kema, and West Sakhalin terranes, which were between 9° to 19° further south in the latest Early Cretaceous relative to present (Table 3.1) (Abrajevitch et al., 2012; Arkhipov et al., 2019; Uno et al., 2011). Evidence from radiolarians also suggests that Hokkaido was

Geological unit	Present latitude	Paleolatitude	Sample age
Kiselevka-Manoma	52.1°N	33±5°N	Albian-Cenomanian (113-94 Ma)
Kema	45.7°N	36±6°N	Albian (113-100 Ma)
West Sakhalin	47.3°N	28±5°N	Early Albian (~110 Ma)
SW Kyushu	32.3°N	18±3°N	Aptian-Albian (125-100 Ma)

Table 3. 1 Published paleolatitudes of Early Cretaceous terranes within NE Asia. (Arkhipov et al., 2019; Abrajevitch et al., 2012; Uno et al., 2011).

located at the sub-tropical or tropical area in the late Jurassic, with a paleolatitude lower than 25° N (Matsuoka, 1996). The Sambagawa belt in Japan restores as an accretionary prism along the Eurasian margin in the mid-Cretaceous (Fig. 3.9b).

3.5.1.2 Reconstructed NW Pacific basin plate tectonics during the Early Cretaceous

According to the compiled igneous activity, stratigraphy, and paleomagnetism evidence in NE Asia, and following an approach to implement the least-complex solution, we reconstruct the most likely plate tectonic boundary conditions within the oceanic realms (Fig. 3.9, 3.10). We make the following choices:

(1) We follow the Hokkaido accreted ocean plate stratigraphy of Ueda and Miyashita (2005) and reconstruct Izanagi plate subduction from the mid-Cretaceous (~100 Ma) to early Cenozoic based on the accreted oceanic crust of progressively younger ages Ueda and Miyashita (2005) and evidence for Izanagi-Pacific ridge subduction between 56 to 46 Ma (Wu and Wu, 2019).

(2) We reconstruct our intra-oceanic arc accretions during the Early Cretaceous by invoking a 'marginal sea plate' (e.g. Fig. 3.9b) within the NW Pacific basin, outboard of the Eurasian margin. Hokkaido ocean plate stratigraphy supports our inferred marginal sea along NE Asia during the Early Cretaceous and indicates the marginal sea was probably formed of older oceanic crust (>100 Myr ages) (cf. Ueda and Miyashita, 2005). Such intra-oceanic subduction within the NW Pacific basin has been suggested by previous studies (e.g. Ueda and Miyashita, 2005; van der Meer et al., 2012).

(3) We reconstruct the intra-oceanic arcs that were later accreted to the Eurasian margin by invoking a convergent plate boundary between the 'marginal sea plate' and the Izanagi plate as a convergent plate boundary. We choose a westward subduction polarity (Fig. 3.10b) with the acknowledgment that reconstructing subduction polarities of intra-oceanic arcs is challenging.

(4) We reconstruct the intra-oceanic arc-trench system of (2) and (3) above within a minimum latitude range of 15°N to 42° N based on published paleolatitudes (Table 3.1). This places our restored intra-oceanic arcs between the latitudes of South China and southern Sikhote-Alin, which effectively spans the entire range of our plate reconstructions (Fig. 3.9, 3.10).

(5) The intra-oceanic subduction zone plate boundary between the marginal sea plate and the Izanagi plate in (2) and (3) was reconstructed as a single, curved subduction zone to accommodate a diachronous 130 to 100 intra-oceanic arc accretion timeframe (see Section 3.4.4, Fig. 3.6c). Other more complex solutions are certainly possible, but we choose this scenario in line with our approach to reconstruct the most straightforward solution.

Following the assumptions above, we interpret a late Jurassic to middle Cretaceous plate tectonic evolution model for the NW Pacific basin and NE Asia, as follows (Fig. 3.9 and 3.10): (1) From 160 to 140 Ma (Fig. 3.10a), a marginal sea plate subducted beneath the Eurasian continent. We follow Wu et al. (2019) and interpret the inboard and outboard migration of magmatism (Fig. 3.3a) to be a result of flat subduction followed by slab rollback; our model indicates the subducting slab was not Izanagi, but would have been a marginal sea; (2) From 140 to 125 Ma (Fig. 3.10b), two co-eval arc-trench systems existed along East Asia; these included the Eurasian continental arc system and an intra-oceanic arc formed by Izanagi plate subduction beneath the marginal sea plate that kept rolling backward. We move the intra-oceanic arc system westward in order to reconstruct its accretion to the Eurasia continent, which results in the closure of the marginal sea (Fig. 3.10b). Destruction of the lower NCC lithosphere occurred during this period (Fig. 3.10b). The 145 to 120 Ma K-rich adakitic rocks in NE China were generated by partial melting of North China craton lower crust (orange diamonds in Fig. 3.4); (3) From 130 to 100 Ma, the marginal sea fully closed and the intra-oceanic arc system(s) accreted to the Eurasian continental margin (Fig. 3.6, 3.9b, 3.10b and c). The outboard migration of NE Asia igneous activity ended ~110 Ma (Fig. 3.3a, b) during this period. The adakitic magmatism in Japan and Sikhote-Alin with 132 to 99 Ma ages (purple and yellow diamonds in Fig. 3.4) were generated by oceanic slab melting following their temporal correlation to intra-oceanic arc accretion (and possible subduction) (see 3.4.4).

Although the schematic plate tectonic model (Fig. 3.9, 3.10) shows only the most straightforward solution, a single intra-oceanic arc-trench along East Asia during the Early Cretaceous, we acknowledge that constraints for the latest accretion time of the intra-oceanic arc fragments show a wide range, from 130 to 100 Ma (Table 3.1). Within these constraints, alternative scenarios involving accretion of multiple arc-trench systems and marginal seas similar to Cenozoic SE Asia (Hall, 2012; Pubellier et al., 2004; Wu et al., 2016) could be possible. Under a more complex scenario with multiple oceanic plates, some of the 132 to 99 Ma adakitic rocks (purple and yellow diamonds in Fig. 3.4) could be generated by collisions between intra-oceanic arcs (Sajona et al., 2000). Regardless of plate tectonic complexities, any reconstructed scenario would imply a 130 to 100 Ma reorganization in plate tectonic boundary conditions along the NE Asian margin that is more complex than depicted in popular Andean-style subduction models (Fig. 3.2a).

3.5.1.3 Philippine Sea and western Pacific modern analog

The present Philippine Sea plate and western Pacific subduction systems along East Asia (Fig. 3.11) shows the importance of recognizing the more complex plate tectonic boundary conditions envisioned in our Early Cretaceous plate reconstruction along NE Asia (Fig. 3.10, 3.11). North of the Japan trench-trench-trench triple junction (TTT), a relatively straightforward subduction system is formed by Andean-style subduction and a single mantle wedge (Fig. 3.11). The subducting Pacific oceanic lithosphere is older (>100 Ma) and colder (Fig. 3.11). In contrast, south of the Japan TTT, a more complex double subduction system is formed that includes the Pacific, a marginal sea (i.e. the Philippine Sea plate), and the Izu-Bonin-Marianas intra-oceanic subduction zone (Fig. 3.11). Recognition of the additional plate tectonic complexities south of the Japan TTT is critical for petrogenesis, since the subducting Philippine Sea oceanic lithosphere is significantly warmer and younger (<55 Ma) compared to the Pacific Ocean lithosphere. Furthermore, near the Japan TTT, overlap of the

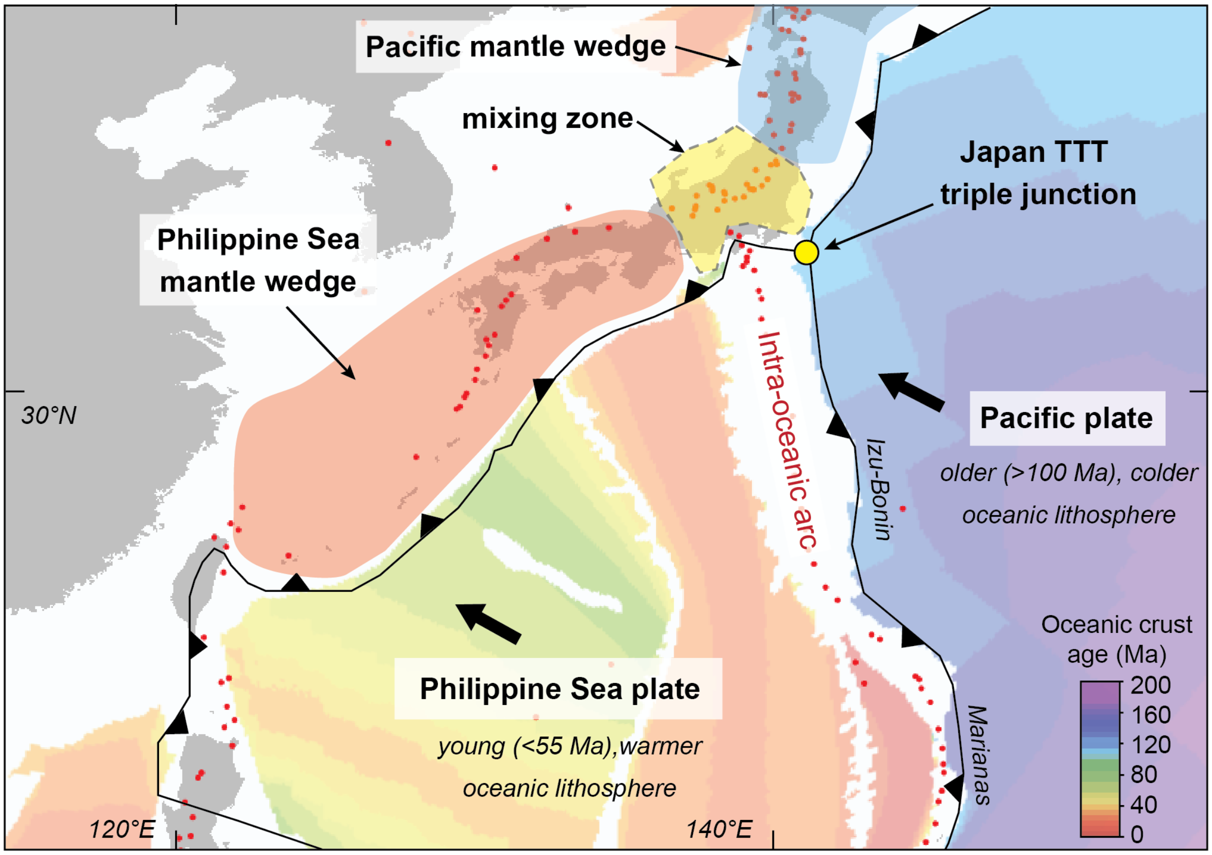

Figure 3. 11 Map of present-day Philippine Sea plate and western Pacific subduction along East Asia shows an analogy of complex plate tectonic conditions produced by marginal sea subduction.

The subducting oceanic plate age and temperature abruptly changes across the Japan trench-trench-trench (TTT) triple junction. Two compositionally-distinct mantle wedges (red and blue polygons) are produced, in addition to a mixed zone (yellow polygon) near the triple junction (after Nakamura et al., 2019). The mixed zone shows an arc-arc collision, elevated slab-derived fluid fluxes, and variable compositions and geochemistry. In this study, we recognize a similarly complex plate tectonic context along NE Asia during Early Cretaceous times that may have implications for petrogenesis during North China craton destruction.

Pacific and Philippine Sea mantle wedges produce a mixing zone that shows elevated slab-derived fluid fluxes and variable magmatic compositions and geochemistry (Nakamura et al., 2008; Nakamura et al., 2019). Other petrological complexities are introduced by the collision of the Izu-Bonin intra-oceanic arc and Japan continental arc near the Japan TTT (Tamura et al., 2010). In the same way, a clearer recognition that NE Asian plate tectonics during Early Cretaceous times was more complex than generally recognized (e.g. Fig. 3.9, 3.10) may allow new details to emerge when these conditions are implemented into future regional tectonic and geodynamic models.

3.5.2 Implications for North China Craton destruction models

Recently proposed mechanisms for the NCC destruction typically consider continuous Izanagi /paleo-Pacific plate subduction under an Andean-type margin (Fig. 3.2a) (Liu et al., 2019; Wu et al., 2019; Zheng et al., 2018). In this study, we show that intra-oceanic arc(s) accreted along the NE Asian Eurasian margin during the Early Cretaceous 130 to 100 Ma (Fig. 3.7). These island arc accretions overlap with the peak of the North China craton destruction between 130 to 120 Ma (Dai et al., 2016; Liu et al., 2019; Ma et al., 2016a; Zheng et al., 2018). Therefore, NCC destruction models must be considered in the context of changing plate boundary conditions during Early Cretaceous times (Fig. 3.9, 3.10). In other words, published NCC destruction models that rely on straightforward Andean-style subduction (Fig. 3.2a) are likely oversimplified.

Specifically, our results challenge NCC destruction models that rely on 'big mantle wedge'-style subduction with a stagnant slab (He, 2014; Li and Wang, 2018; Liu et al., 2019), since these models rely on continuous, long-lived subduction of a single plate beneath the Eurasian margin (e.g. Andean-style models in Fig. 3.2a). In contrast, our models suggest a more complex Early Cretaceous reorganization of the subduction zone, and possible slab detached occurred (Fig. 3.10). Some NCC destruction models invoke back-arc extension and rollback of the Izanagi plate relative to NE China to explain the outboard migration of continental arc magmatism during the Early Cretaceous (Zhu et al., 2012a). Such models may require revisions since our models indicate the Izanagi plate was not subducting beneath the NE Asian margin before 130 Ma (Fig. 3.10), therefore, reconstructed East Asia-Izanagi convergence rates (Engebretson, 1985) should not be applied to geodynamic models of NCC destruction.

Moreover, the geodynamic evolution of the mantle beneath NE China is likely more complex than generally recognized if intra-oceanic arc accretion is considered. Details for the replacement of old NCC subcontinental lithospheric mantle (SCLM) by juvenile material at ~115 Ma (Event 3 in Fig. 3.8) (Dai et al., 2016; Liu et al., 2019; Ma et al., 2016a; Zheng et al., 2018) remains controversial. Previously proposed ideas include: (1) mantle metasomatism with oceanic slab-derived adakitic melt (event 5 in Fig. 3.8) (Zheng et al., 2018); and, (2) lateral filling of asthenospheric mantle induced by slab rollback (Event 1 in Fig. 3.8) (Dai et al., 2016). Indeed, both of these mechanisms can replace the old NCC SCLM with juvenile mantle lithosphere. However, the juvenile adakitic melt is unlikely to have replaced the entire SCLM. On the other hand, the ~115 Ma SCLM replacement (Event 3 in Fig. 3.8) started 20

Myrs after the beginning of slab rollback at 140 Ma (Event 1 in Fig. 3.8). Considering models of instantaneous return flow induced by slab rollback (Kincaid and Griffiths, 2003), the 20 Myrs delay seems too long for slab rollback to be the main mechanism. Instead, a double subduction system similar to Figures 3.9 and 3.10 can allow for sufficient exchange of asthenospheric mantle beneath the oceanic and continental crust by toroidal flow (Holt et al., 2017; Zhang et al., 2017), or by direct flow through a slab gap that forms after intra-oceanic arc accretion, when the marginal sea is fully subducted and breaks off (Fig. 3.10c). These mantle evolution scenarios beneath the NCC during its destruction should be further investigated by geodynamic modeling.

From the perspective of continental lithospheric evolution, the Early Cretaceous was a critical time for the growth of the modern Eurasian continental lithosphere along NE Asia. Juvenile mantle lithosphere was added beneath the eastern Eurasian continent during the Early Cretaceous and Archean mantle lithosphere was lost. Intra-oceanic arc(s) floored by juvenile lithosphere accreted along the NE Asian continental margin. Juvenile magmatism derived from partial melting of the oceanic slabs, newly linked here to intra-oceanic arc accretion (i.e. 132-99 Ma adakitic rocks with depleted isotopic composition, purple and yellow diamonds in Fig. 3.4d-e), was also emplaced along the NE Asian continental margin. It is reasonable to conclude that accretion of one or several intra-oceanic arcs during Early Cretaceous times along East Asia, as shown in this study, is a sufficiently large tectonic event to have induced the addition of juvenile material to the NE Asian lithosphere, either directly or indirectly. More work is needed to further investigate these links.

3.6 Conclusion

The accretion of intra-oceanic arcs along Japan, Sikhote-Alin, and the Russian Far East during 130 to 100 Ma is incompatible with popular Andean-style plate models of the NE Asian margin during Cretaceous times. Here we present an alternative NE Asia plate tectonic reconstruction during Cretaceous times that synthesizes available constraints on regional intra-oceanic arc accretions and timings. This model provides a more geologically plausible plate tectonic context for North China craton peak destruction and thinning ~125 Ma. During the Early Cretaceous, subduction boundary conditions along the eastern Eurasian continental margin were perturbed by the intra-oceanic arc accretion(s); subduction was not continuous. Slab melting during 132 to 99 Ma produced adakitic rocks that show depleted Nd-Sr isotopic compositions in Japan and Sikhote-Alin. Changes in mantle circulation due to the intra-oceanic arc accretion(s) and subduction zone reorganizations may have added juvenile mantle to the NE Asian continental lithosphere. Geodynamic models incorporating intra-oceanic subduction and additional plates may help to further understand the role of island arc accretion in cratonic lithosphere thinning, destruction, and evolution of the subcontinental lithospheric mantle.

CHAPTER 4: EVOLVING CONTINENTAL ARC ALONG A GROWING ACCRETIONARY MARGIN IN SIKHOTE-ALIN (RUSSIAN FAR EAST) AND ADJACENT NORTHEAST ASIA

4.1 Introduction

Continental growth takes place in active margins where juvenile oceanic material and mantle-derived arc magma are added (Cawood et al., 2009; Condie, 2007; Reymer and Schubert, 1986). Particularly, the northwest Pacific margin (i.e. East Asia) has long been considered as a continuously growing continental margin since Mesozoic (Sengör and Natal'In, 1996). However, the spatial-temporal evolution history of the East Asian active margin is complicated by the late Cenozoic marginal sea opening. In this study, we focus on the ~1500 km-wide 42° to 52°N NE Asian margin at Sikhote-Alin (Russian Far East) and adjacent area, which has been less deformed by the late Cenozoic marginal Sea opening (Abrajevitch et al., 2012; Didenko et al., 2014; Khanchuk et al., 2015; Otofuji et al., 2002; Otofuji et al., 1995). We present new zircon U-Pb chronology (n=94) and whole-rock geochemical data (62 major elemental, 53 trace elemental, and 22 Nd-Hf isotopic analysis) from igneous rocks across the Sikhote-Alin area. We combine our new igneous age and geochemical results with other published data (n>60) from Sikhote-Alin (generally restricted between 42° to 47°N part of the area). We described the igneous rock spatial-temporal distributions together with igneous rocks from adjacent NE Asia (i.e. Sakhalin in Russian Far East, Hokkaido, and NE China). We then discuss the spatiotemporal and geochemical evolution of the continental arc in northeast Asia between 140 Ma to the Present.

4.2 Sampling and method

In this study, we have 94 rock samples collected from Sikhote-Alin by colleagues of Far East Geological Institute at Vladivostok (Fig. 4.1, Table 4.1), including 70 plutonic rocks, 15 volcanic rocks, and 9 pyroclastic rocks. Part of each rock sample was crushed and ground into powder for whole-rock geochemistry (i.e. major, trace element, and Nd-Hf isotopic analysis), while another part was used for zircon U-Pb chronology. For whole-rock geochemistry, we performed major and trace element analysis for 38 plutonic rocks and 15 volcanic rocks, and picked 22 rocks to proceed with Nd-Hf isotope geochemistry, while the 9 pyroclastic rocks only went through major element analysis.

Zircon grains were separated from the 94 rock samples using conventional techniques and final purification by hand-picking. They were mounted in epoxy resin beds and half-sectioned after the resin bed had dried. For examination of zircon internal texture and selection of analytical spots, we took Cathodoluminescence (CL) and Energy Dispersive Spectrometer (EDS) images for the zircons, using an FEI XL30 Environmental Scanning Electron Microscope (ESEM) in the Jackson School of Geosciences at the University of Texas at Austin, and a JEOL JSM 6360LV SEM in the Institute of Earth Sciences at the Academia Sinica in Taiwan. We then conduct zircon U-Pb dating on three sets of Laser Ablation

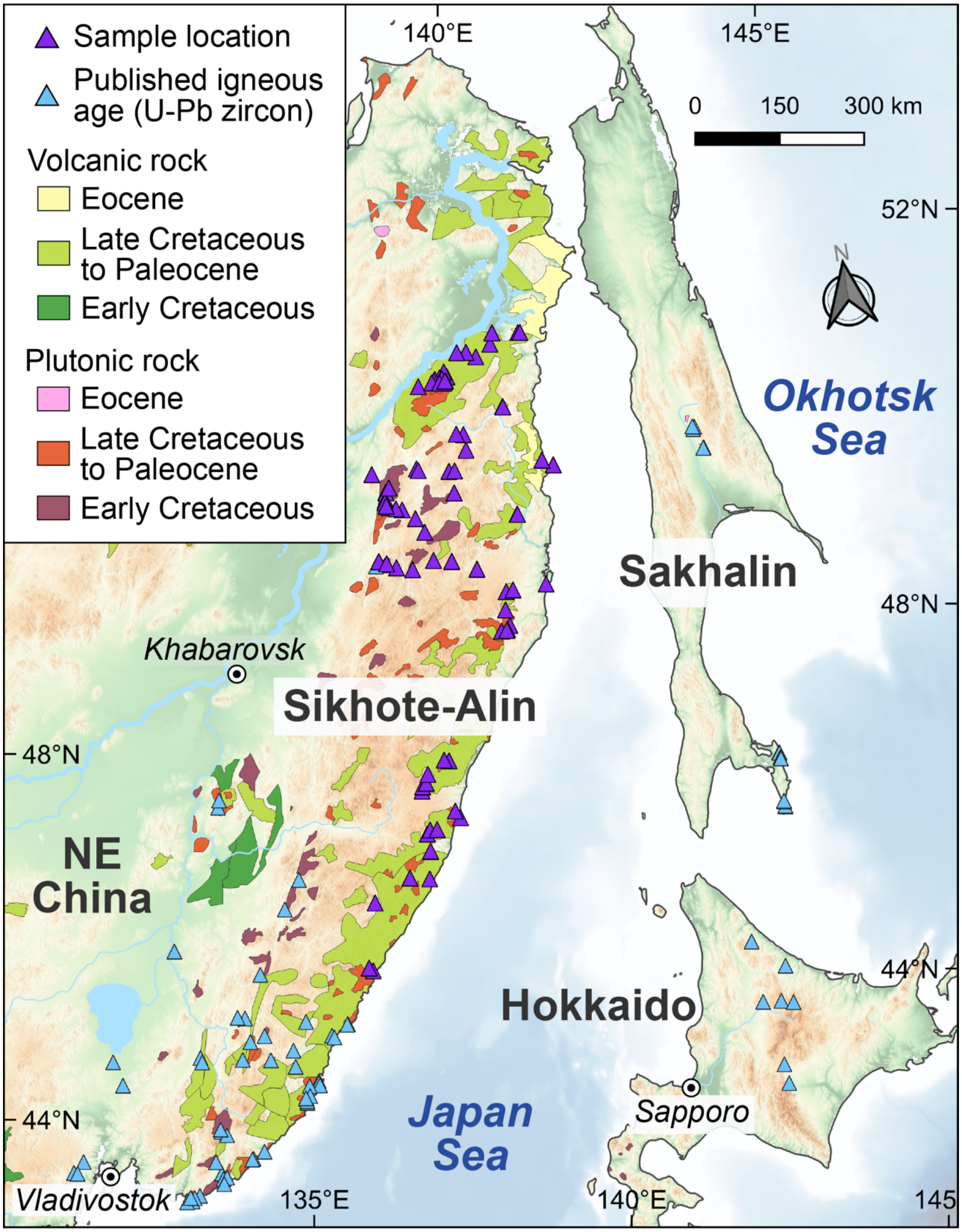

Figure 4. 1 Cretaceous to Eocene igneous rock distribution in northeast Asia and sample locations of new analysis (purple triangles) and published ages (blue triangles).

Table 4. 1 Result of zircon U-Pb dating for igneous rocks.

See Appendix C for the detailed results.

#	Sample	Rock type	Age (Ma, 2σ error)			Rock unit
1	KH16-01	granodiorite	52.4	± 1.1	Mean age	Verhneudominskii complex
2	KH16-03	granodiorite	53.7	± 0.9	Mean age	Verhneudominskii complex
3	KH16-04	granodiorite	54.5	± 1.0	Mean age	Verhneudominskii complex
4	KH16-08	granodiorite	74.7	± 0.9	Mean age	Verhneudominskii complex
5	KH16-09	basaltic andesite	54.7	± 0.8	Intercept age	Verhneudominskii complex
6	KH16-10	granodiorite	76.8	± 0.6	Mean age	Verhneudominskii complex
7	KH16-13	andesitic tuff	75.0		Youngest peak	Bol'binskaya Formation
8	KH16-17	dacite	63.4	± 1.0	Intercept age	Kuznetsovskaya Formation
9	KH16-20	granodiorite	80.4	± 0.9	Intercept age	Verhneudominskii complex
10	KH16-21	granodiorite	80.4	± 1.0	Mean age	Verhneudominskii complex
11	KH16-22	granodiorite	84.0	± 1.2	Intercept age	Verhneudominskii complex
12	KH16-24	basaltic andesite	52.5	± 0.4	Mean age	Siziman sequence
13	KH16-27	quartz monzonite	83.9	± 0.8	Mean age	Nizhneamurskii or Verhneudominskii
14	KH16-28	quartz monzonite	82.2	± 0.8	Mean age	Nizhneamurskii or Verhneudominskii
15	KH16-29	granodiorite	80.8	± 0.8	Mean age	Nizhneamurskii or Verhneudominskii
16	KH16-31	granodiorite	84.8	± 2.4	Intercept age	Nizhneamurskii or Verhneudominskii
17	KH16-32	rhyolitic tuff	87.0	± 0.9	Mean age	Bol'binskaya Formation
18	KH16-33	rhyolitic tuff	83.7	± 0.6	Mean age	Tatarkinskaya Formation
19	KH16-34	andesitic tuff	85.2	± 0.9	Mean age	Tatarkinskaya Formation
20	KH16-35	granodiorite	83.8	± 0.5	Mean age	Nizhneamurskii or Verhneudominskii
21	KH16-37	quartz monzonite	84.7	± 0.7	Intercept age	Verhneudominskii complex
22	KH16-39	andesitic tuff	85.4	± 0.8	Mean age	Bol'binskaya Formation
23	KH16-40	granodiorite	79.7	± 0.8	Intercept age	Nizhneamurskii or Verhneudominskii
24	KH16-41	granodiorite	82.9	± 0.8	Mean age	Nizhneamurskii or Verhneudominskii
25	KH16-43	dacite	84.6	± 1.1	Mean age	Siziman or Bol'binskaya Formation
26	KH16-53	quartz monzodiorite	52.1	± 0.4	Intercept age	Nizhneamurskii complex (phase 1)
27	KH16-55	granite	72.3	± 2.1	Intercept age	Verhneudominskii or Hungariyskiy
28	KH16-56	granite	110.5	± 0.9	Intercept age	Verhneudominskii complex (phase 3)
29	KH16-58	diorite	162.1	± 2.2	Mean age	Hungariyskiy complex
30	KH16-60	granodiorite	125.7	± 1.2	Mean age	Hungariyskiy complex
31	KH16-64	granite	109.4	± 1.9	Mean age	Hungariyskiy complex
32	KH16-67	granite	108.3	± 1.3	Mean age	Dzhaurskaya Formation
33	KH16-68	quartz monzodiorite	74.0	± 1.0	Mean age	Verhneudominskii or Hungariyskiy
34	KH16-69	granite	73.0	± 0.4	Intercept age	Verhneudominskii complex (phase 3)
35	KH16-71	granite	70.5	± 0.9	Mean age	Nizhneamurskii or Hungariyskiy
36	KH16-72	granodiorite	123.9	± 0.9	Mean age	Bappinskiy or Hungariyskiy complex
37	KH16-73	granite	74.3	± 1.3	Intercept age	Bappinskiy or Hungariyskiy complex
38	KH16-76	granite	73.3	± 0.8	Mean age	Nizhneamurskii complex (phase 3)
39	KH16-77	granite	71.6	± 0.8	Mean age	Nizhneamurskii complex (phase 3)
40	KH16-81a	basaltic andesite	108.0		Youngest peak	Bol'binskaya or Tatarkinskaya Fm.
41	KH16-81b	basaltic andesite	75.6	± 0.9	Mean age	Bol'binskaya or Tatarkinskaya Fm.
42	KH16-82	basalt	72.1	± 1.2	Intercept age	Udominskaya Formation
43	KH16-84	monzodiorite	62.0		Youngest peak	Pribrezhnyy complex (Phase 2)
44	KH16-85	quartz monzodiorite	75.6	± 0.6	Mean age	Pribrezhnyy complex (Phase 2)
45	KH16-86	granodiorite	63.0		Youngest peak	Pribrezhnyy complex (Phase 2)
46	KH16-88	quartz monzodiorite	66.2	± 0.9	Mean age	Pribrezhnyy complex (Phase 3)
47	KH16-89	granodiorite	87.4	± 0.9	Intercept age	Pribrezhnyy complex (Phase 3)
48	KH16-92	granite	78.5	± 2.0	Intercept age	Pribrezhnyy complex (Phase 2)

#	Sample	Rock type	Age (Ma, 2σ error)				Rock unit
49	KH16-93	granite	53.9	±	0.6	Intercept age	Pribrezhnyy complex (Phase 2
50	KH16-97	tuff breccia	63.1	±	0.5	Mean age	Tatarkinskaya or Kuznetsovska
51	KH16-98	granite	70.7	±	0.5	Mean age	Verhneudominskii complex (ph
52	KH16-99a	quartz monzodiorite	81.7	±	0.5	Mean age	Verhneudominskii complex (ph
53	KH16-102a	granite	71.6	±	1.3	Mean age	Sandinskiy complex
54	KH16-102b	granite	122.3	±	2.0	Mean age	Sandinskiy complex
55	KH16-103a	diorite	52.1	±	1.5	Intercept age	Bappinskiy complex (phase 3)
56	KH16-103b	granite	109.3	±	1.7	Intercept age	Bappinskiy complex (phase 3)
57	KH16-103c	granite	106.2	±	0.6	Intercept age	Bappinskiy complex (phase 3)
58	KH16-105a	granite	107.8	±	0.9	Mean age	Verhneudominskii or Hungariys
59	KH16-105b	granodiorite	107.9	±	0.8	Mean age	Verhneudominskii or Hungariys
60	KH16-107	granite	57.6	±	1.2	Intercept age	Verhneudominskii complex (ph
61	KH16-110	granite	106.6	±	1.0	Mean age	Hungariyskiy complex
62	KH16-111	tuff	53.5	±	0.5	Intercept age	Dekastrinskaya Formation
63	KH16-114a	granite	108.6	±	1.2	Mean age	Sandinskiy complex
64	KH16-114b	rhyolite	58.6	±	0.5	Mean age	Dyke in KH16-114a
65	KH16-116a	granite	84.0	±	0.7	Intercept age	Yoliyskiy complex
66	KH16-116b	granite	83.6	±	0.7	Mean age	Yoliyskiy complex
67	KH16-118	diorite	59.9	±	1.4	Intercept age	Pribrezhnyy complex (Phase 3
68	KH16-119	granodiorite	59.6	±	1.1	Mean age	Pribrezhnyy complex (Phase 3
69	KH16-120	granite	59.2	±	0.8	Mean age	Yoliyskiy complex
70	KH16-122	granodiorite	62.5	±	0.5	Mean age	Yoliyskiy complex
71	KH16-123	granite	59.9	±	0.6	Mean age	Yoliyskiy complex
72	KH16-124	granodiorite	60.1	±	1.1	Intercept age	Bappinskiy complex (phase 3)
73	KH16-126	granite	66.8	±	0.9	Intercept age	Yoliyskiy complex
74	KH16-127	granodiorite	63.6	±	2.2	Intercept age	Bappinskiy complex (phase 3)
75	KH16-128	granite	52.6	±	0.6	Mean age	Yoliyskiy complex
76	KH16-129	granodiorite	82.4	±	1.9	Intercept age	Yoliyskiy complex
77	P15-13	basalt	65.0			Youngest peak	Kuznecovskaya
78	P15-20	quartz monzodiorite	37.5	±	4.0	Intercept Age	Ol'ginskii Complex
79	P15-30	granodiorite	67.9	±	0.7	Mean age	Ol'ginskii Complex
80	P16-01	rhyolitic tuff	53.0	±	0.5	Mean age	Bogopol'skaya Formation
81	P16-02	basaltic andesite	62.0			Youngest peak	Primorskaya series
82	P16-04	granodiorite	75.9	±	0.6	Mean age	Ol'ginskii Complex
83	P16-05	porphyritic rhyolite	89.8	±	0.6	Mean age	Primorskaya series
84	P16-06	porphyritic andesite	91.6	±	0.9	Mean age	Samarginskaya Formation
85	P16-07	granodiorite	90.8	±	1.0	Mean age	Ulunginskii complex
86	P16-08	granite	58.8	±	0.6	Mean age	Primorskii complex
87	P16-09	granite	58.4	±	0.7	Youngest peak	Primorskii complex
88	P16-16	granite	63.6	±	0.6	Mean age	Primorskii complex
89	P16-17	porphyritic granite	55.3	±	1.6	Mean age	Primorskii complex
90	P16-18	granodiorite	43.0			Youngest peak	Primorskii complex
91	P16-19	porphyritic rhyolite	66.3	±	0.5	Intercept Age	Primorskaya series
92	P16-22	rhyolitic tuff	54.1	±	0.5	Intercept Age	Bogopol'skaya Formation
93	P16-25	basalt	65.0			Youngest peak	Ukturskaya Formation
94	P16-28	rhyolite	86.8	±	0.8	Mean age	Samarginskaya Formation

Inductively Coupled Plasma Mass Spectrometry (LA-ICP-MS) equipment: (1) an Analyte 193 coupled to a Varian 810 ICP-MS in the Department of Earth and Atmospheric Sciences at the University of Houston, (2) an Analyte 193 coupled to an Agilent 7500s ICP-MS in the Department of Geosciences at the National Taiwan University and (3) an Analyte 193 coupled to an Agilent 7900s ICP-MS in the Institute of Earth Sciences at the Academia Sinica in Taiwan. We performed data reduction through the Iolite 2.5 (Paton et al., 2011), and calculated the age result using the Isoplot 4.15 (Ludwig, 2012).

The whole-rock major element composition of the samples was measured by an Agilent 725 Inductively Coupled Plasma Optical Emission Spectrometer (ICP-OES) in the Department of Earth and Atmospheric Sciences at the University of Houston, after the powdered rock samples have proceeded with the loss on ignition (L.O.I) test and $LiBO_2$ fusion digestion. The trace element composition of the samples was analyzed by an Agilent 8800 ICP-QQQ-MS in the Department of Earth and Atmospheric Sciences at the University of Houston, after microwave-assisted acid digestion was applied to the powdered rock samples. Whole-rock Nd-Hf isotopic analyses were carried out to the rock samples using a NuPlasma II Multicollector-Inductively Coupled Plasma Mass Spectrometer (MC-ICP-MS) in the Department of Earth and Atmospheric Sciences at the University of Houston, after the powdered rock sample proceeded with microwave-assisted acid digestion and cation-exchange chromatography for Nd and Hf isolation.

4.3 Result

4.3.1 Zircon U-Pb ages

We performed U-Pb chronology for more than 2000 zircon grains from the 94 rock samples in this study. A summary of the zircon U-Pb age result is given in Table 4.1 and Fig. 4.2, and detailed age data is in Appendix C. The studied zircons generally show well-developed oscillatory zoning under CL images, with some grains also exhibiting sector zoning (Fig. 4.3). The zircon Th/U ratios range from 0.04 to 4, with a majority between 0.1 to 1.4 (Fig. 4.4). Igneous ages of the rocks were determined mostly by their weight-mean $^{206}Pb/^{238}U$ zircon age, or intercept age on Terra-Wasserburg and conventional Concordia Wetherill plots if the data shows the presence of common lead in some zircons (Table 4.1, Appendix C). However, some samples have scattered zircon ages that may imply a complicated zircon crystallization history, and a straightforward igneous age is difficult to define. In this case, we use the youngest peak $^{206}Pb/^{238}U$ age as the determining igneous age. The igneous rock samples yield U-Pb zircon ages between 125.7 to 37.5 Ma and a 162.1 Ma age from the KH16-58 gabbro (Table 4.1 and Fig. 4.2). Among the ~2000 analyzed zircons, there are ~250 inherited zircons that have $^{206}Pb/^{238}U$ age older than 140 Ma, and ~70 of them yield Precambrian age (Fig. 4.4).

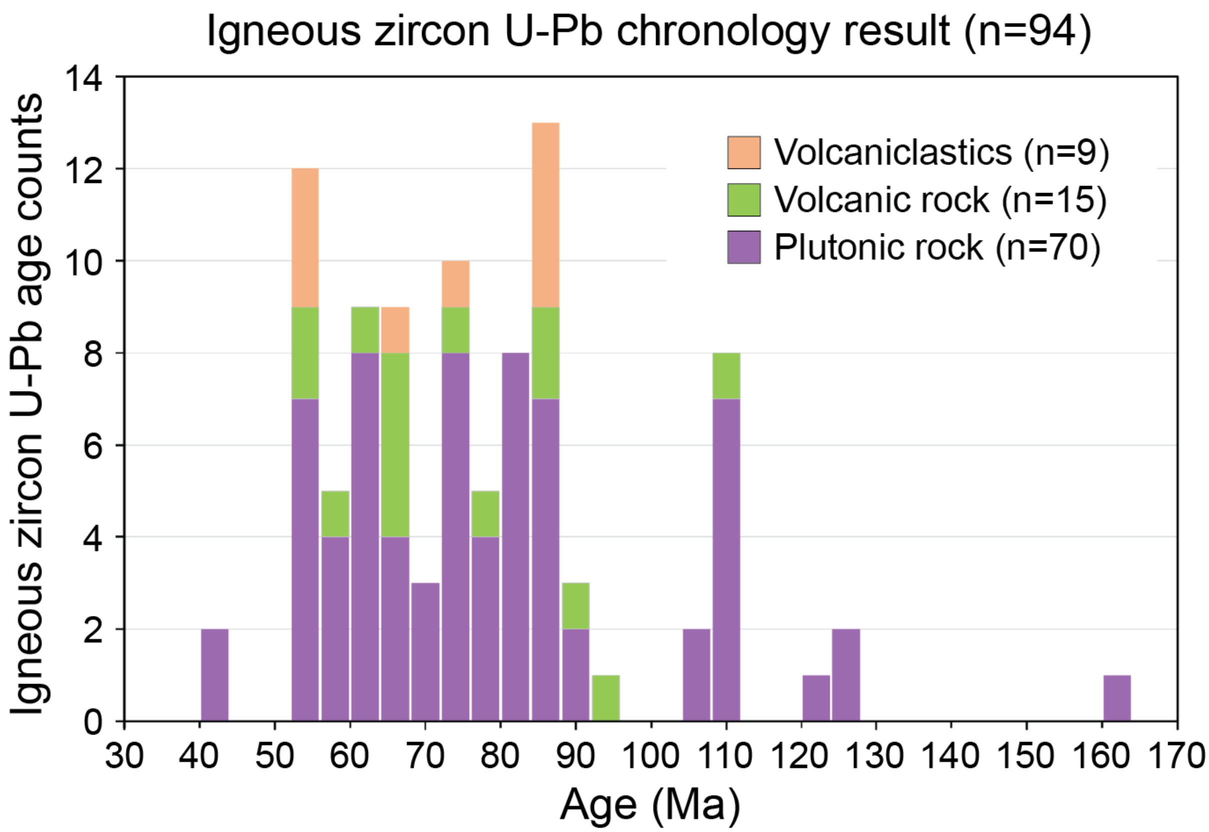

Figure 4. 2 Spatial distribution of the zircon U-Pb age result.

Locations of the samples are shown in Fig. 4.1.

Figure 4. 3 Zircon cathodoluminescence (CL) image.

The laser analysis locations are displayed as red (35 µm diameter) and blue (25 µm diameter) circles. The zircons are generally subhedral or euhedral in shape, with well-developed oscillatory or sector zoning in zircon under CL images.

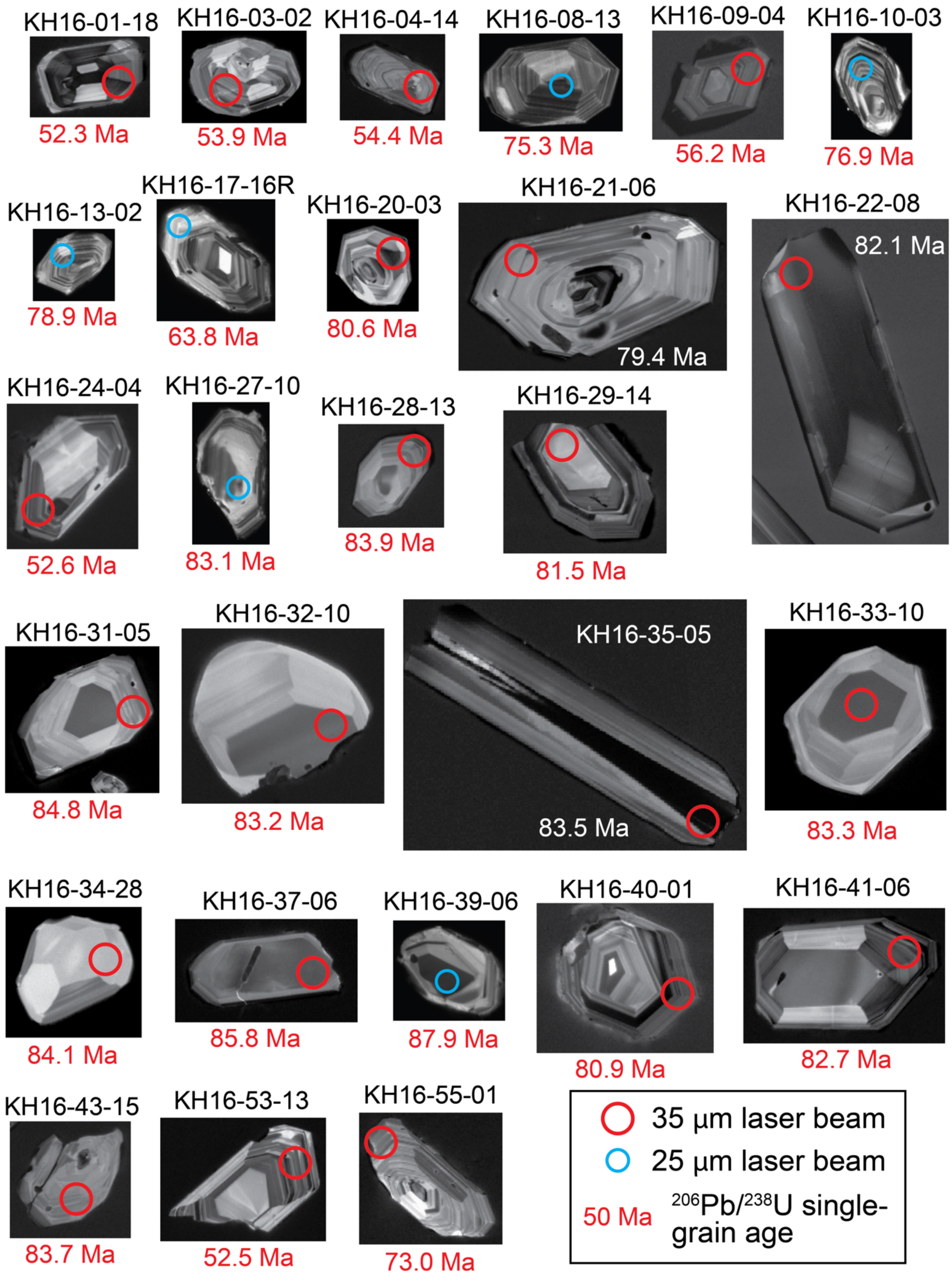

KH16-01-18
52.3 Ma
KH16-03-02
53.9 Ma
KH16-04-14
54.4 Ma
KH16-08-13
75.3 Ma
KH16-09-04
56.2 Ma
KH16-10-03
76.9 Ma
KH16-13-02
78.9 Ma
KH16-17-16R
63.8 Ma
KH16-20-03
80.6 Ma
KH16-21-06
79.4 Ma
KH16-22-08
82.1 Ma
KH16-24-04
52.6 Ma
KH16-27-10
83.1 Ma
KH16-28-13
83.9 Ma
KH16-29-14
81.5 Ma
KH16-31-05
84.8 Ma
KH16-32-10
83.2 Ma
KH16-35-05
83.5 Ma
KH16-33-10
83.3 Ma
KH16-34-28
84.1 Ma
KH16-37-06
85.8 Ma
KH16-39-06
87.9 Ma
KH16-40-01
80.9 Ma
KH16-41-06
82.7 Ma
KH16-43-15
83.7 Ma
KH16-53-13
52.5 Ma
KH16-55-01
73.0 Ma
35 μm laser beam
25 μm laser beam
50 Ma $^{206}Pb/^{238}U$ single-grain age


KH16-56-01
111.5 Ma
KH16-58-08
162.8 Ma
KH16-60-02
124.4 Ma
KH16-64-02
109.3 Ma
KH16-67-08C
109.5 Ma
KH16-68-12
73.0 Ma
KH16-69-06
73.4 Ma
KH16-71-04
72.6 Ma
KH16-72-24
125.3 Ma
KH16-73-04
75.6 Ma
KH16-76-20R
74.6 Ma
KH16-77-09
71.7 Ma
KH16-81b-09
76.3 Ma
KH16-82-26
72.5 Ma
KH16-85-04
77.5 Ma
KH16-88-19
65.5 Ma
KH16-89-16b
87.5 Ma
KH16-92-08
77.9 Ma
KH16-93-07
53.8 Ma
KH16-97-17
63.3 Ma
KH16-98-04
70.9 Ma
KH16-99a-14
82.2 Ma
KH16-102a-14
73.7 Ma
KH16-102b-03
121.2 Ma
KH16-103a-12
53.3 Ma
KH16-103b-19C
111.1 Ma
KH16-103c-11
106.3 Ma
KH16-105a-14
107.3 Ma
35 μm laser beam
25 μm laser beam
50 Ma $^{206}Pb/^{238}U$ single-grain age

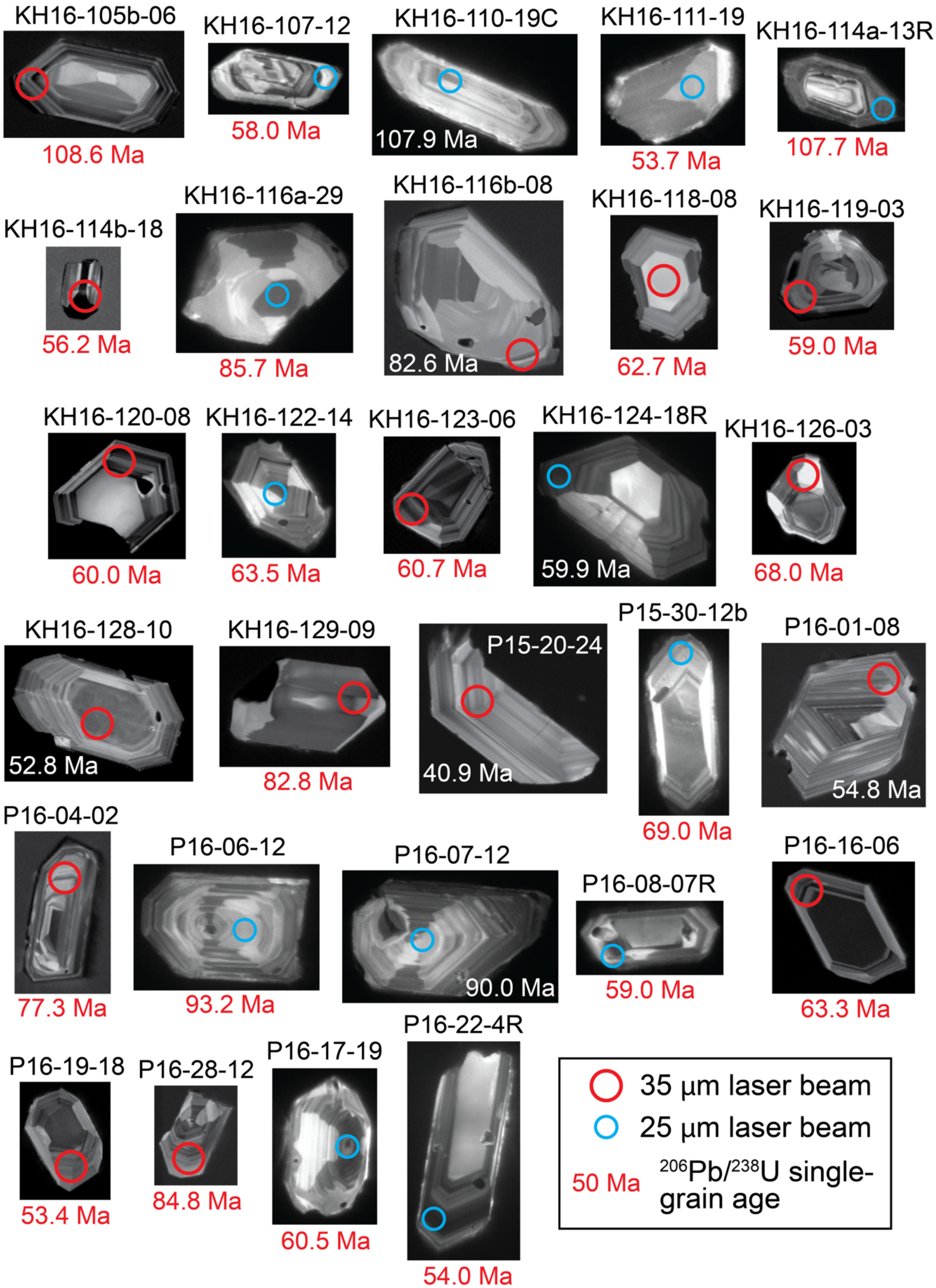
KH16-105b-06
108.6 Ma
KH16-107-12
58.0 Ma
KH16-110-19C
107.9 Ma
KH16-111-19
53.7 Ma
KH16-114a-13R
107.7 Ma
KH16-114b-18
56.2 Ma
KH16-116a-29
85.7 Ma
KH16-116b-08
82.6 Ma
KH16-118-08
62.7 Ma
KH16-119-03
59.0 Ma
KH16-120-08
60.0 Ma
KH16-122-14
63.5 Ma
KH16-123-06
60.7 Ma
KH16-124-18R
59.9 Ma
KH16-126-03
68.0 Ma
KH16-128-10
52.8 Ma
KH16-129-09
82.8 Ma
P15-20-24
40.9 Ma
P15-30-12b
69.0 Ma
P16-01-08
54.8 Ma
P16-04-02
77.3 Ma
P16-06-12
93.2 Ma
P16-07-12
90.0 Ma
P16-08-07R
59.0 Ma
P16-16-06
63.3 Ma
P16-19-18
53.4 Ma
P16-28-12
84.8 Ma
P16-17-19
60.5 Ma
P16-22-4R
54.0 Ma
35 μm laser beam
25 μm laser beam
50 Ma
206Pb/238U single-grain age

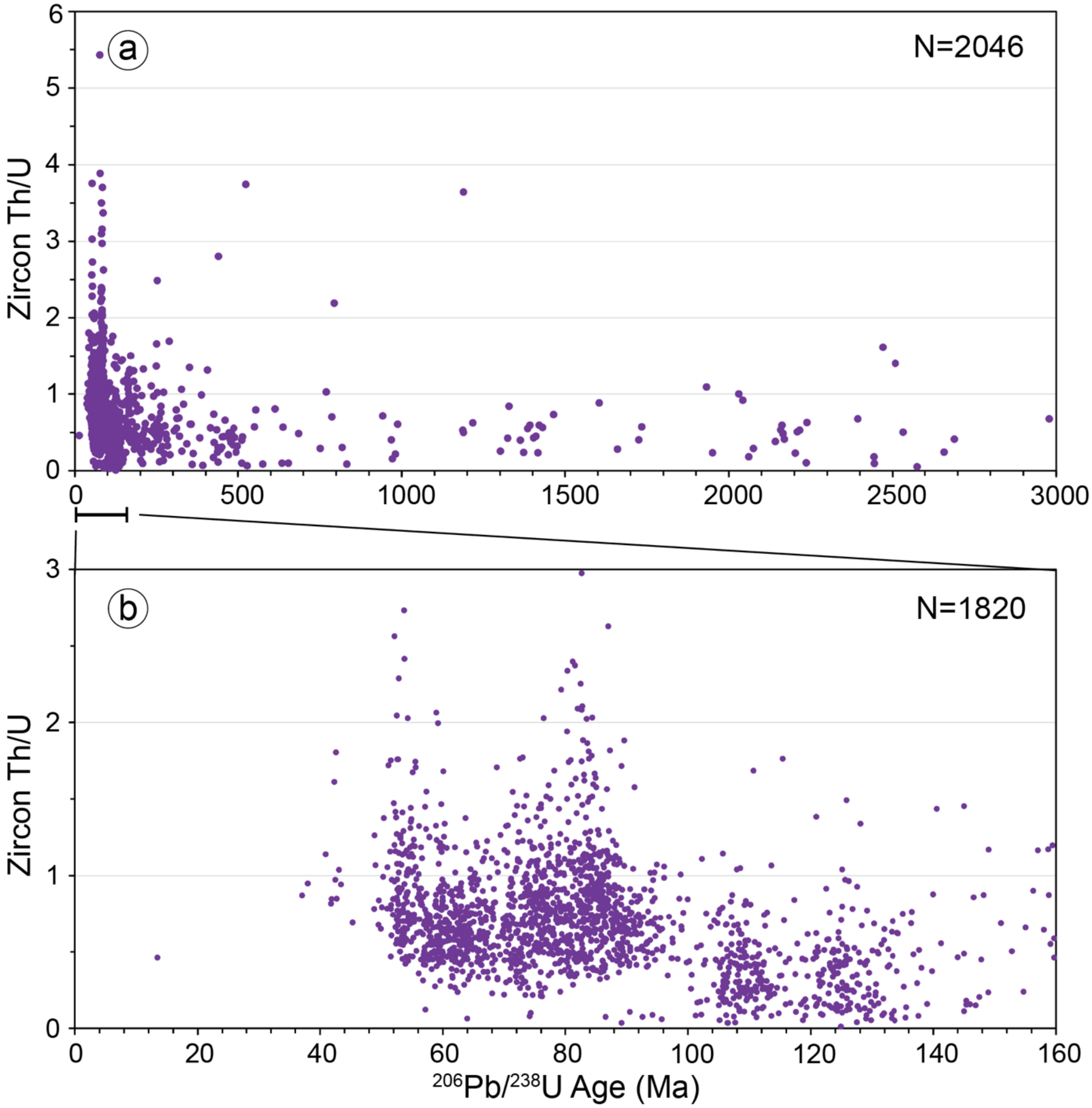

Figure 4. 4 Zircon Th/U ratio result.

The zircons have $^{206}Pb/^{238}U$ ages mostly younger than 160 Ma (n=1820), with some between 3000 to 160 Ma (n=226). They have Th/U ratios ranging between 0.01 and 0.54.

4.3.2 Whole-rock elemental composition

Whole-rock elemental analyses result are presented in Appendix D. The 53 igneous rocks yield a wide range of volatile-free SiO_2 between 49-78 % (Fig. 4.5b-c), including 39 acid rocks (SiO_2 >63%), 10 intermediate rocks (SiO_2 = 52-63%), and 4 basic rocks (SiO_2 = 45-52%) (Le Maitre et al., 2005). The 9 pyroclastic rocks have a similar SiO_2 content range between 51-75%. The igneous rocks are identified as a calc-alkaline association in the cationic classification diagram (or the "Q-P" plot, Fig. 4.5a) (Debon and Le Fort, 1988), and calc-alkalic to calc-alkalic rocks in the modified alkali-lime index (Fig. 4.5c) (Frost and Frost, 2008). The plutonic rocks were plotted within the Metaluminous and Peraluminous fields in the A/CNK vs. A/NK diagram (Fig. 4.5d) (Maniar and Piccoli, 1989). Using the threshold A/CNK< 1.1 and CIPW normative corundum< 1%, most of the plutonic rocks were defined as I-type granites, only 6 plutonic rocks are S-type granites with A/CNK > 1.1 and CIPW corundum >1% (Fig. 4.5d and Appendix D) (Chappell and White, 2001). The Fe-index diagram (Frost and Frost, 2008) shows that most of the igneous rocks are the Magnesian type or Ferroan type with high silica content (SiO_2 >70%), while two volcanic rocks are Ferroan type with intermediate silica content (Fig. 4.5e). The Y+Nb vs. Rb tectonic discrimination diagram (Pearce, 1996) reveals a volcanic arc origin for most of the igneous rocks (Fig. 4.5f). The Th-Hf-Ta plot (Wood, 1980) for mafic rocks agrees with this result, except for the KH16-58 gabbro that has an OIB origin (Fig. 4.5g). The C1 chondrite-normalized rare earth element (REE) diagram and primitive mantle-normalized multi-element spider diagram (Sun and McDonough, 1989) of the samples are shown in Fig. 4.6.

Figure 4. 5 Whole-rock geochemistry of the igneous rock samples.

(a) the cationic classification diagram, or the “Q-P” plot (Debon & Le Fort,1988). ad: adamellite (dellenite), dq: qtz diorite, qtz gabbro (qtz andesite, qtz basalt), gd: granodiorite, granogabbro (rhyodacite), go: gabbro, diorite (basalt, andesite), gr: granite (rhyolite), mz: monzonite (latite), mzdq: qtz monzodiorite, qtz monzo-gabbro (qtz lantiandesite, qtz latibasalt), mzgo: monzogabbro, monzodiorite (latibasalt, latiandesite), mzq: qtz monzonite (qtz latite), s: syenite (trachyte), sq: qtz syenite (qtz trachyte), to: tonalite, trondjemite (dacite). (b) SiO_2 vs. Nb/Y diagram for volcanic rock (Winchester & Floyd, 1977), (c) the modified alkali-lime index diagram (Frost & Frost, 2008). (d) the A/NK vs. A/CNK diagram for plutonic rock (Maniar & Piccoli, 1989) with an A/CNK=1.1 boundary line between S- and I-type granites (Chapell & White, 1992), (e) the Fe-index diagram (Frost & Frost, 2008). See Appendix D for detailed whole-rock geochemistry results. (f) Rb vs. Y+Nb tectonic discrimination diagram (Pearce, 1996), (g) Th-Hf-Ta tectonic discrimination diagram for mafic rocks (Wood, 1980). See Appendix D for detailed results.

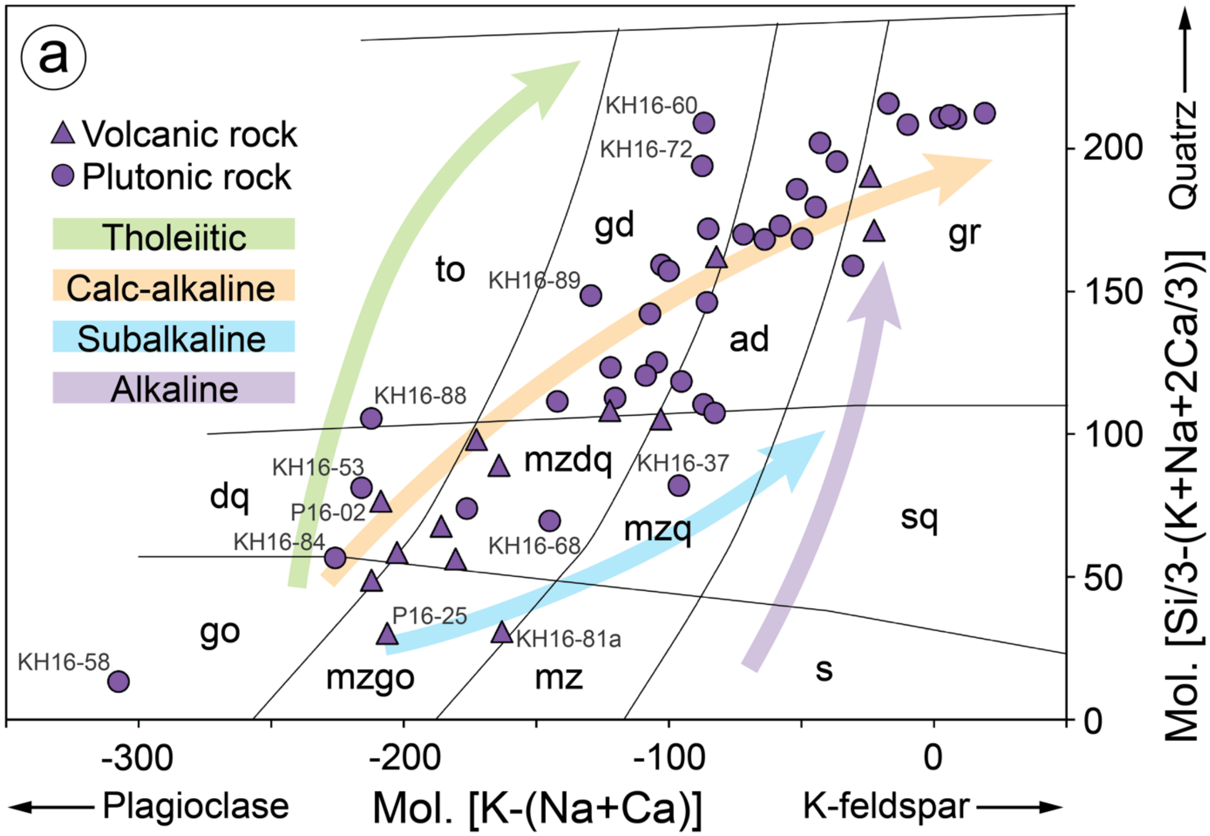
a
Volcanic rock
Plutonic rock
Tholeiitic
Calc-alkaline
Subalkaline
Alkaline
KH16-60
KH16-72
KH16-89
KH16-88
KH16-53
P16-02
KH16-84
KH16-68
KH16-37
P16-25
KH16-81a
KH16-58
to
gd
ad
gr
mzdq
dq
mzq
sq
go
mzgo
mz
s
-300
-200
-100
0
0
50
100
150
200
Plagioclase
Mol. [K-(Na+Ca)]
K-feldspar
Quatrz
Mol. [Si/3-(K+Na+2Ca/3)]

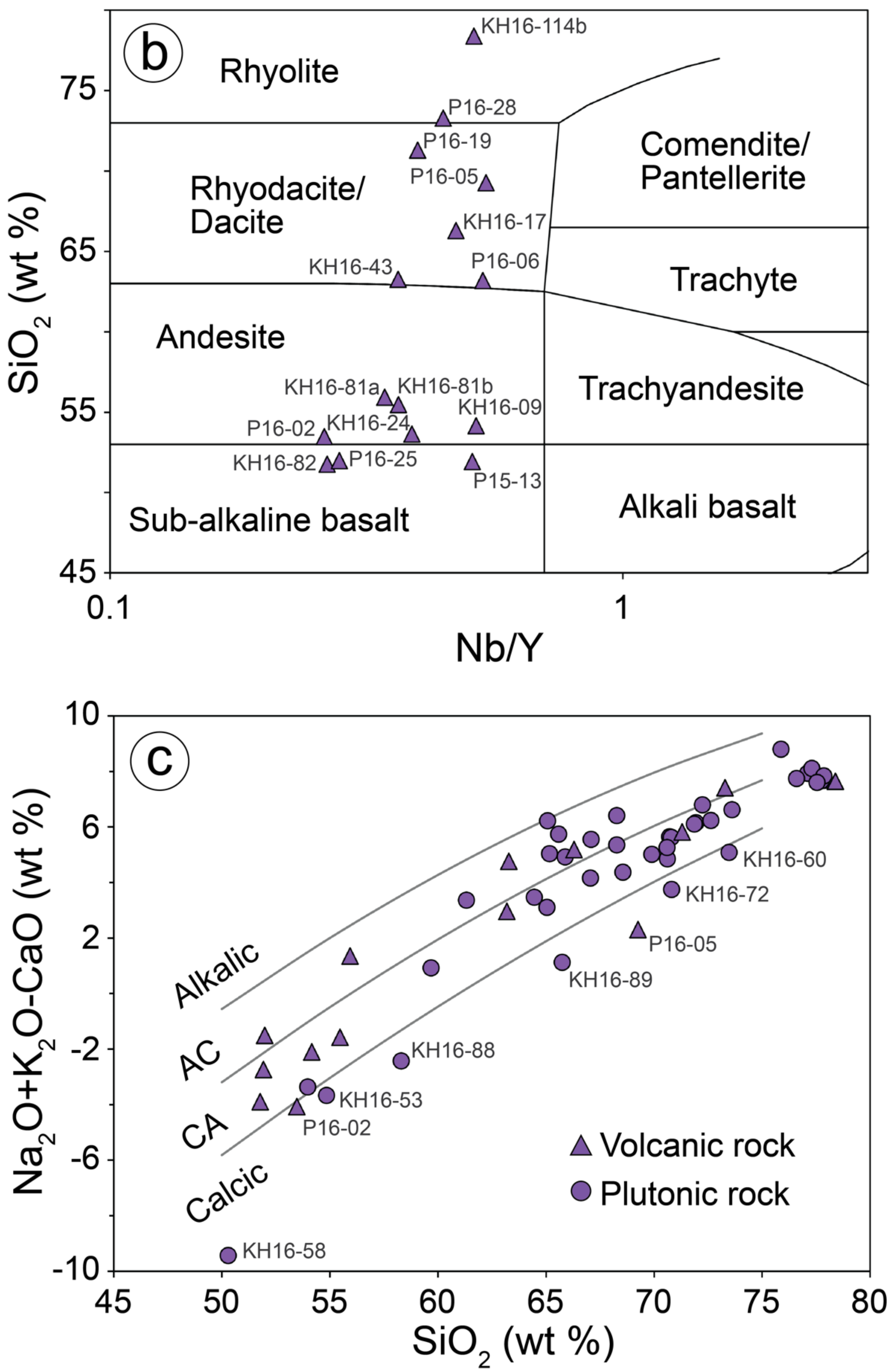
b
Rhyolite
Rhyodacite/ Dacite
Andesite
Sub-alkaline basalt
Comendite/ Pantellerite
Trachyte
Trachyandesite
Alkali basalt
KH16-114b
P16-28
P16-19
P16-05
KH16-17
KH16-43
P16-06
KH16-81a
KH16-81b
KH16-09
P16-02
KH16-24
KH16-82
P16-25
P15-13
SiO2 (wt %)
Nb/Y
c
Alkalic
AC
CA
Calcic
KH16-60
KH16-72
P16-05
KH16-89
KH16-88
KH16-53
P16-02
KH16-58
Volcanic rock
Plutonic rock
Na2O+K2O-CaO (wt %)
SiO2 (wt %)

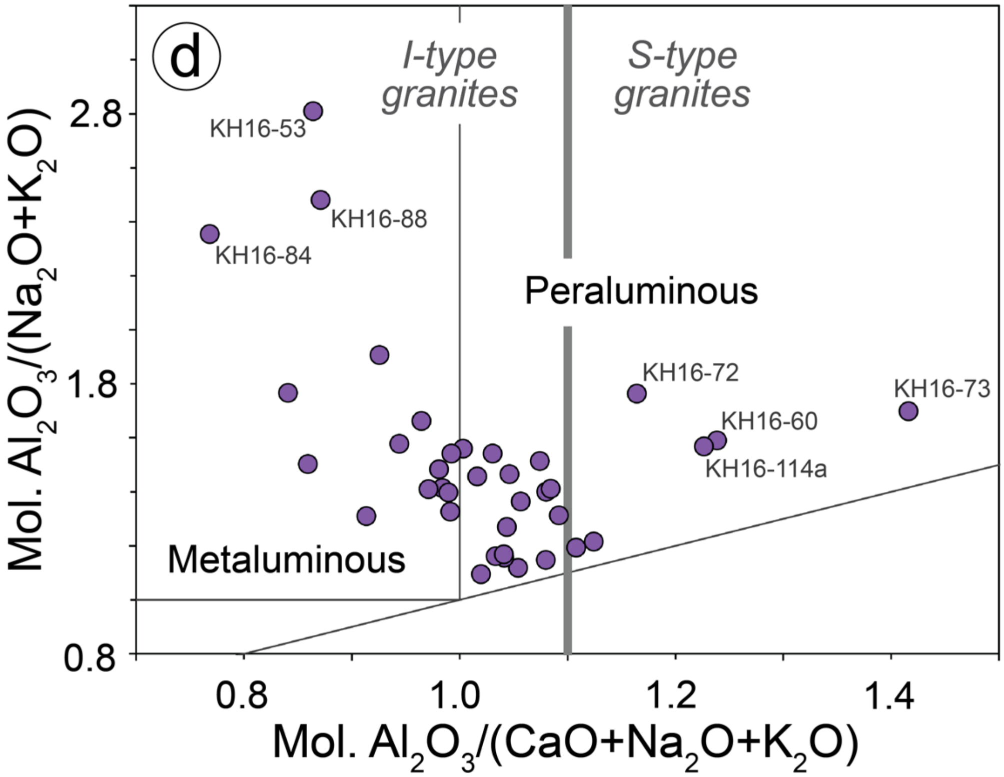
d
I-type granites
S-type granites
Peraluminous
Metaluminous
KH16-53
KH16-88
KH16-84
KH16-72
KH16-73
KH16-60
KH16-114a
Mol. Al2O3/(Na2O+K2O)
Mol. Al2O3/(CaO+Na2O+K2O)
2.8
1.8
0.8
0.8
1.0
1.2
1.4

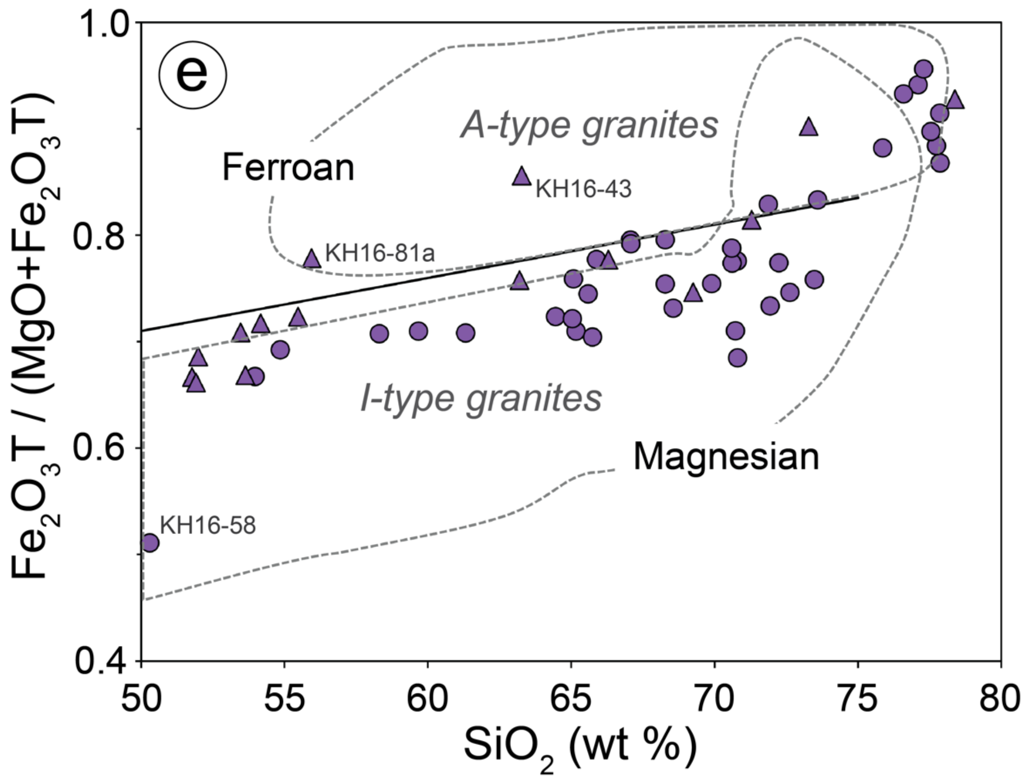
e
A-type granites
Ferroan
KH16-43
KH16-81a
I-type granites
Magnesian
KH16-58
Fe2O3T / (MgO+Fe2O3T)
SiO2 (wt %)
1.0
0.8
0.6
0.4
50
55
60
65
70
75
80

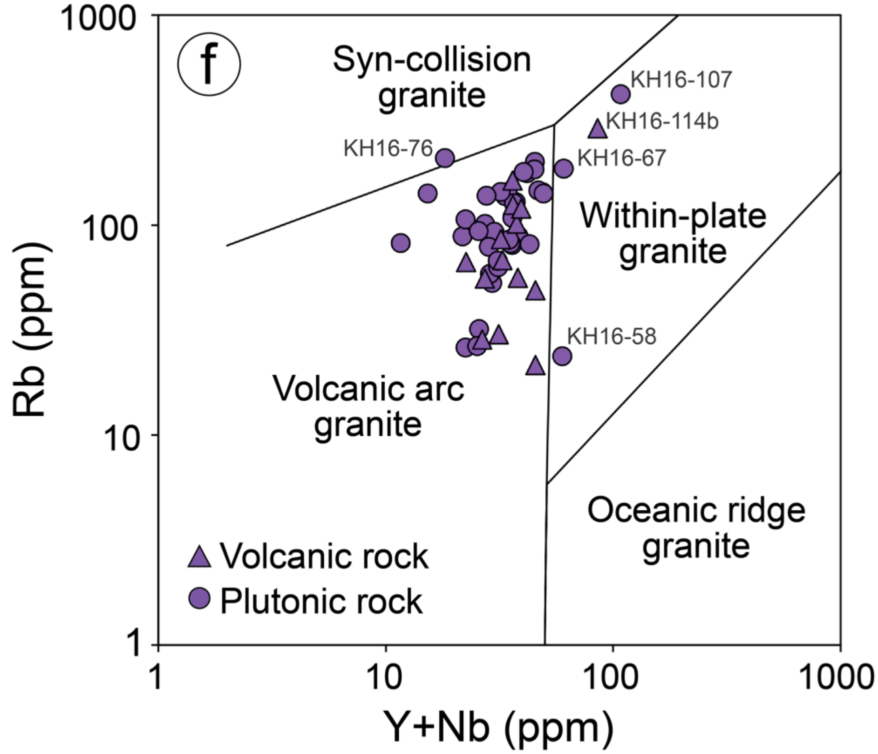
f
Syn-collision granite
Within-plate granite
Volcanic arc granite
Oceanic ridge granite
KH16-107
KH16-114b
KH16-76
KH16-67
KH16-58
Volcanic rock
Plutonic rock
Rb (ppm)
Y+Nb (ppm)
1000
100
10
1
1
10
100
1000

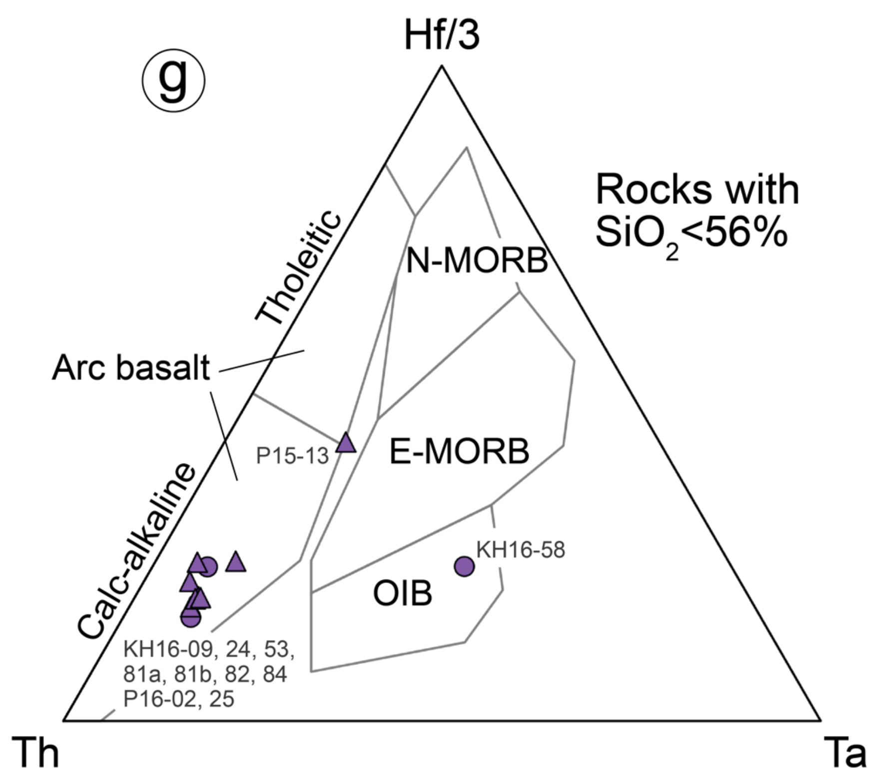
g
Hf/3
Th
Ta
Rocks with SiO_2<56%
Tholeitic
Arc basalt
Calc-alkaline
N-MORB
E-MORB
OIB
P15-13
KH16-58
KH16-09, 24, 53, 81a, 81b, 82, 84
P16-02, 25

Figure 4. 6 C1 chondrite-normalized rare earth element diagram and primitive mantle-normalized multi-element spider diagrams for the igneous rocks from this study. The plotting method follows Sun & McDonough (1989).

Samples with igneous ages between (a-b) 43-40 Ma, (c-d) 60-52 Ma, (e-f) 70-60 Ma, (g-h) 80-70, (i-j) 92-80 Ma, and (k,l) 162 and 125-105 Ma.

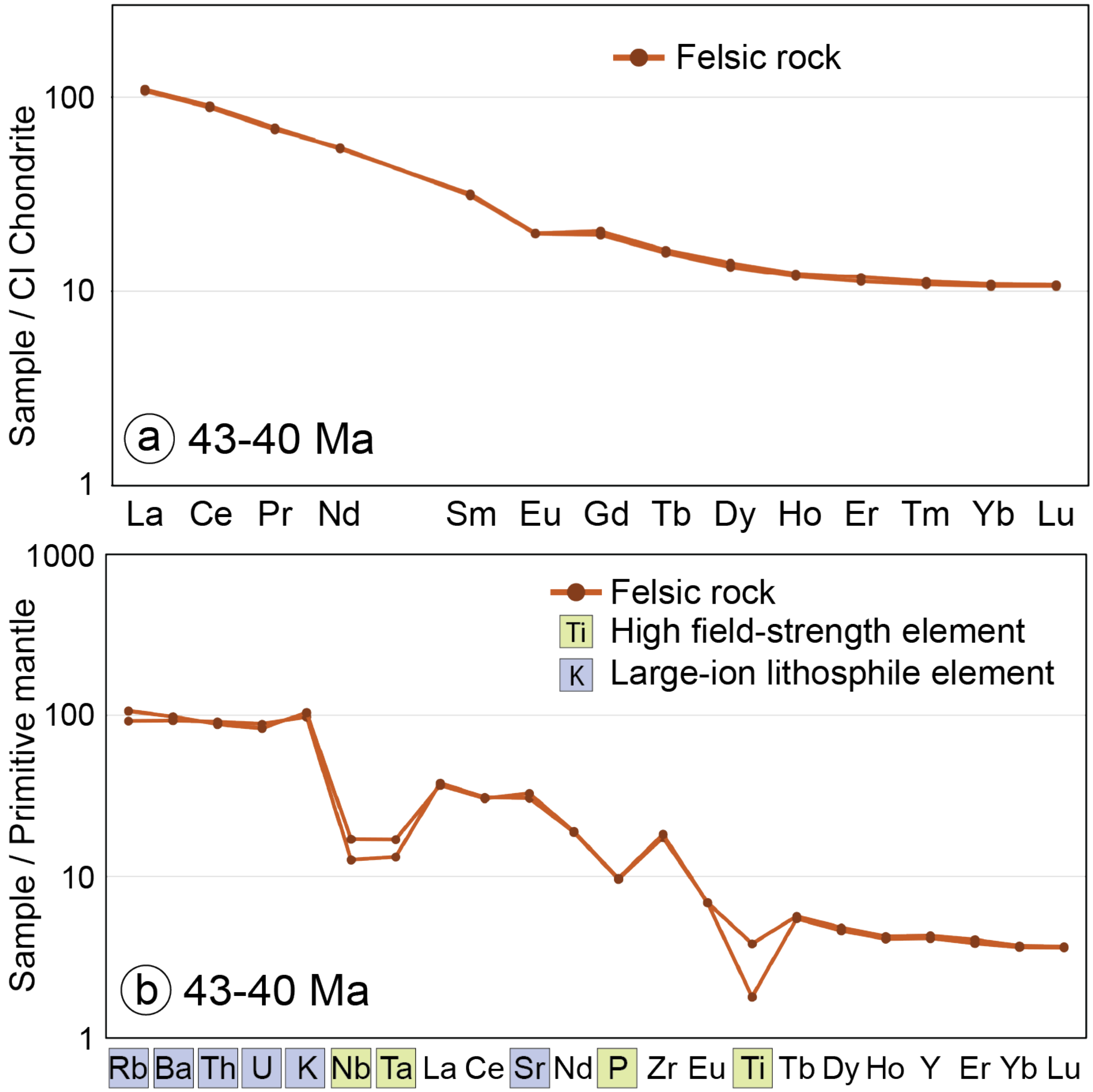
Felsic rock
Sample / CI Chondrite
100
10
1
a 43-40 Ma
La Ce Pr Nd Sm Eu Gd Tb Dy Ho Er Tm Yb Lu
1000
Felsic rock
Ti High field-strength element
K Large-ion lithosphile element
Sample / Primitive mantle
100
10
1
b 43-40 Ma
Rb Ba Th U K Nb Ta La Ce Sr Nd P Zr Eu Ti Tb Dy Ho Y Er Yb Lu

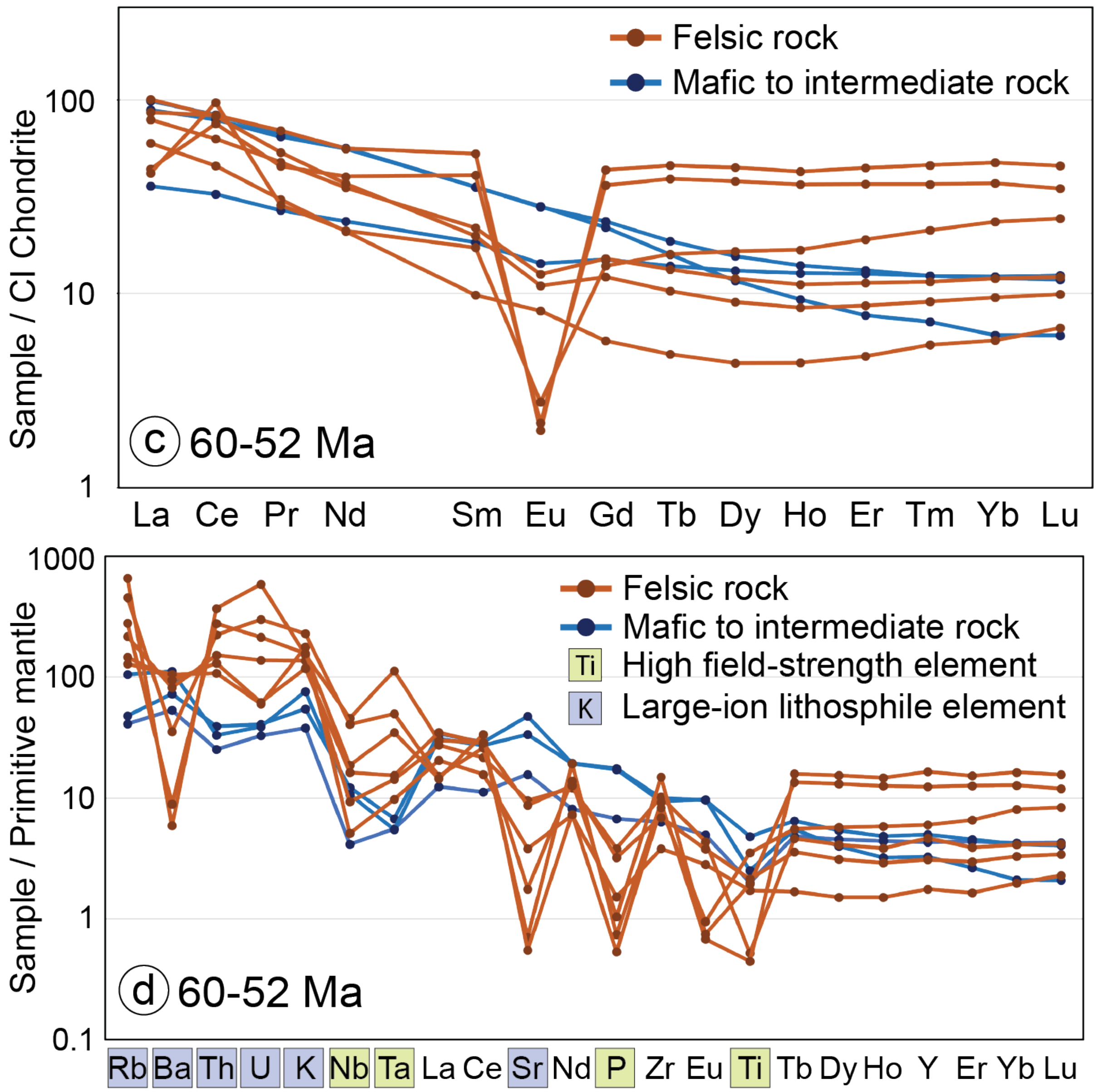
Felsic rock
Mafic to intermediate rock
Sample / CI Chondrite
100
10
1
c 60-52 Ma
La Ce Pr Nd Sm Eu Gd Tb Dy Ho Er Tm Yb Lu
1000
100
10
1
0.1
Sample / Primitive mantle
Felsic rock
Mafic to intermediate rock
Ti High field-strength element
K Large-ion lithosphile element
d 60-52 Ma
Rb Ba Th U K Nb Ta La Ce Sr Nd P Zr Eu Ti Tb Dy Ho Y Er Yb Lu

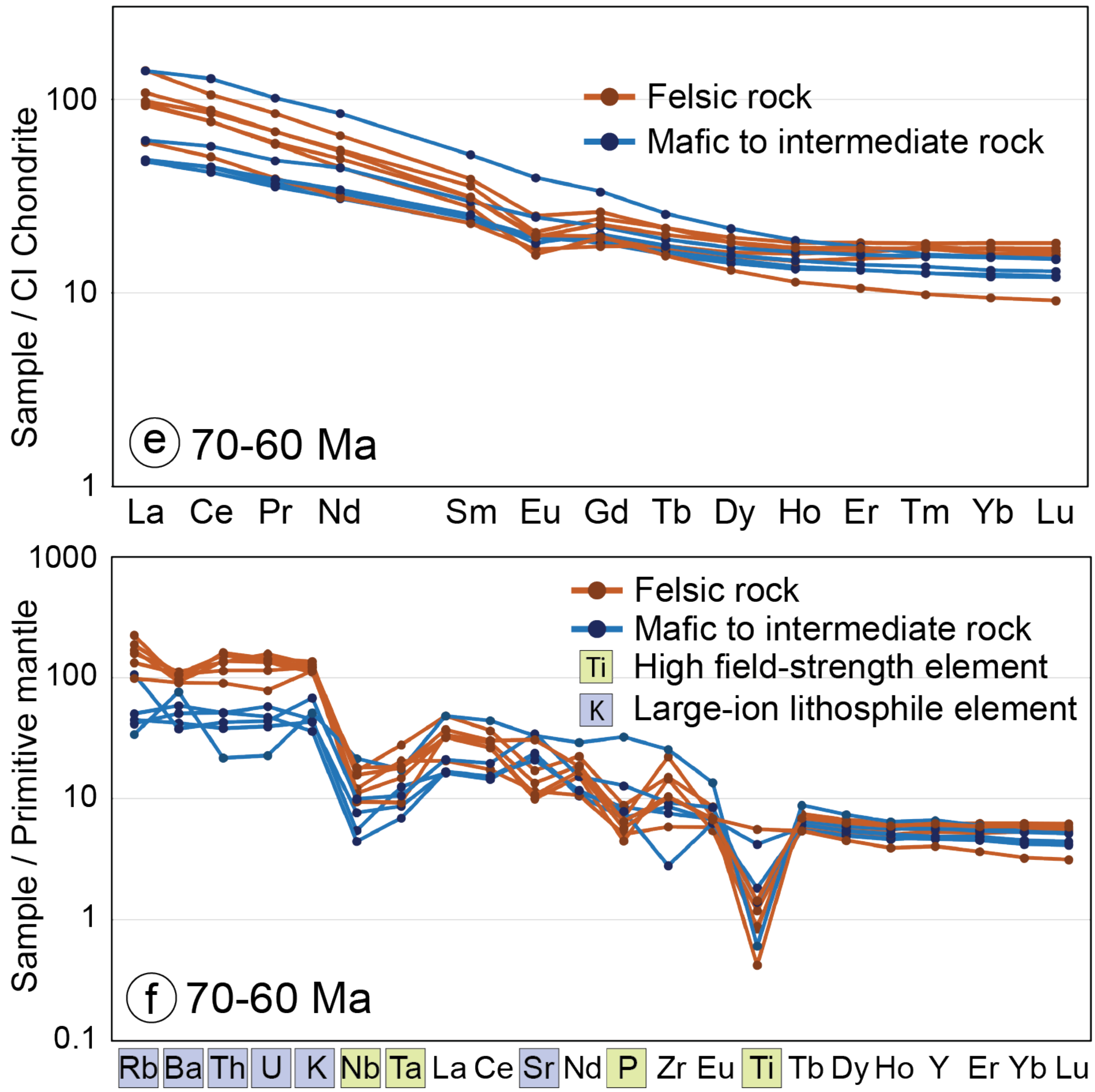
Felsic rock
Mafic to intermediate rock
Sample / CI Chondrite
100
10
1
e 70-60 Ma
La Ce Pr Nd Sm Eu Gd Tb Dy Ho Er Tm Yb Lu
1000
Felsic rock
Mafic to intermediate rock
Ti High field-strength element
K Large-ion lithophile element
Sample / Primitive mantle
100
10
1
0.1
f 70-60 Ma
Rb Ba Th U K Nb Ta La Ce Sr Nd P Zr Eu Ti Tb Dy Ho Y Er Yb Lu

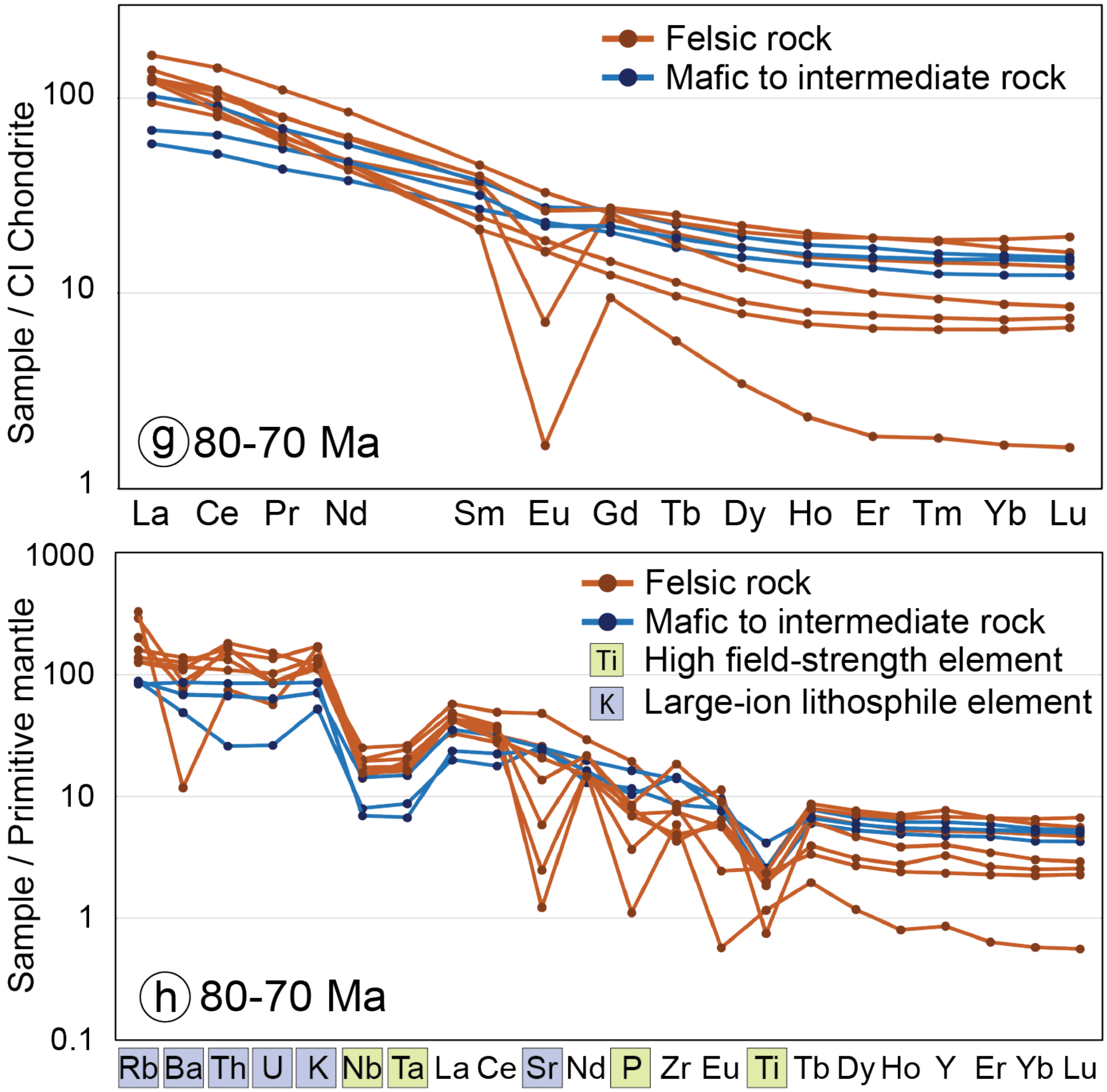

Felsic rock
Mafic to intermediate rock
Sample / CI Chondrite
100
10
1
g 80-70 Ma
La Ce Pr Nd Sm Eu Gd Tb Dy Ho Er Tm Yb Lu
1000
Felsic rock
Mafic to intermediate rock
Ti High field-strength element
K Large-ion lithosphile element
Sample / Primitive mantle
100
10
1
0.1
h 80-70 Ma
Rb Ba Th U K Nb Ta La Ce Sr Nd P Zr Eu Ti Tb Dy Ho Y Er Yb Lu

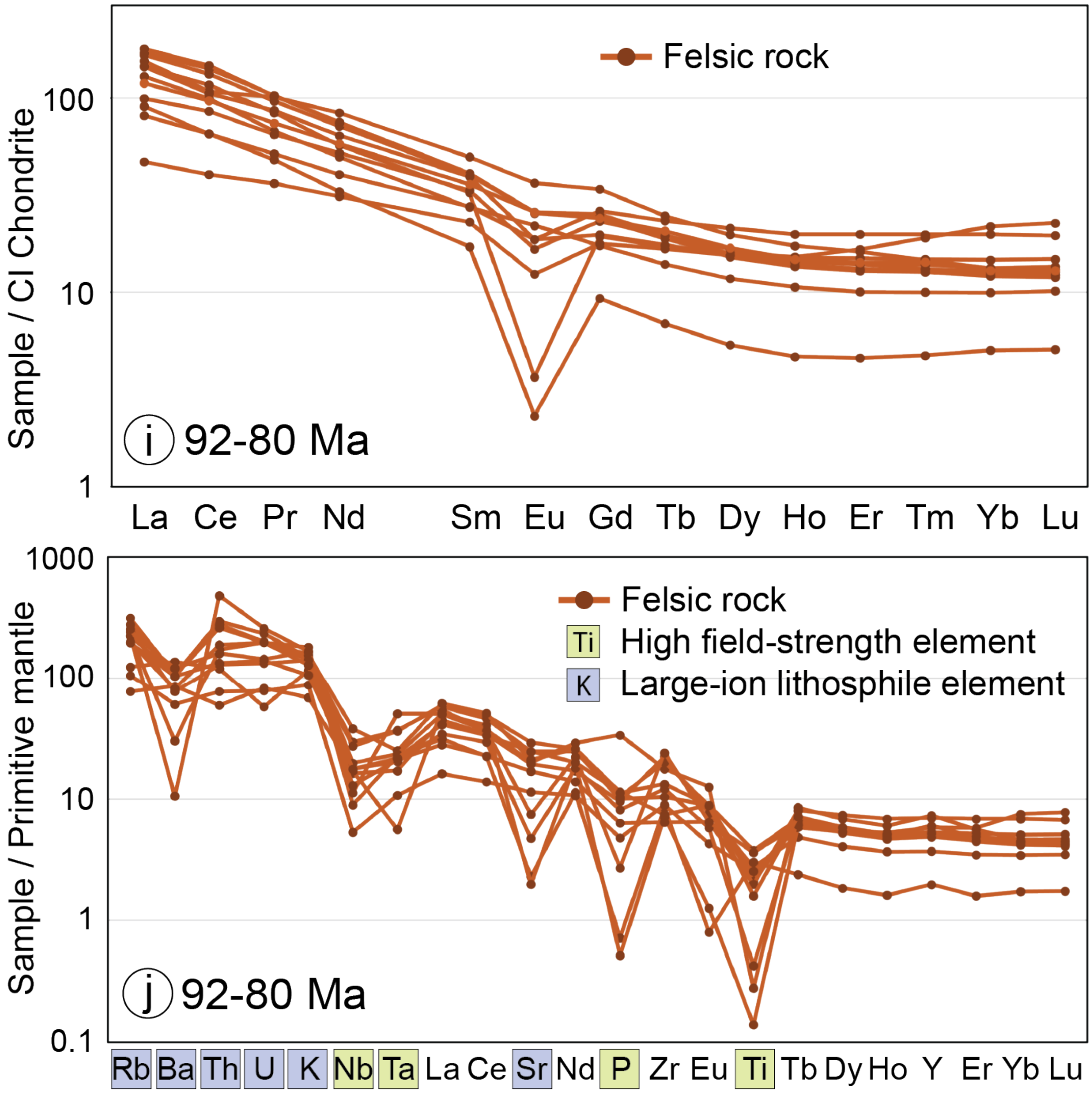

Felsic rock
Sample / CI Chondrite
100
10
1
i 92-80 Ma
La Ce Pr Nd Sm Eu Gd Tb Dy Ho Er Tm Yb Lu
1000
100
10
1
0.1
Sample / Primitive mantle
Felsic rock
Ti High field-strength element
K Large-ion lithosphile element
j 92-80 Ma
Rb Ba Th U K Nb Ta La Ce Sr Nd P Zr Eu Ti Tb Dy Ho Y Er Yb Lu

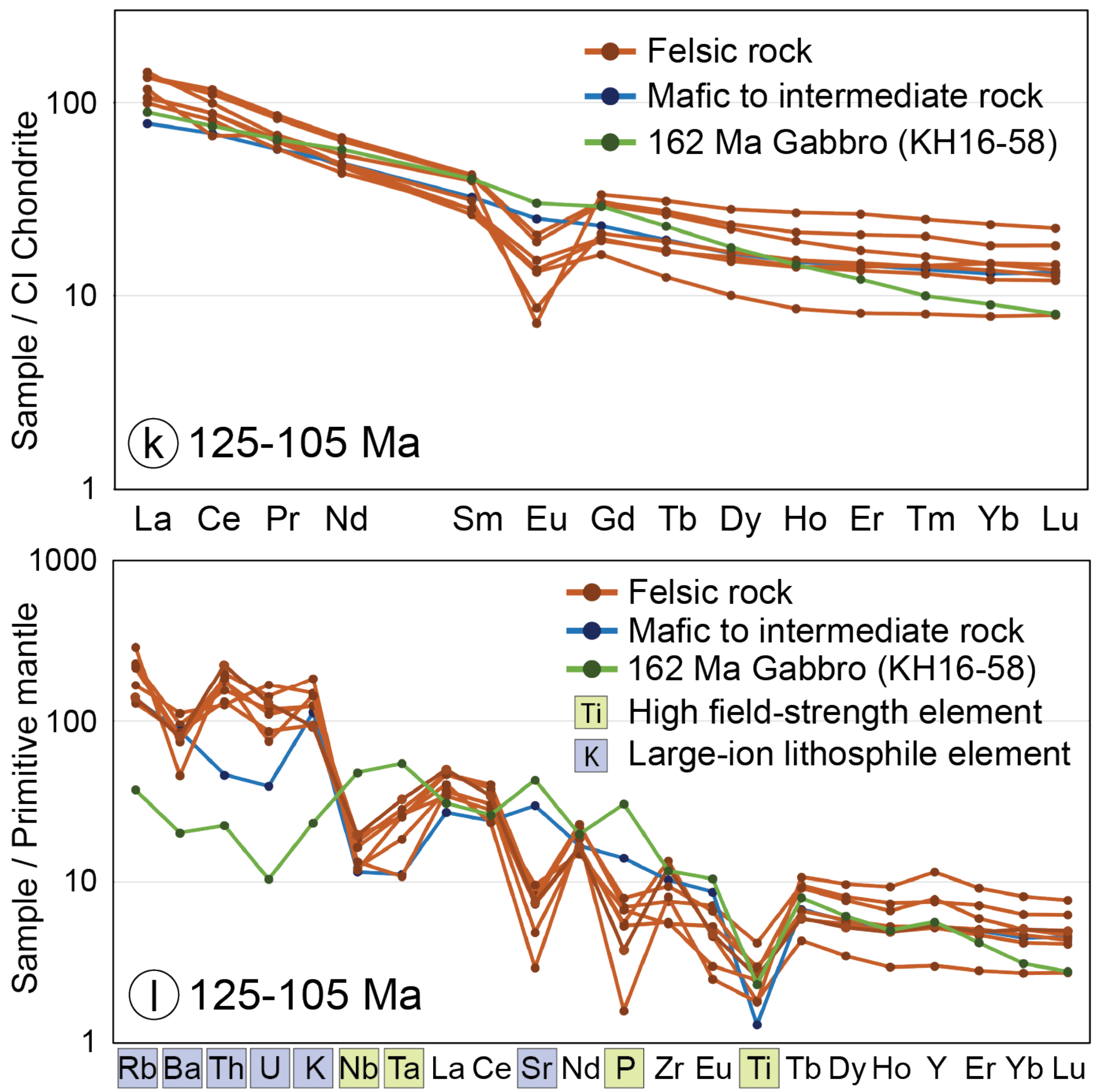
Felsic rock
Mafic to intermediate rock
162 Ma Gabbro (KH16-58)
Sample / CI Chondrite
100
10
1
k 125-105 Ma
La Ce Pr Nd Sm Eu Gd Tb Dy Ho Er Tm Yb Lu
1000
Felsic rock
Mafic to intermediate rock
162 Ma Gabbro (KH16-58)
Ti High field-strength element
K Large-ion lithosphile element
Sample / Primitive mantle
100
10
1
l 125-105 Ma
Rb Ba Th U K Nb Ta La Ce Sr Nd P Zr Eu Ti Tb Dy Ho Y Er Yb Lu

4.3.3 Whole-rock Nd-Hf isotopic composition

Whole-rock initial $^{143}Nd/^{144}Nd$ and $^{176}Hf/^{177}Hf$ ratios are calculated from the measured ratios using $^{147}Sm/^{144}Nd$ = (Sm/Nd) /1.645, $^{176}Lu/^{177}Hf$ = (Lu/Hf) /1.992 (Allègre, 2008), $\lambda^{147}Sm = 6.54\times10^{-12}\ y^{-1}$ (DePaolo and Wasserburg, 1976) and $\lambda^{176}Lu = 1.867\times10^{-11}\ y^{-1}$ (Söderlund et al., 2004), and expressed as εNd(t) and εHf(T) values that compare the initial ratios of samples with those of a chondritic reservoir (CHUR) (Blichert-Toft and Albarède, 1997; Jacobsen and Wasserburg, 1980) at the igneous age time determined by U-Pb zircon chronology. The igneous rock samples yield a range of εNd(t) = -6.6 to +5.5 and εHf(T) = -0.8 to 12.8 (Fig. 4.7) that generally lie along a terrestrial Nd-Hf isotopic array (Vervoort and Blichert-Toft, 1999; Vervoort et al., 2000).

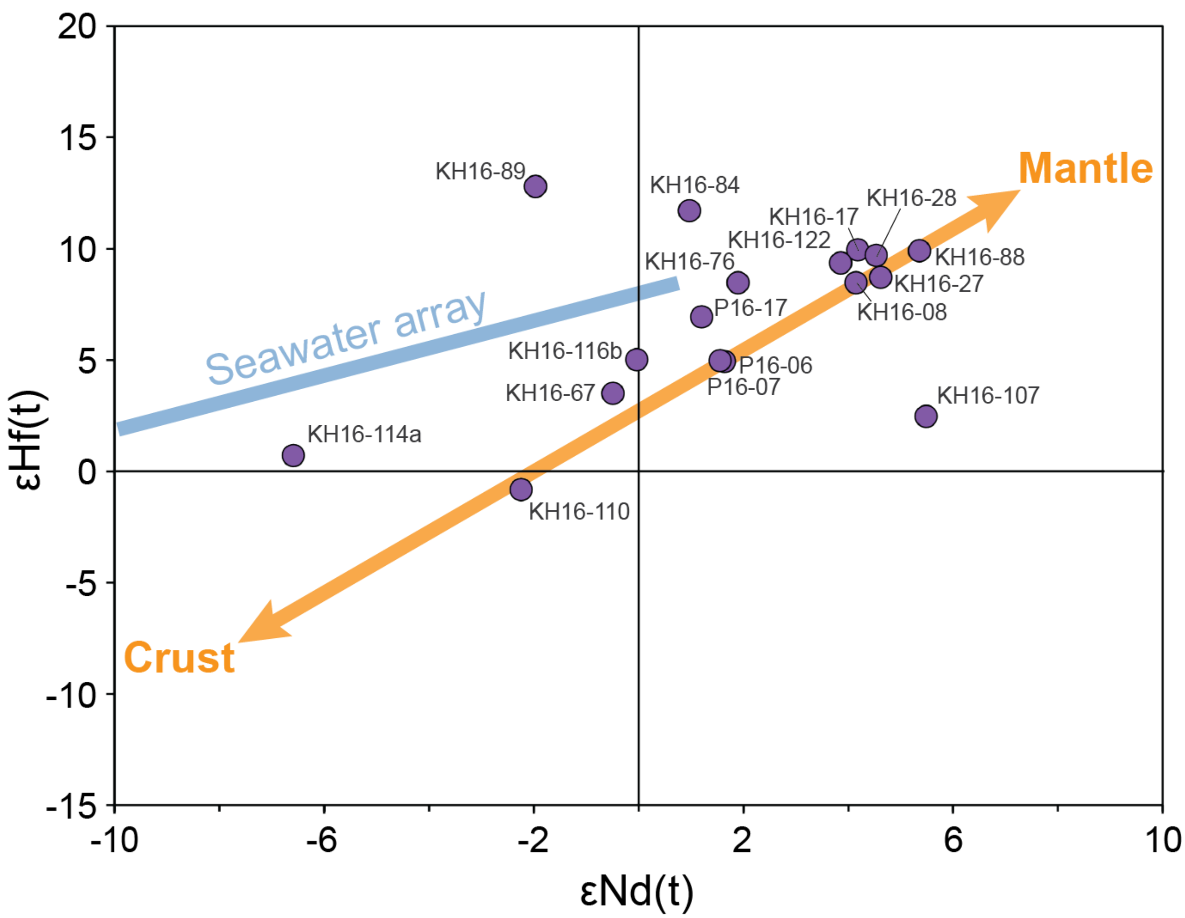

Figure 4. 7 Whole-rock Nd-Hf isotopic composition of rock samples in this study.

Mantle-crust terrestrial array and seawater array after Vervoort et al. (1999) and Alberede et al. (1998). This plot shows the studied igneous rocks generally have depleted Nd-Hf isotopic composition with εNd(t) = -6.6 to +5.5 and εHf(T) = -0.8 to 12.8. See Appendix D for detailed results.

4.4 Discussion

4.4.1 A summary of Sikhote-Alin igneous activity

4.4.1.1 General review

The Cretaceous to Cenozoic igneous rocks occupy a ~1500 km wide margin along the Sikhote-Alin area, Russian Far East (Fig. 4.1). Their significant implications for NW Pacific geodynamics and NE Asia continental crust evolution have been discussed in previous studies (Grebennikov and Popov, 2014; Grebennikov et al., 2016; Jahn et al., 2015; Khanchuk et al., 2019; Khanchuk et al., 2016; Khanchuk et al., 2013; Tang et al., 2016; Wu and Wu, 2019). However, previous U-Pb zircon age and geochemical constraints for the igneous rocks mainly came from the southernmost Sikhote-Alin margin (~500 km width) (light blue triangles in Fig. 4.1). The rocks along a ~1000 km margin to the north are essentially unstudied (Fig. 4.1). Here we combine published data from the southern Sikhote-Alin and our new results for the northern Sikhote-Alin igneous rocks (purple triangles in Fig. 4.1) into a spatiotemporal zircon U-Pb age record (Fig. 4.8, 4.9) and a whole-rock igneous geochemistry database (Fig. 4.10) to discuss a more complete history of magmatic evolution in Sikhote-Alin.

A zircon U-Pb age-constrained 150 to 40 Ma spatiotemporal magmatic record for Sikhote-Alin (Fig. 4.8, 4.9) was compiled by merging our new results (n= 84, Table 4.1) and published data (n=61) (Jahn et al., 2015; Tang et al., 2016; Tsutsumi et al., 2016; Wu et al., 2017b; Zhao et al., 2017). For this compilation, we exclude our 9 samples of volcaniclastics

Figure 4. 8 Spatial distribution of igneous activity in Sikhote-Alin, Sakhalin, and Hokkaido constrained by U-Pb zircon chronology.

The U-Pb zircon age database is our compilation of results from this study (n=84) and other published data (n=61) (Alexandrov et al., 2018; Jahn et al., 2014; 2015; Liao et al., 2018; Tang et al., 2016; Tsutsumi et al., 2016; Wu et al., 2017b; Zhao et al., 2017; 2018).

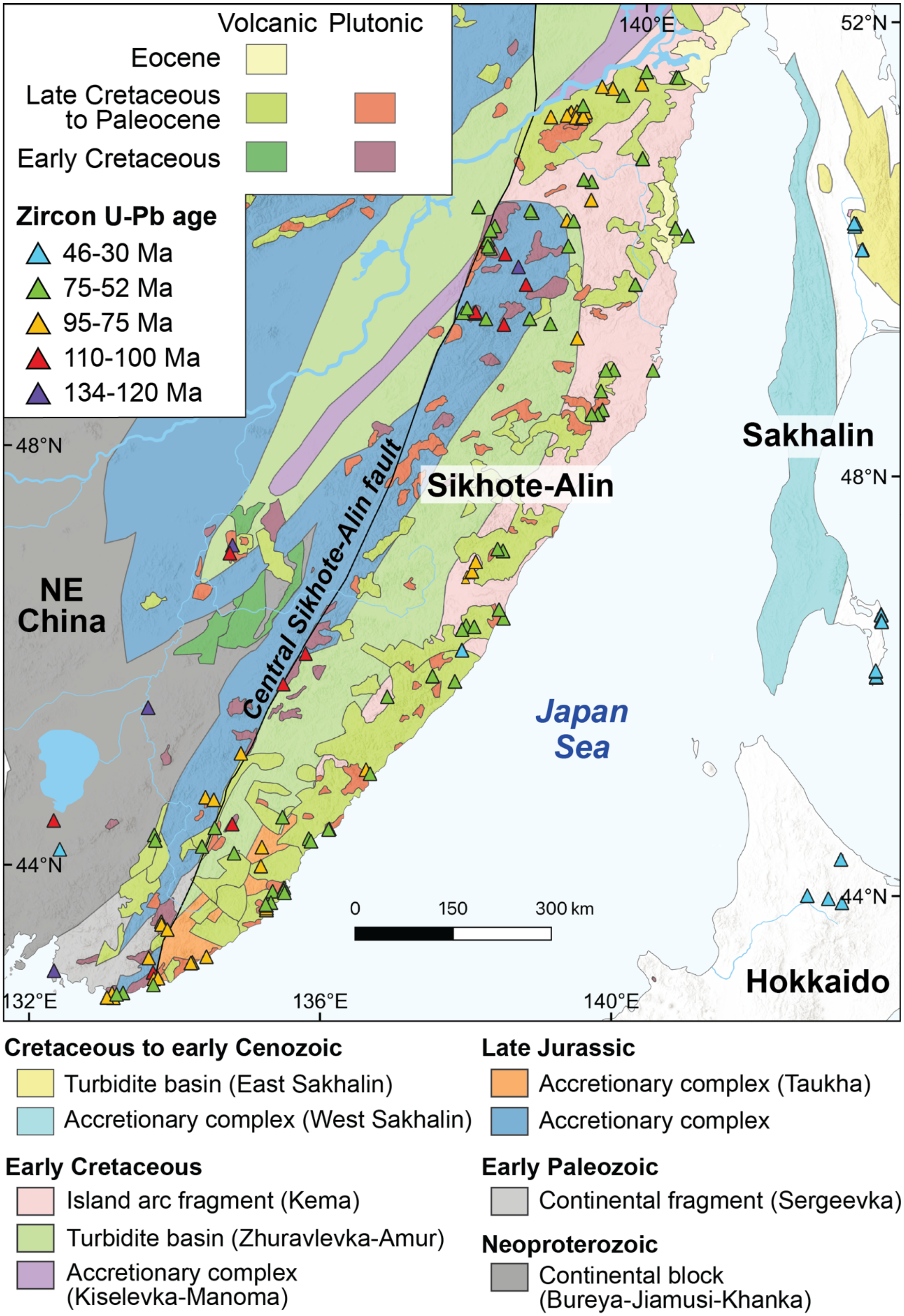
Volcanic
Plutonic
Eocene
Late Cretaceous to Paleocene
Early Cretaceous
Zircon U-Pb age
46-30 Ma
75-52 Ma
95-75 Ma
110-100 Ma
134-120 Ma
140°E
52°N
48°N
44°N
132°E
136°E
NE China
Sikhote-Alin
Central Sikhote-Alin fault
Sakhalin
Japan Sea
Hokkaido
0
150
300 km
Cretaceous to early Cenozoic
Turbidite basin (East Sakhalin)
Accretionary complex (West Sakhalin)
Early Cretaceous
Island arc fragment (Kema)
Turbidite basin (Zhuravlevka-Amur)
Accretionary complex (Kiselevka-Manoma)
Late Jurassic
Accretionary complex (Taukha)
Accretionary complex
Early Paleozoic
Continental fragment (Sergeevka)
Neoproterozoic
Continental block (Bureya-Jiamusi-Khanka)

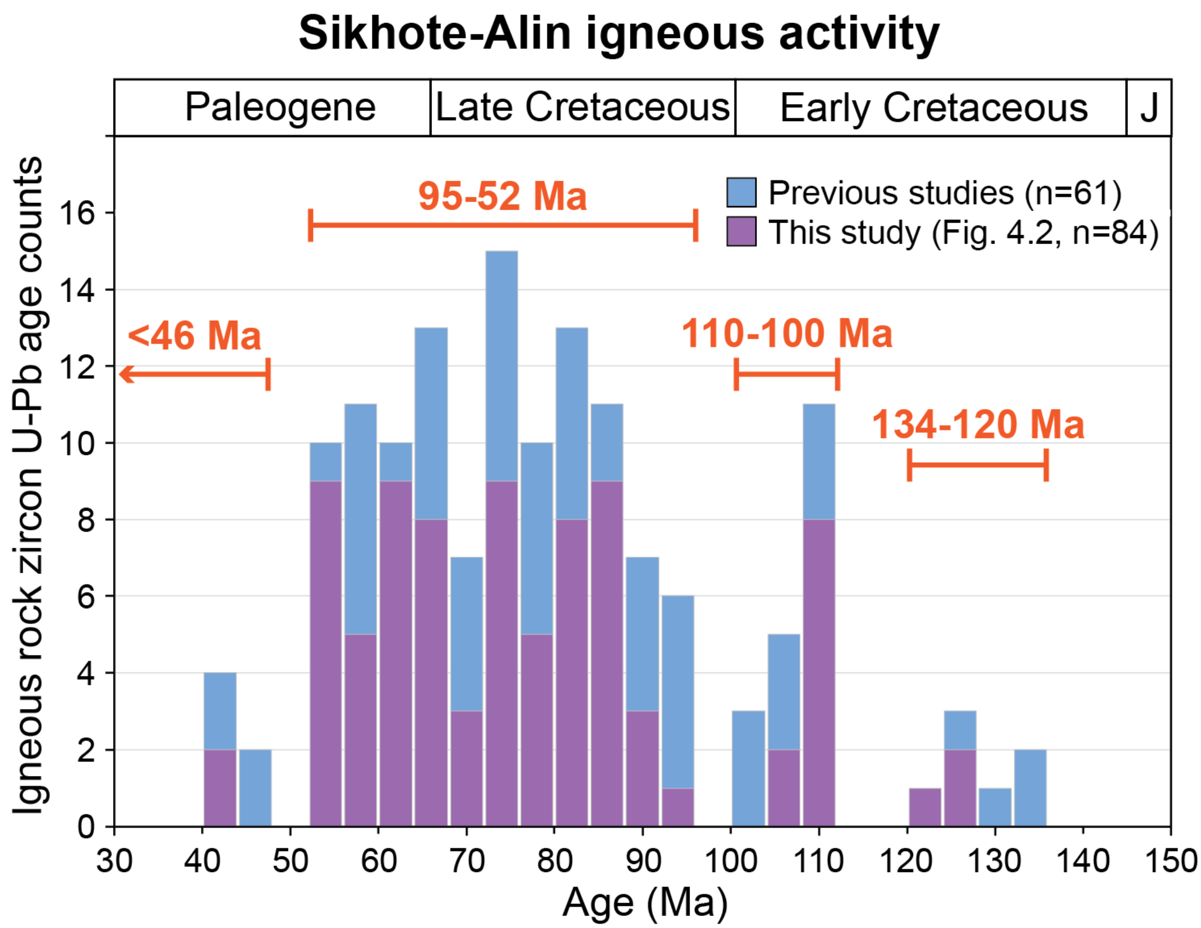

Figure 4. 9 Temporal distribution of Sikhote-Alin igneous activity constraint by U-Pb zircon chronology.

We separate the igneous activity into four groups based on the >4 Ma gaps in U-Pb zircon ages. See Fig. 4.1 for the locations of the dated igneous rocks in previous and this study.

Figure 4. 10 Chemical-temporal evolution of Sikhote-Alin igneous activity.

(a) the modified alkali-lime index diagram (Frost and Frost, 2008), (b) Ta/Yb vs. Th/Yb diagram (Gorton and Schandl, 2000). (c) Y+Nb vs. Rb tectonic discrimination diagram for plutonic rock (Pearce et al., 1984), (d) Th-Hf-Ta tectonic discrimination diagram for mafic rocks (Wood, 1980). (e) Igneous age vs. A/CNK diagram with a S- and I-type granites discrimination following (Chappell and White, 1992). (f) Age vs. Nd isotopic composition plot of igneous rocks in northern and southern Sikhote-Alin. Samples are color-coded by their location either north or south of 48°N latitudes. The plot reveals a general contrast in isotopic compositions between northern and southern Sikhote-Alin across 48°N.

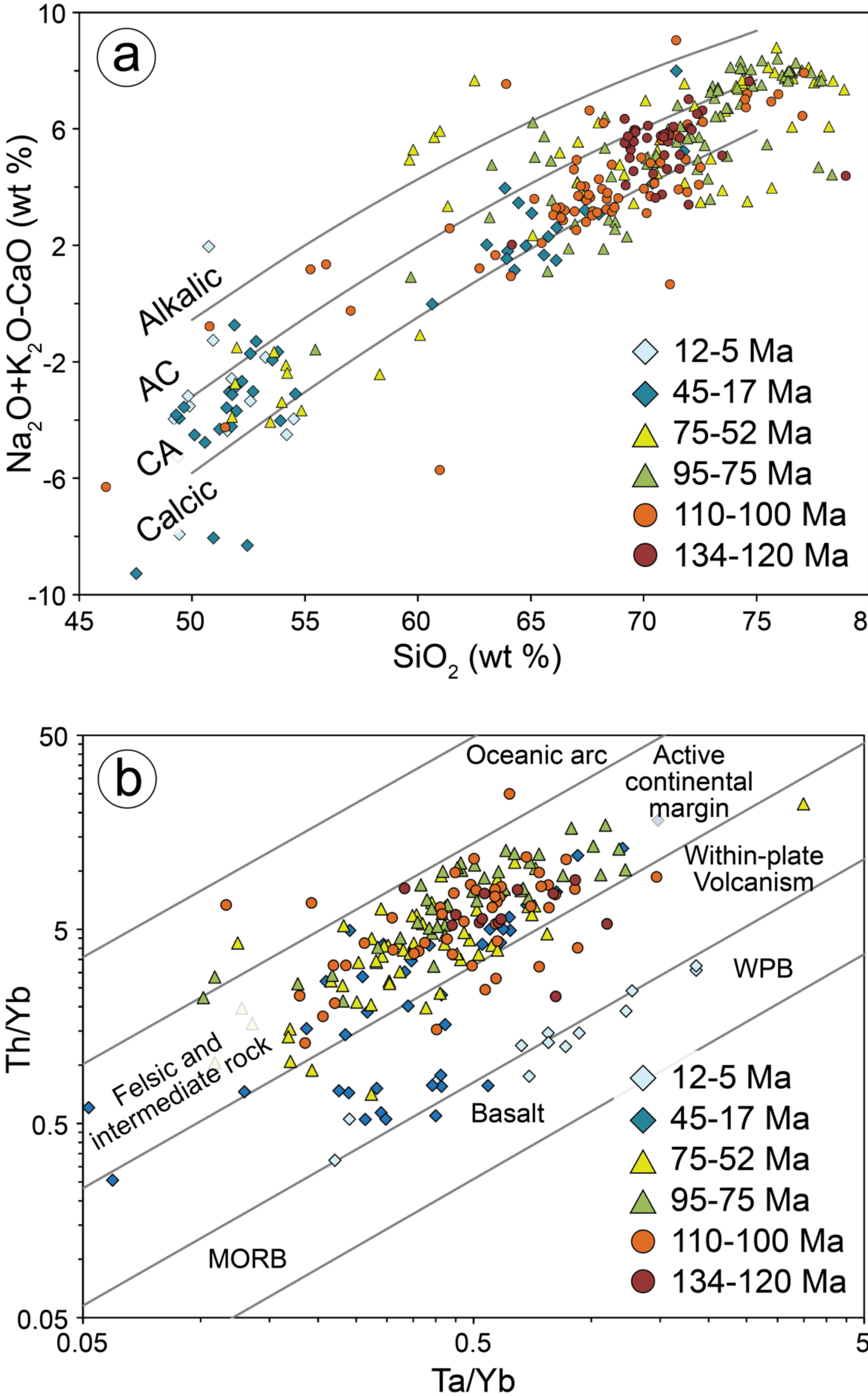

a
Alkalic
AC
CA
Calcic
12-5 Ma
45-17 Ma
75-52 Ma
95-75 Ma
110-100 Ma
134-120 Ma
Na_2O+K_2O-CaO (wt %)
SiO_2 (wt %)
10
6
2
-2
-6
-10
45
50
55
60
65
70
75
80
b
Oceanic arc
Active continental margin
Within-plate Volcanism
WPB
Felsic and intermediate rock
Basalt
MORB
12-5 Ma
45-17 Ma
75-52 Ma
95-75 Ma
110-100 Ma
134-120 Ma
Th/Yb
Ta/Yb
50
5
0.5
0.05
0.05
0.5
5

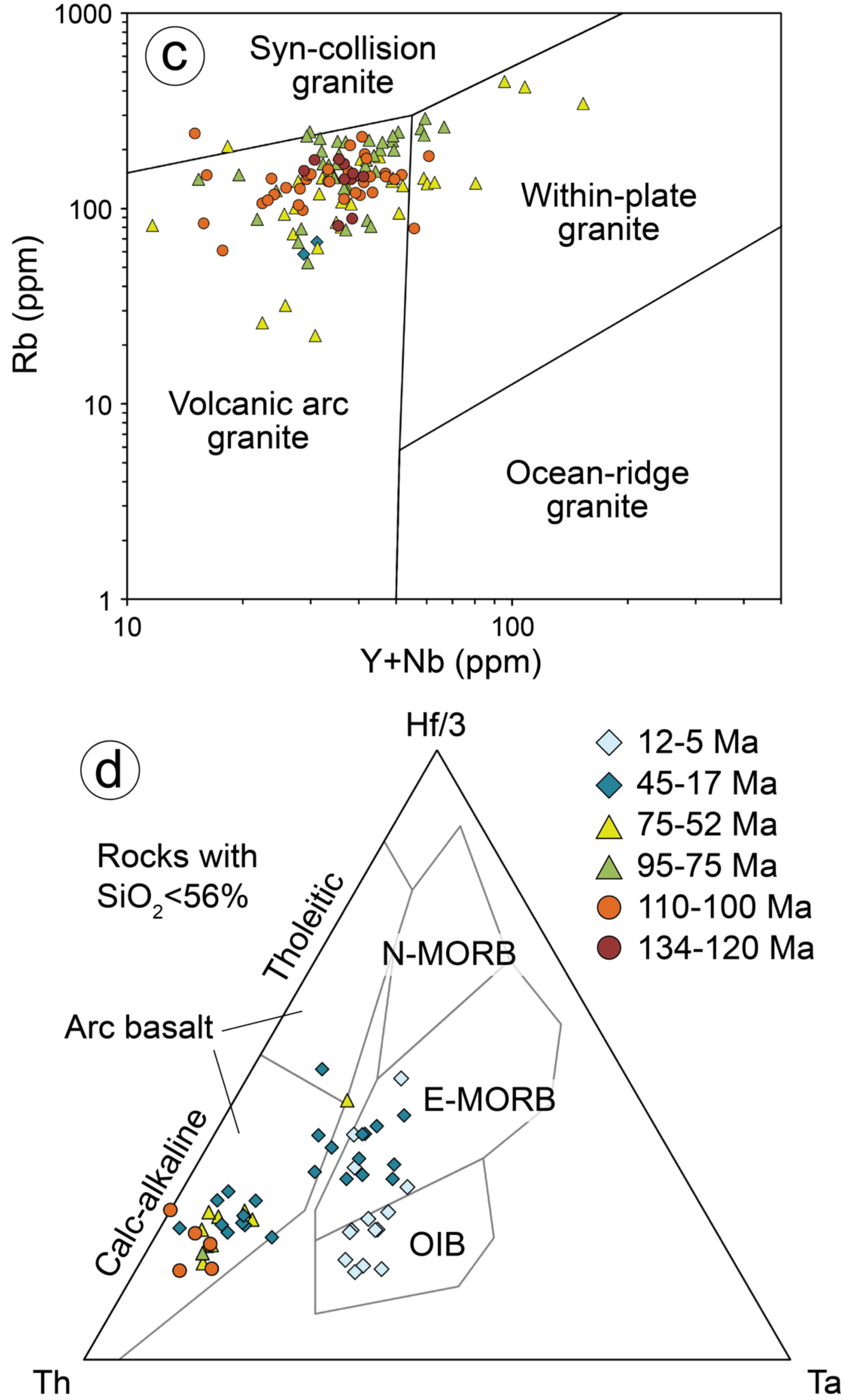
c
Syn-collision granite
Within-plate granite
Volcanic arc granite
Ocean-ridge granite
Rb (ppm)
Y+Nb (ppm)
1000
100
10
1
10
100
d
Hf/3
Th
Ta
Rocks with SiO_2<56%
Tholeitic
Calc-alkaline
Arc basalt
N-MORB
E-MORB
OIB
12-5 Ma
45-17 Ma
75-52 Ma
95-75 Ma
110-100 Ma
134-120 Ma

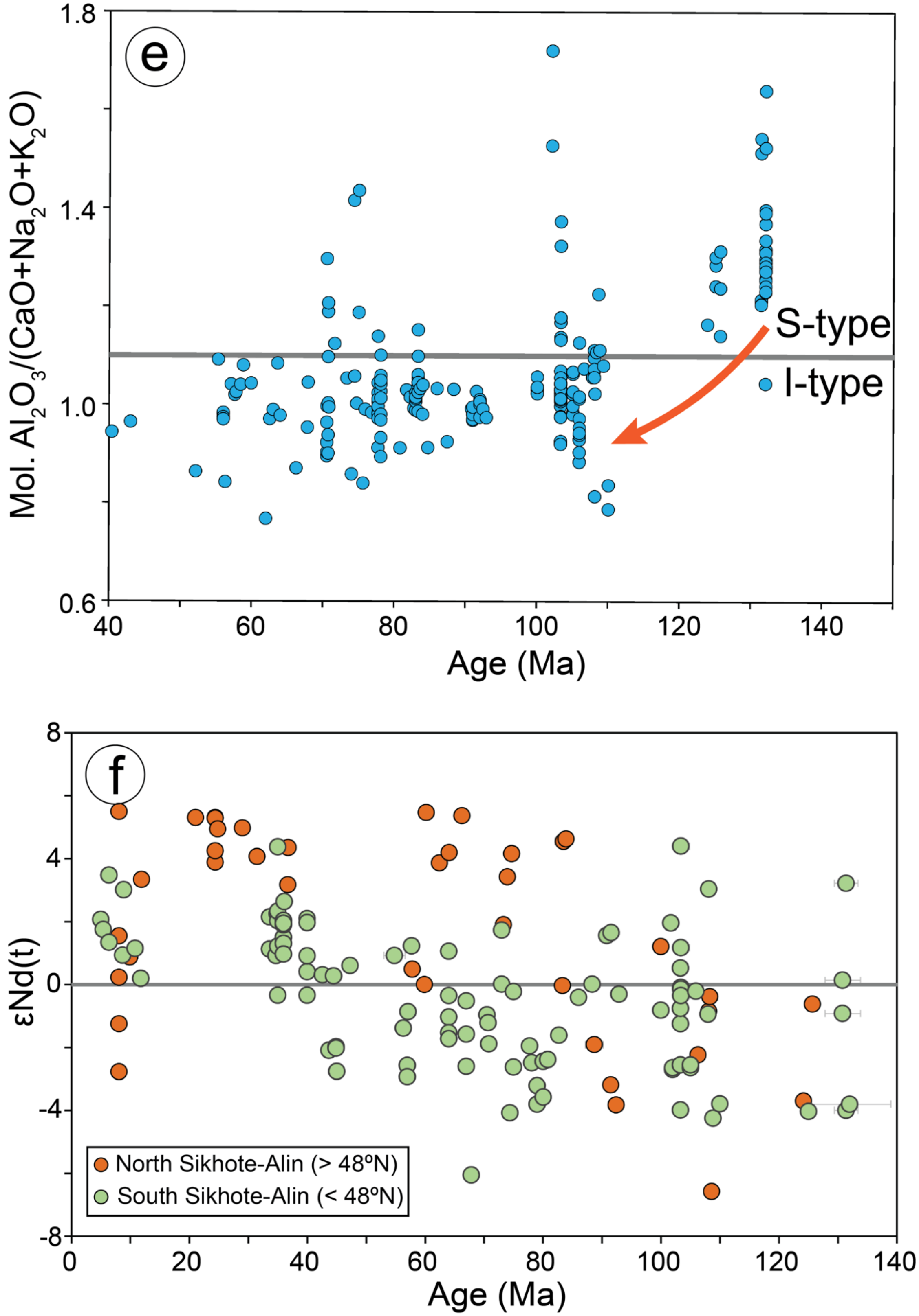

e
Mol. Al2O3/(CaO+Na2O+K2O)
S-type
I-type
Age (Ma)
f
εNd(t)
North Sikhote-Alin (> 48ºN)
South Sikhote-Alin (< 48ºN)
Age (Ma)

for they may not represent in situ record, and one sample dated 160 Ma because it does not fit within our age window. The record reveals 4 episodes of Sikhote-Alin igneous activity: (1) 134-120 Ma, (2) 110-100 Ma, (3) 95-52 Ma, and (4) <46 Ma, based on the >4 Ma gaps in the U-Pb ages (Fig. 4.9).

The newly compiled whole-rock geochemistry database for 134 to 5 Ma Sikhote-Alin igneous rocks (n=361, Fig. 4.10) includes our new data (Appendix C) and published data (Belyansky et al., 2011; Gonevchuk et al., 2011; Gvozdev, 2010; Jahn et al., 2015; Khanchuk et al., 2008; Kruk et al., 2014; Okamura et al., 2004; Tang et al., 2016; Valuy, 2014; Wu et al., 2017b; Zhao et al., 2017). Ages are constrained by the 145 compiled zircon U-Pb ages in this study (Fig. 4.8, 4.9), 32 whole-rock K-Ar ages (Chekryzhov et al., 2010; Okamura et al., 1998), 2 biotite K-Ar ages (Gonevchuk et al., 2011; Gonevchuk et al., 2015), and a muscovite K-Ar age (Sato et al., 2006). The record reveals the 134 to 52 Ma igneous rocks generally show calc-alkalic characteristics (Fig. 4.10a) and magmatic arc signature (Fig. 4.10b-d), i.e., enrichment in Th, Rb, and other large-ion lithophile element elements (LILE) relative to Ta, Hf, Y, Nb, and other high field strength elements (HFSE) (Pearce, 2003; Pearce et al., 1984; Wood, 1980). In comparison, the younger 45 to 5 Ma Sikhote-Alin igneous rocks have a more complicated chemical composition, that shows active margin signatures and E-MORB and OIB signatures (Fig. 4.10b, d). These could be generated from an intra-plate setting, including all basalts with ages younger than 15 Ma (Okamura et al., 2004).

Some Sikhote-Alin igneous rocks with age 132 to 98 Ma and 46 to 39 Ma have adakitic signature (i.e., Sr/Y>40, La/Yb>20) (Defant and Drummond, 1990; Moyen, 2009). This has been shown in previous studies (Chashchin et al., 2011; Wu et al., 2017b). On the contrary, the 125-105 Ma and 46-38 Ma samples in this study have moderate Sr/Y=1 to 33, La/Yb= 7 to 19, and Eu depletion (Fig. 4.6, Appendix D) like typical arc magmatic rocks. This reveals the complexity of Sikhote-Alin igneous activity during the early Cretaceous and late Eocene, with both adakitic rocks and typical arc rocks generated simultaneously.

When using the S-I-A alphabet classification scheme (Chappell and White, 2001; Frost et al., 2001; Whalen et al., 1987) to classify the Sikhote-Alin plutonic rocks, nearly all the 134 to 120 Ma rocks were identified as S-type granites, by their A/CNK >1.1 (Fig. 4.10e), average Na_2O = 3.3%, restricted SiO_2 variation with 70.9 wt.% average and 1σ = 2.1 wt.% (n=39) (red circles in Fig. 4.10a). In comparison, most of the 110 to 52 Ma and 42 to 37 Ma plutonic rocks are I-type granites that have A/CNK <1.1 (Fig. 4.10e), higher average Na_2O = 3.6%, CIPW corundum <1% (Appendix D), and a broader spectrum of SiO_2 with 69.2 wt.% in average and 1σ = 6.4 wt.% (n=221) (Fig. 4.10a). Among the 110 to 52 Ma I-type granites (Fig. 4.10e, 10a) (Jahn et al., 2015; Tang et al., 2016; Zhao et al., 2017), some of 65 to 52 Ma felsic plutonic rocks also show high Fe/Mg, Ga/Al and slight enrichment in HFSE (e.g. Zr, Nb, Y and rare-earth elements like Ce). These may identify as A-type granite (Fig. 4.11a, b) (Grebennikov and Maksimov, 2021; Grebennikov and Popov, 2014; Grebennikov et al., 2016), and the "within-plate granite" in the Y+Nb vs. Rb plot (Fig. 4.10c). The A-type granites are significant for they are mostly associated with anorogenic/ post-orogenic/ extensional environments (Loiselle and Wones, 1979; Martin, 2006) (although not necessarily, according to Bonin, 2007; King et al., 1997; Whalen et al., 1987). However, it is not always straightforward to distinguish between A-type granite and highly fractionated I-type granite from their chemical signature (Bonin, 2007; Whalen et al., 1987; Wu et al., 2017a). We will discuss the petrogenesis of the 65 to 52 Ma felsic rocks in Section 4.4.1.3.

4.4.1.2 Late Cretaceous to early Eocene (95-52 Ma) highly evolved magmatism in Sikhote-Alin

Late Cretaceous to early Cenozoic (95 to 52 Ma) Sikhote-Alin magmatic arc shows a significantly higher average SiO_2= 70.0 wt.% (1σ = 6.7, n= 147) when compared to the classic Cordilleran continental arcs that have average SiO_2 from 55.6 to 64.0 wt.% in different areas (Ducea et al., 2015). In addition, the widely-distributed high silica magmatism along the ~1500 km Sikhote-Alin margin persisted for more than 40 Myrs, which is longer than those that have similar average SiO_2 in some areas of the Cordillera, but was limited in occurrence to a maximum of 20 Myrs (Kirsch et al., 2016). Here we discuss the petrogenesis of 95 to 52 Ma high silica magmatic rocks.

Silica saturation (i.e. high silica) in magmatic rocks can either result from the magmatic fractionation in the magma chamber or can be inherited from the source rock. Melting of a quartz-rich fertile sedimentary source rock is the original interpretation for an association of silica and aluminum saturation (i.e., A/CNK >1.1) in S-type granites (Chappell and White, 1992; Chappell and White, 2001), which is consistent with the 134 to120 Ma S-type granites in Sikhote-Alin (average SiO_2= 70.9 wt.%, 1σ = 2.1, n= 39) (Fig. 4.10e). However, the sedimentary source rock generation is inconsistent with the geochemistry of the 95 to 52 Ma

Figure 4. 11 Chemical indicators for magmatic fractionation.

(a) Zr+Nb+Ce+Y vs. FeO*/MgO and (b) 10000×Ga/Al vs. Zr diagrams for putonic rocks (Whalen et al., 1987) with the A-type and I/S-type granite fractionation trend (Wu et al., 2017a) (c) Zr/Hf vs. Nb/Ta and (d) Eu/Eu* vs. Ba plots as an indicator for magmatic differentiation (Bau, 1996; Dostal and Chatterjee, 2000; Wu et al., 2017a). Samples are color-coded by age groupings assigned in Fig. 4.9.

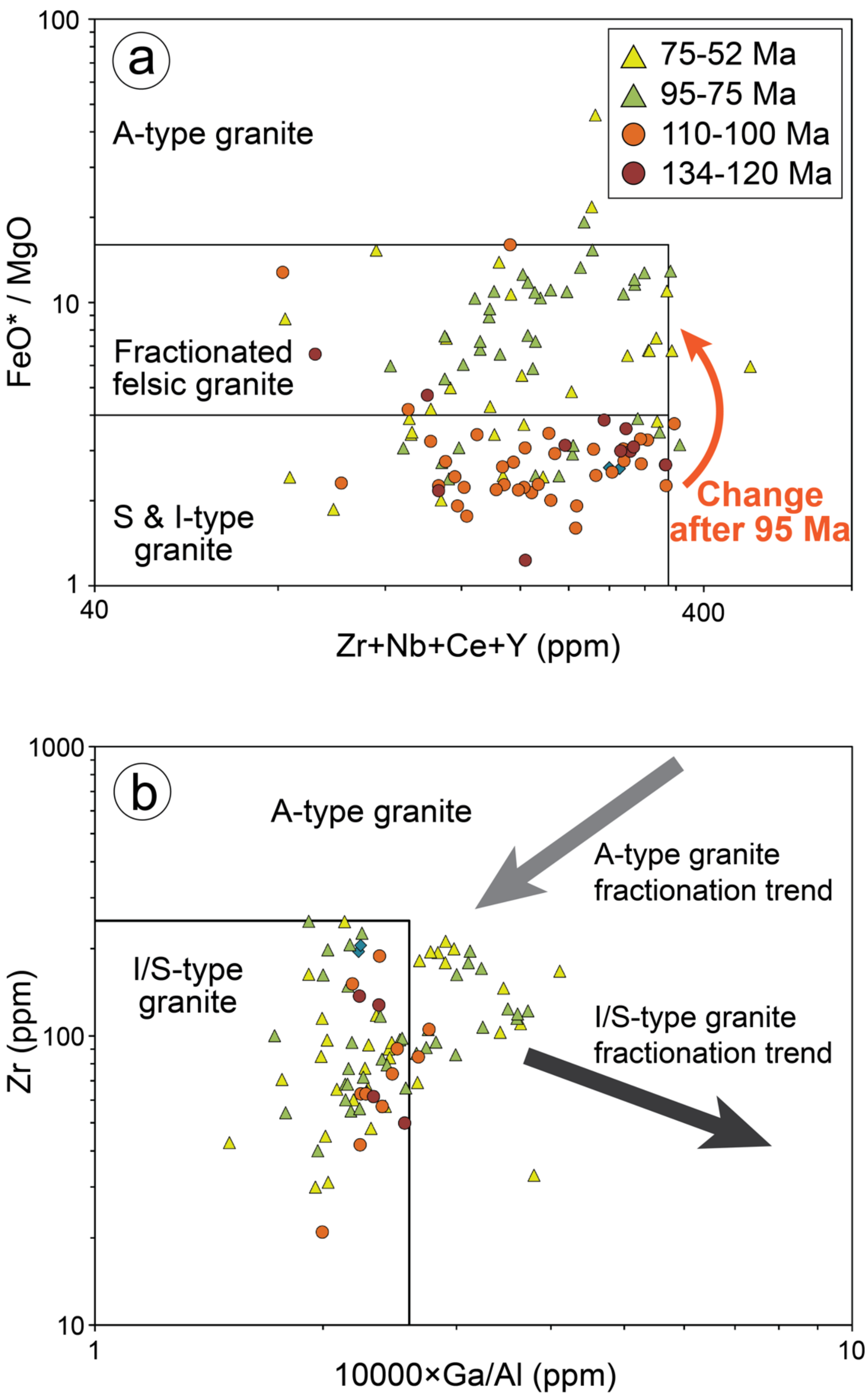
a
75-52 Ma
95-75 Ma
110-100 Ma
134-120 Ma
A-type granite
Fractionated felsic granite
S & I-type granite
Change after 95 Ma
FeO* / MgO
Zr+Nb+Ce+Y (ppm)
100
10
1
40
400
b
A-type granite
A-type granite fractionation trend
I/S-type granite
I/S-type granite fractionation trend
Zr (ppm)
10000×Ga/Al (ppm)
1000
100
10
1
10

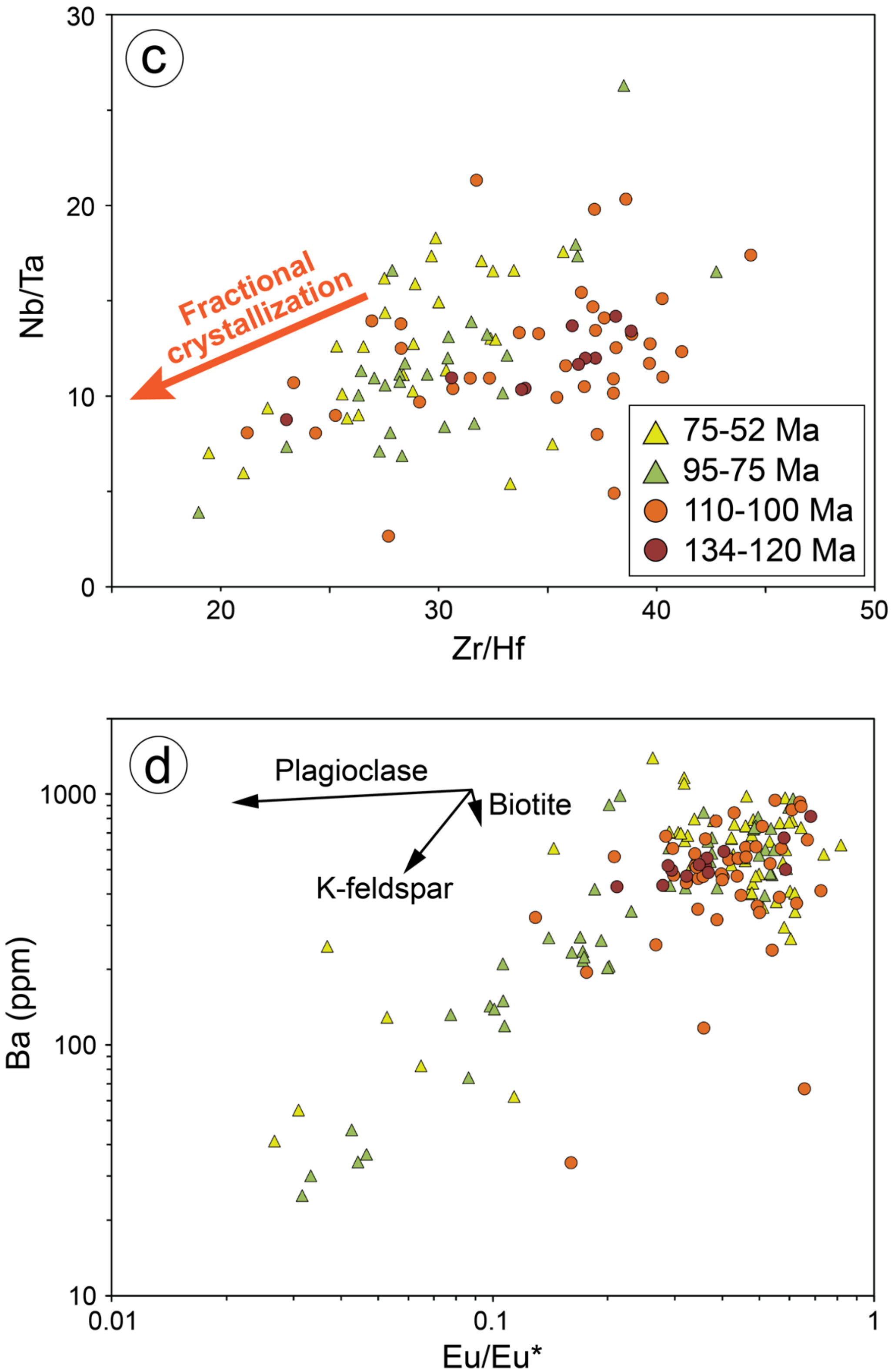
c
30
20
10
0
Nb/Ta
Fractional crystallization
20
30
40
50
Zr/Hf
75-52 Ma
95-75 Ma
110-100 Ma
134-120 Ma
d
Plagioclase
Biotite
K-feldspar
1000
100
10
Ba (ppm)
0.01
0.1
1
Eu/Eu*

granites, for they mainly have I-type signatures that indicate their aluminum undersaturation (i.e., A/CNK <1.1, Fig. 4.10e). Note that among all the 110 to 52 Ma I-type granites in Sikhote-Alin (Fig. 4.10e), the 95 to 52 Ma I-type granites have higher average silica contents (average SiO_2= 70.0 wt.%, 1σ = 6.7, n= 147) compared to the 110 to 100 Ma I-type granites (average SiO_2= 67.6 wt.%, 1σ = 5.6, n= 74).

On the other hand, high silica granites have been interpreted as the residual melt from an extensive crystallization differentiation during storage in crustal magma chamber (Bonin, 1999; Lee and Morton, 2015; Wu et al., 2017a). The extensive magmatic fractionation changes the chemistry of residual melt by increasing in FeO*/MgO and incompatible elements (e.g., Li, K, Rb, and Cs), and decreasing in Nb/Ta, Zr/Hf, compatible elements (e.g., Cr, Ni, and Co), and feldspar-compatible elements (Eu, Sr, and Ba) (Bau, 1996; Dostal and Chatterjee, 2000; Gelman et al., 2014; Lee and Morton, 2015; Miyashiro and Shido, 1975; Wu et al., 2017a). When comparing to the geochemistry of 134 to 100 Ma igneous rocks in Sikhote-Alin, most of the 95 to 52 Ma igneous rocks have higher FeO*/MgO (Fig. 4.11a), lower Zr/Hf, Nb/Ta, Ba, and stronger negative Eu anomaly (i.e. low Eu/Eu*) (Fig. 4.11c, d), which fit a petrogenesis that involves extensive crystallization differentiation in their late-stage magmatic evolution. The decreasing Ba coincides with Eu/Eu* from part of the 95 to 52 Ma igneous rocks (Fig. 4.11d). This indicates the K-feldspar fractionation was the principal process during late-stage feldspar fractionation, since Ba is compatible in K-feldspar but incompatible in plagioclase, whereas Eu is compatible in the two feldspar types (Bachmann et al., 2005; Gelman et al., 2014).

In addition, extensive crystallization differentiation of silica-rich magma requires high temperature or enrichment volatiles to decrease the magma viscosity (Lesher and Spera, 2015). This prevents the elevated silica content and rising viscosity that causes the termination of further magma differentiation (Lee and Morton, 2015; Russell, 2014; Wu et al., 2017a). Although no estimated magma temperature (e.g. zircon saturation temperature) has been reported in Sikhote-Alin, the zircon Th/U might give some indications, since the high Th/U zircons imply their origin from a high-temperature magma without Th-bearing minerals (e.g. monazite or allanite) saturation (Harrison et al., 2007; Kirkland et al., 2015). Therefore, we newly compiled a Sikhote-Alin igneous zircon Th/U database (Fig. 4.12a) that includes numbers calculated from the new zircon U-Pb isotopic dating results (n= 1788, Fig. 4.4) and previous studies (n=729) (Jahn et al., 2015; Zhao et al., 2017). The database reveals the 95 to 52 Ma zircons have a significantly higher average Th/U= 0.96 relative to an average Th/U= 0.58 from the 140 to 100 Ma zircons (Fig. 4.12). Considering the high zircon Th/U corresponds to high zircon saturation temperatures (Harrison et al., 2007; Kirkland et al., 2015), this result could imply hotter 95 to 52 Ma magmatism compared to the 134 to 100 Ma magmatism in Sikhote-Alin. This would further support an interpretation that the 95 to 52 Ma Sikhote-Alin magmatism was highly fractionated under high temperature.

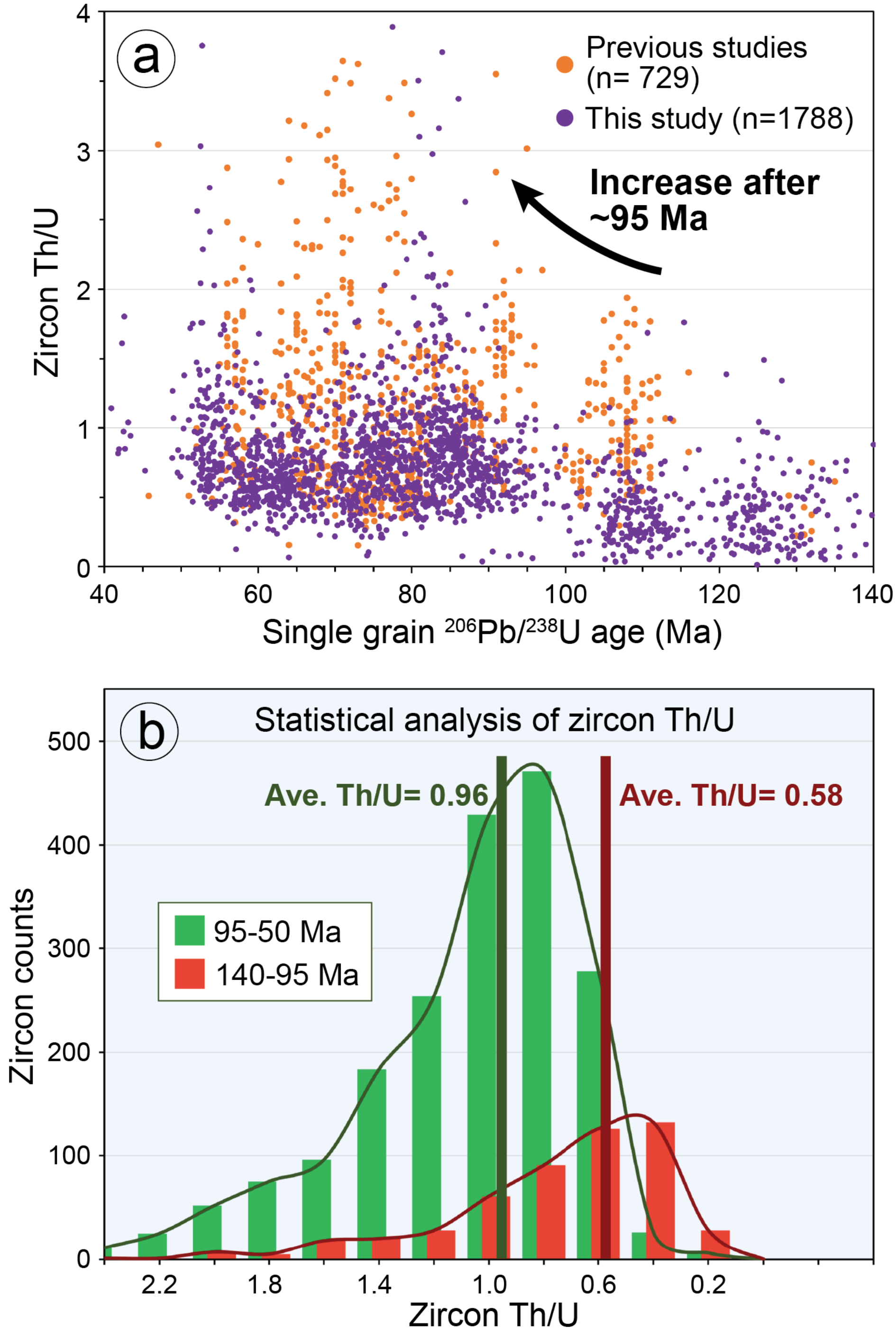

Figure 4. 12 Th/U of 140 to 40 Ma igneous zircons from Sikhote-Alin.

(a) single-grain zircon $^{206}Pb/^{238}U$ age vs. zircon Th/U. (b) Statistical analysis of 140 to 95 Ma and 95 to 50 Ma igneous zircon Th/U.

4.4.1.3 A-type or highly fractionated I-type granites in Sikhote-Alin?

The S-I-A alphabet classification for granites was designed to distinguish magma with different residual components (Chappell and White, 1992; Chappell and White, 2001; Whalen et al., 1987). However, classifying extremely felsic granites (SiO_2 >70%) can be difficult, for they have minimal residual components from extensive magmatic differentiation (Bonin, 2007; Chappell, 1999; White and Chappell, 1977). Particularly, HFSE enriched felsic granites can either be classified as highly fractionated I-type (Jiang et al., 2009; PérEz-SobA and Villaseca, 2010, 2019; Qiu et al., 2017; Wu et al., 2003) or A-type granites (King et al., 2001; King et al., 1997). It is sometimes difficult to discriminate between the two granite types.

Previous studies have suggested the 65 to 52 Ma felsic plutonic rocks in Sikhote-Alin are A-type granites associated with ignimbrites (Grebennikov and Maksimov, 2021; Grebennikov and Popov, 2014; Grebennikov et al., 2016). According to our newly compiled database, the Sikhote-Alin plutonic rocks with 10000×Ga/Al >2.6 (i.e., one of the key definitions for A-type granite from Whalen et al., 1987) have a wider age range between 95 to 52 Ma (yellow and green triangles in Fig. 4.11b). However, the HFSEs (e.g. Zr, Nb, Ce, and Y) are not significantly enriched in these rocks compared to typical S- and I- type granites (Fig. 4.11a, b). In addition, as previously discussed in sections 4.4.4.1 and 4.4.1.2, petrogenesis of some 95 to 52 Ma I-type granites (Fig. 4.10e) involved extensive crystallization differentiation (Fig. 4.11). Therefore, it is likely that the high Ga/Al is a result of magmatic fractionation (Bonin, 1999; Whalen et al., 1987; Wu et al., 2017a) in the 95 to 52 Ma magmatism, rather than partial melting of a source rock that should generate significantly-enriched HFSEs A-type granite (Collins et al., 1982; Creaser et al., 1991; Eby, 1992; Martin, 2006). An alternative petrogenesis for the A-type granites in the region is fractionation from an alkalic and tholeiitic mafic magma (Bonin, 1999, 2007; Eby, 1992; Turner et al., 1992); however, alkalic and tholeiitic mafic rock is absent in our database for the 95 to 52 Ma magmatism in Sikhote-Alin. Instead, those 95 to 52 Ma mafic rocks with SiO_2< 56 wt.% have calc-alkaline composition, revealed by their low to medium Na_2O+K_2O-CaO= -4.1 to -1.5 (Fig. 4.10a), low $Fe_2O_3T/(MgO+Fe_2O_3T)$= 0.66 to 0.72 (n=10), and trace element composition enriched in LILE (e.g., Th) but depleted in HFSE (e.g. Hf and Ta) (Fig. 4.10d). Therefore, we conclude the Sikhote-Alin 95 to 52 Ma igneous rocks are mainly I-type granites. Some of them have gone through extensive fractionation that has caused their chemical composition to overlap with A-type granites (i.e. highly fractionated I-type granites).

4.4.2 Implications for continental growth in NE Asia

Continents grow along active margins through the accretion of juvenile oceanic material and mantle-derived arc magmatism (Cawood et al., 2009; Condie, 2007; Reymer and Schubert, 1986). Recycled crustal material may also be incorporated into the arc magmatic source region by dehydration and/or melting of the subducting slab, and may then re-enter the continental margin by arc magmatism (Stern, 2011). The NE Asian margin has indeed been laterally growing through the Mesozoic to the Cenozoic, at least between the latitudes 42 °N to 52 °N, where juvenile terranes accreted since the Jurassic (Fig. 4.8)

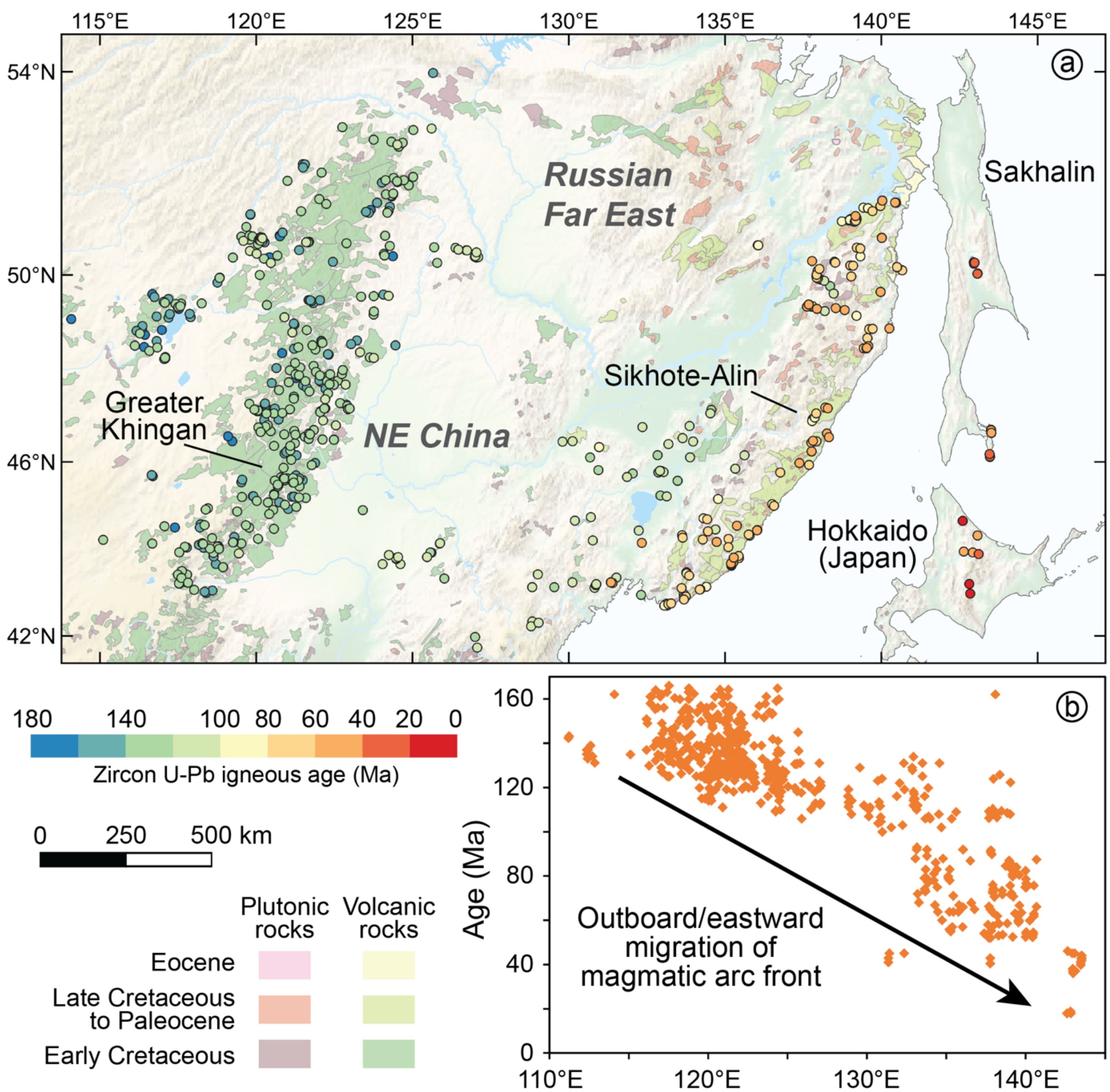

Figure 4. 13 140 to 0 Ma outboard/eastward migration of 42°N to 54°N NE Asia magmatism.

(a) Igneous rock distribution with U-Pb zircon age constraints in Sikhote-Alin (This study; Jahn et al., 2015; Tang et al., 2016; Tsutsumi et al., 2016; Wu et al., 2017b; Zhao et al., 2017), Sakhalin (Alexandrov et al., 2018; Liao et al., 2018; Zhao et al., 2018), Hokkaido (Jahn et al., 2014), and NE China (Gou et al., 2019 and references therein). (b) Present longitude vs. age of igneous rocks.

(Khanchuk et al., 2016; Ueda, 2016; Zharov, 2005). To further investigate the role of simultaneous arc magmatism along the margin, we compiled a zircon U-Pb constrained spatiotemporal igneous history of NE Asia (Fig. 4.13), including Sikhote-Alin, Sakhalin, and Hokkaido (same data source as Fig. 4.8), and NE China (Gou et al., 2019) and references therein).

Despite the likelihood that some terranes have moved in a limited margin-parallel fashion (Kemkin, 2008; Otofuji et al., 2002; Otofuji et al., 1995), the spatiotemporal igneous history of 42 °N to 52 °N NE Asia reveals a generally outboard/ eastern migration of arc magmatism between 140 Ma to present (Fig. 4.13). Particularly, the magmatism has migrated into the earlier accreted juvenile terranes in Silhote-Alin and Sakhalin (Fig. 4.8). The Cretaceous to Cenozoic Sikhote-Alin magmatism shows more enriched εNd(t) between -5 to +5 (Fig. 4.10f) compared to a depleted mantle reservoir with εNd around +10 (Sun and McDonough, 1989). It suggests the magma contained at least some recycled crustal material that was emplaced in or on to the continental margin, and further modified the accreted terranes. Here we present a schematic model to summarize the continental growth between 42 °N to 52 °N latitudes of the NE Asian margin since early Cretaceous (Fig. 4.14):

(1) Early Cretaceous (Fig. 4.14a): the arc magmatism moved outboard (eastward) (Fig. 4.8, 4.13) from inboard NE China into Sikhote-Alin. The early Cretaceous accretionary belt was developing along the margin. An intra-oceanic arc was accreted along the margin

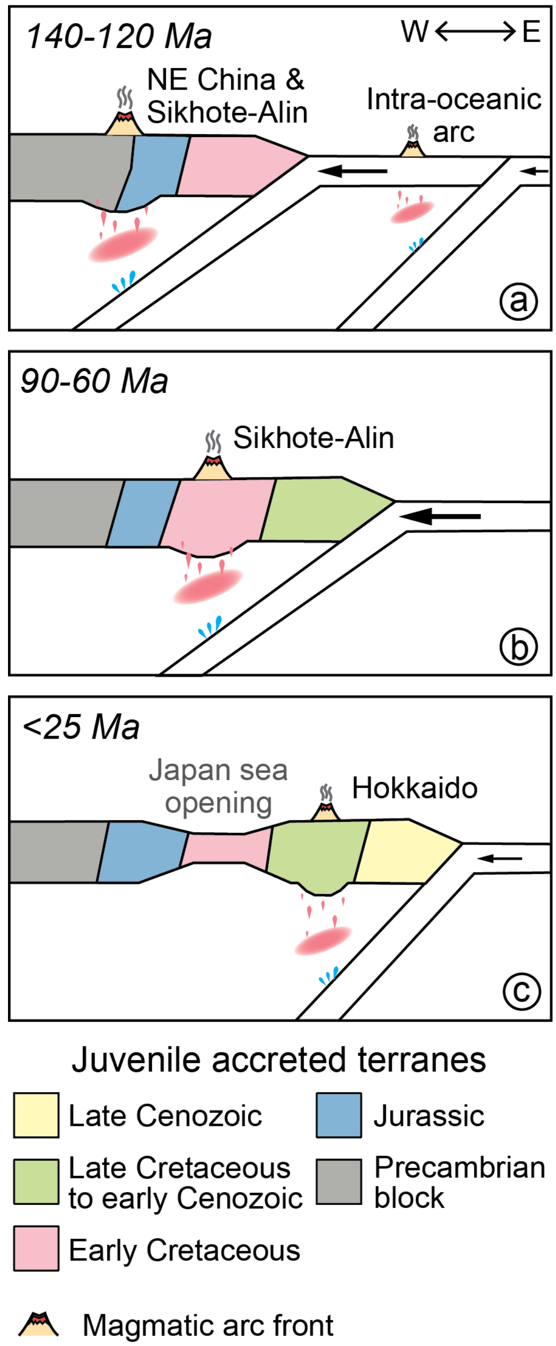

Figure 4. 14 Continental arc evolution of NE China, Sikhote-Alin, Sakhalin, and Hokkaido at 42°N to 52°N on latitudes from the Early Cretaceous to present based on the result from this study.

(a) Early Cretaceous (140 to 120 Ma) (b) Late Cretaceous to early Cenozoic (90 to 60 Ma) (c) Late Cenozoic (<25 Ma).

during 130-100 Ma (see chapter 3). The early Cretaceous magmatism was emplaced within the Jurassic accretionary belt (Samarka, Nadanhada-Bikin, and Khabarovsk terranes) and Precambrian-early Paleozoic terranes (Bureya-Jiamusi-Khanka block and the Sergeevka terrane) (Fig. 4.8).

(2) Late Cretaceous to Paleocene (Fig. 4.14b): the arc magmatism moved eastward into early Cretaceous terranes (Zhuravlevka-Amur and Kema) (Fig. 4.8, 4.13). The Late Cretaceous to Paleocene arc magmatism was characterized by high volumes (~1090 km^2/Ma) and average silica content (average SiO_2= 70.0 wt.%) (Fig. 4.10 and discussion in 4.4.1.2).

(3) Middle to late Cenozoic (Fig. 4.14c): the magmatic arc front moved eastward and outboard from Sikhote-Alin into the Sakhalin and Hokkaido area (Fig. 4.13). The Cenozoic arc magmatism after 40 Ma was emplaced within the Late Cretaceous to early Cenozoic terranes (east and west Sakhalin terranes, and Hidaka belt in Hokkaido) (Fig. 4.8).

4.5 Conclusion

In this study, we present new zircon U-Pb age (n=94) and whole-rock geochemical data (n=62) from igneous rock across Sikhote-Alin (Russian Far East). We combined our new result with published data (n>60) and shows four episodes of magmatism along a ~1500 km-wide NE Asian margin at Sikhote-Alin since the Early Cretaceous: (1) 134 to 120 Ma S-type magmatism, (2) 110 to 100 Ma I-type magmatism, (3) 95 to 52 Ma highly evolved I-type magmatism, and (4) <46 Ma I-type magmatism. The 134 to 52 Ma igneous rocks are generally calc-alkaline rocks with magmatic arc signature (i.e. enriched in LILE relative to HFSE), and εNd(t) isotopic values between -7 to +6. The 95 to 52 Ma episode has a significantly silica-enriched composition (average SiO_2= 70.0 wt.%) as a result of extensive crystallization differentiation. We compiled a zircon U-Pb constrained spatiotemporal igneous history between 42 °N to 52 °N latitude of NE Asia (NE China, southern Russian Far East, and Hokkaido), and discussed it with regional geology. The result implies a growing NE Asian continental margin during the Mesozoic to the Present, with juvenile terrane accretion followed by outboard (eastward) migration of arc magmatism that brings recycled crustal material to modify the newly accreted terranes.

CHAPTER 5: LINKS BETWEEN NORTHEAST ASIAN MAGMATIC ARC AND SUBDUCTION DYNAMICS

5.1 Introduction

The flare-ups and lulls in magmatism that coincide with episodic chemical variations in evolving continental arc have been recognized as "arc tempos" (Chapman et al., 2021; DeCelles et al., 2009; Ducea et al., 2015). Two groups of models have been suggested to explain the continental arc tempos (Fig. 5.1): (1) the "internal feedback" model invokes intra-arc processes that are relatively independent from subduction zone dynamics, including crustal thickening, melting, and/or delamination (DeCelles et al., 2014; Ducea, 2001; Ducea et al., 2015), and (2) the "external control" models apply processes outside the continental arc crust, such as mantle thermal structure or fluid flux that are generally controlled by subducting-plate parameters (Ardila et al., 2019; De Silva et al., 2015; Zellmer, 2008). It is

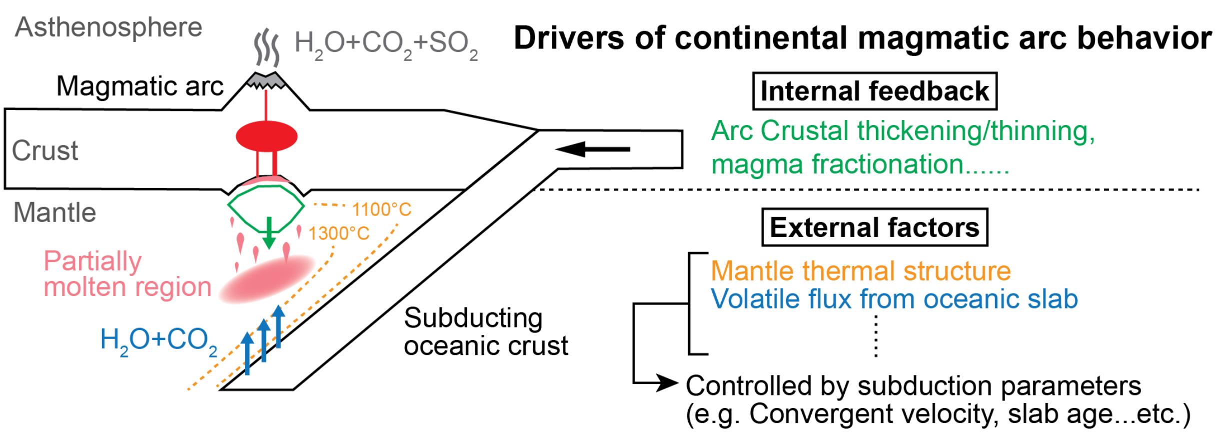

Figure 5. 1 Subduction zone cross-section showing internal and external factors that may drive continental magmatic arc behavior.

Also possible that the arc tempo drivers could be a combination of internal and external factors. However, subducting-plate parameters have been difficult to establish (e.g. Kirsch et al., 2016) due to the challenge of reconstructing subducted and lost oceanic lithosphere. In addition, current arc tempo models largely rely on data from the eastern Pacific (i.e. Cordillera).

In this study, we investigate the arc tempos in the Cretaceous to Cenozoic western Pacific margin (i.e. NE Asia) (Fig. 5.2), using a paired geologic/plate tectonic dataset: (1) a large (n>800) NE Asian magmatic database of published and unpublished results; and (2) and a digital, fully-kinematic 'tomographic' NE Asian-Pacific plate tectonic reconstruction model. We discretize the magmatic database (e.g. whole-rock SiO_2 and Nd isotopic composition) into time windows for multivariate statistical analysis. We extract subduction zone parameters (e.g. convergence rate, and slab age) from the relatively independent plate reconstruction model (constructed from seafloor spreading constraints, paleomagnetism, and tomography). We then test the correlation between external factors (i.e. subduction zone parameters from the plate kinematic model) and arc magmatic evolution, limiting our analysis to SiO_2 and Nd isotopic compositions, with an aim to explore whether our newly compiled magmatic database could be used to more fully investigate arc tempos in a future study.

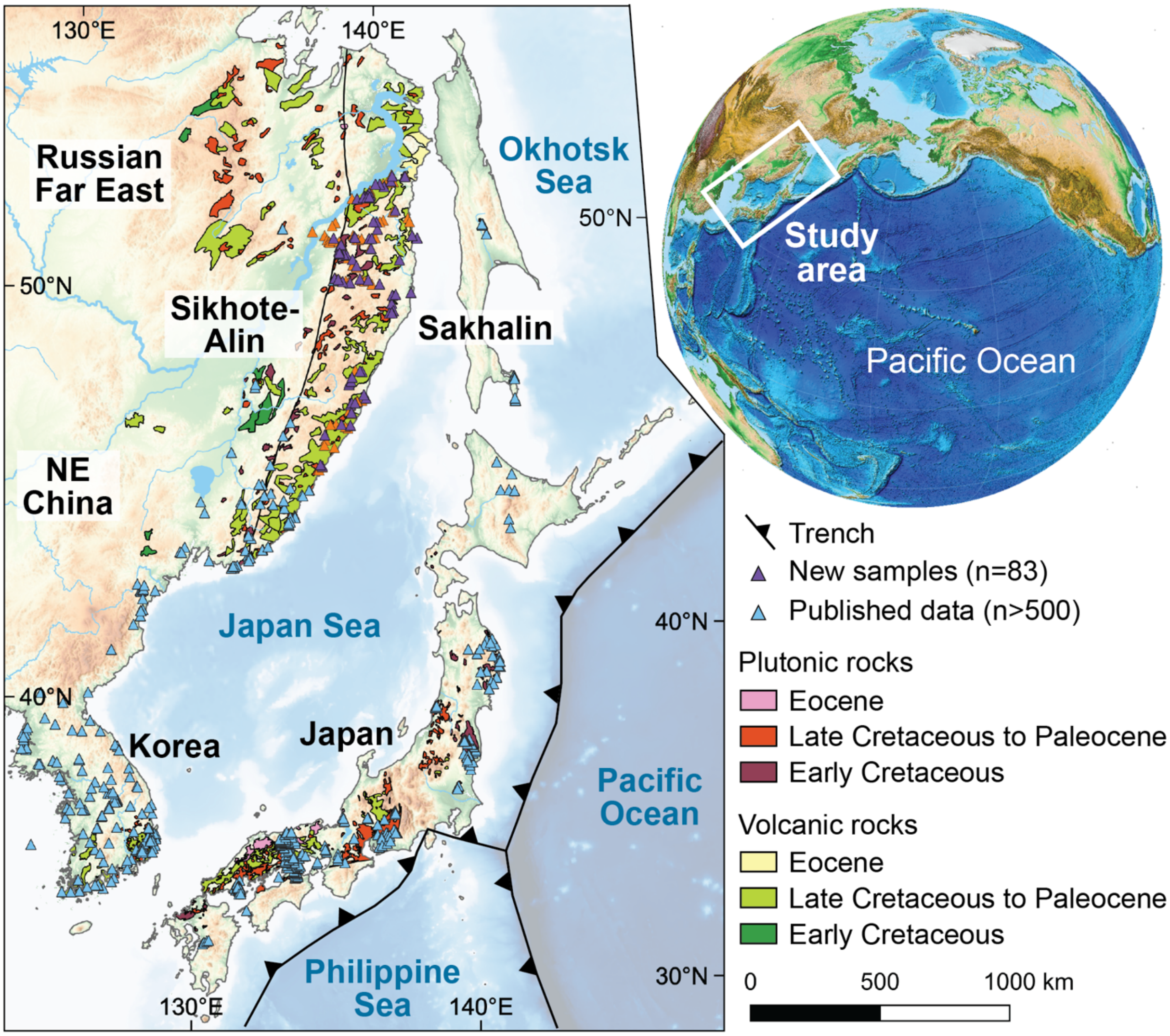

Figure 5. 2 Map showing sample locations for the large (n>500) geochronology and geochemistry database of NE Asia compiled in this study.

The GIS database of Cretaceous to Cenozoic igneous rocks is shown by the colored polygons.

5.2 Method

I newly compiled a magmatic database that includes >80 new zircon U-Pb ages/whole-rock geochemical analyses (result shown in Chapter 4), and published igneous-rock major elements (~1300) and Nd isotopic geochemistry (~800) data with age constrained by zircon U-Pb (~570), Monazite U-Pb (13), whole-rock Rb-Sr (~130), and whole-rock/hornblende K-Ar (~90) chronology (Belyansky et al., 2011; Cheong and Jo, 2017; Iida et al., 2015; Ito et al., 2010; Jahn et al., 2014; Jahn et al., 2015; Khanchuk et al., 2008; Kim et al., 2003; Kim et al., 2016; Koike and Tsutsumi, 2018; Kon et al., 2015; Kon and Takagi, 2012; Nakajima et al., 2004; Osozawa et al., 2019; Sagong et al., 2005; Sakashima et al., 2003; Sato et al., 2016; Skrzypek et al., 2016; Sueoka et al., 2018; Suzuki and Adachi, 1998; Takahashi et al., 2010; Takahashi et al., 2012; Takahashi et al., 2016; Tang et al., 2016; Tani et al., 2016; Watanabe et al., 2000; Wu et al., 2007; Wu et al., 2017b; Zhai et al., 2016; Zhang et al., 2012; Zhao et al., 2017).. The magmatic database has been discretized into time-sequence variations of the chemical composition of magmatic rocks constrained by the igneous age dating results. In addition, we applied a 'tomographic' NE Asian-Pacific plate tectonic model built in GPlates (Wu et al., in revision) to restore NE Asia subduction since the Cretaceous. We extracted the following plate-tectonic parameters (Fig. 5.4) between 110 to 0 Ma for the location 40 °N, 140 °E on the continental-oceanic plate boundary from the Gplate model: (1) plate convergence azimuth, (2) convergence velocity, and (3) trench-orthogonal convergence velocity calculated from the portion of convergence velocity toward 320° azimuth (i.e. NW direction).

We correlated the NE Asia magmatic geochemistry to the trench-orthogonal convergence velocity between 100 to 0 Ma in collaboration with PhD candidate Lingling Chen and Dr. Mikyoung Jun from the Department of Mathematics at UH. We applied a time-varying coefficient linear regression model (TVLM) (Casas and Fernandez-Casal, 2019) on the magmatic and plate-tectonic databases using the tvReg package in the software R. The TVLM with one predictor variable (y_t) can be expressed by

$$y_t = \beta_0(z_t) + \beta_1(z_t)x_t + \epsilon_t, \qquad t = 1, \dots, T,$$

where $\beta_i's, i = 0, 1,$ are the functions of the variable z_t, which is called the smoothing variable. The $\beta_i{}'s$ are defined as an unknown functions of a random variable $f(z_t)$ (Robinson, 1989). The main approach to estimate $\beta_i{}'s$ include an ordinary least squares regression, kernel-local polynomial smoothing, polynomial spline, and a smoothing spline (Hastie and Tibshirani, 1993; Huang et al., 2002; Wu et al., 1998). In this study, the whole-rocks SiO_2 and Nd isotopic composition (Fig. 5.3a, b) were treated as the variable y_t that responded to the orthogonal convergent velocity (Fig. 5.4c) (predictor variable x_t) through time (z_t).

5.3 Result

The 110 to 0 Ma NE Asian-Pacific plate tectonic model predicts a plate convergence azimuth (Fig. 5.3a) ranging from 263° to 345° (i.e. W to NNW direction), an absolute convergence velocity (Fig. 5.3b) from 2.2 to 24.7 cm/yr, and an orthogonal convergence velocity (Fig. 5.3c) from 2.2 to 23.0 cm/yr. When using a 5 Myrs-moving average model to deduce the 140 to 0 Ma NE Asia magmatic rock database, the rocks show an average SiO_2 from 52.5 to 74.7 wt.% (i.e. basaltic andesitic to rhyolitic composition) (Fig. 5.4a), and an average εNd(t) from -9.8 to 6.2 (Fig. 5.4b). The TVLM yields coefficients (β_1) range between -3.8 to 0.2 for SiO_2 and -0.3 to 3 for εNd(t) corresponding to 100-20 Ma orthogonal convergence velocity.

Figure 5. 3 NE Asian subduction boundary conditions.

The subduction boundary conditions extracted from the NE Asia plate tectonic reconstruction (Wu et al., in revision) shows the continental margin experienced a wide range of plate convergence rates, slab ages, and other factors. (a) Absolute convergence velocity between the oceanic plate and the NE Asian margin. (b) Plate convergence azimuth. (c) Trench-orthogonal convergent velocity.

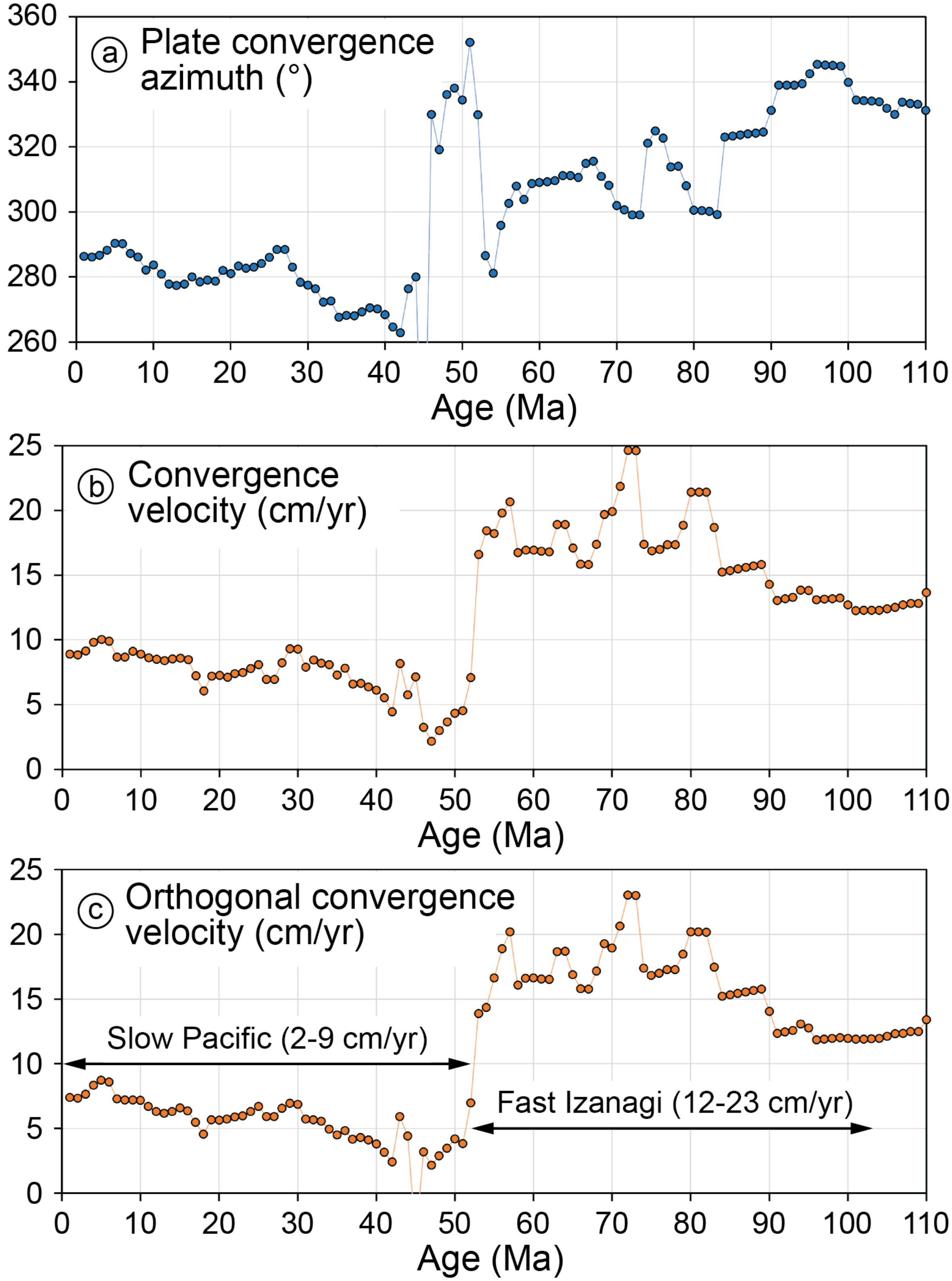
a Plate convergence azimuth (°)
360
340
320
300
280
260
0 10 20 30 40 50 60 70 80 90 100 110
Age (Ma)
b Convergence velocity (cm/yr)
25
20
15
10
5
0
0 10 20 30 40 50 60 70 80 90 100 110
Age (Ma)
c Orthogonal convergence velocity (cm/yr)
Slow Pacific (2-9 cm/yr)
Fast Izanagi (12-23 cm/yr)
25
20
15
10
5
0
0 10 20 30 40 50 60 70 80 90 100 110
Age (Ma)

Figure 5. 4 NE Asia magmatic/plate tectonic database plotted as a function of time

(a) whole-rock volatile-free SiO_2 and (b) Nd isotopic composition of igneous rocks in NE Asia, and (c) subducting plate and (d) plate convergence velocity along the NE Asian margin from the plate reconstruction (Wu et al., in revision).

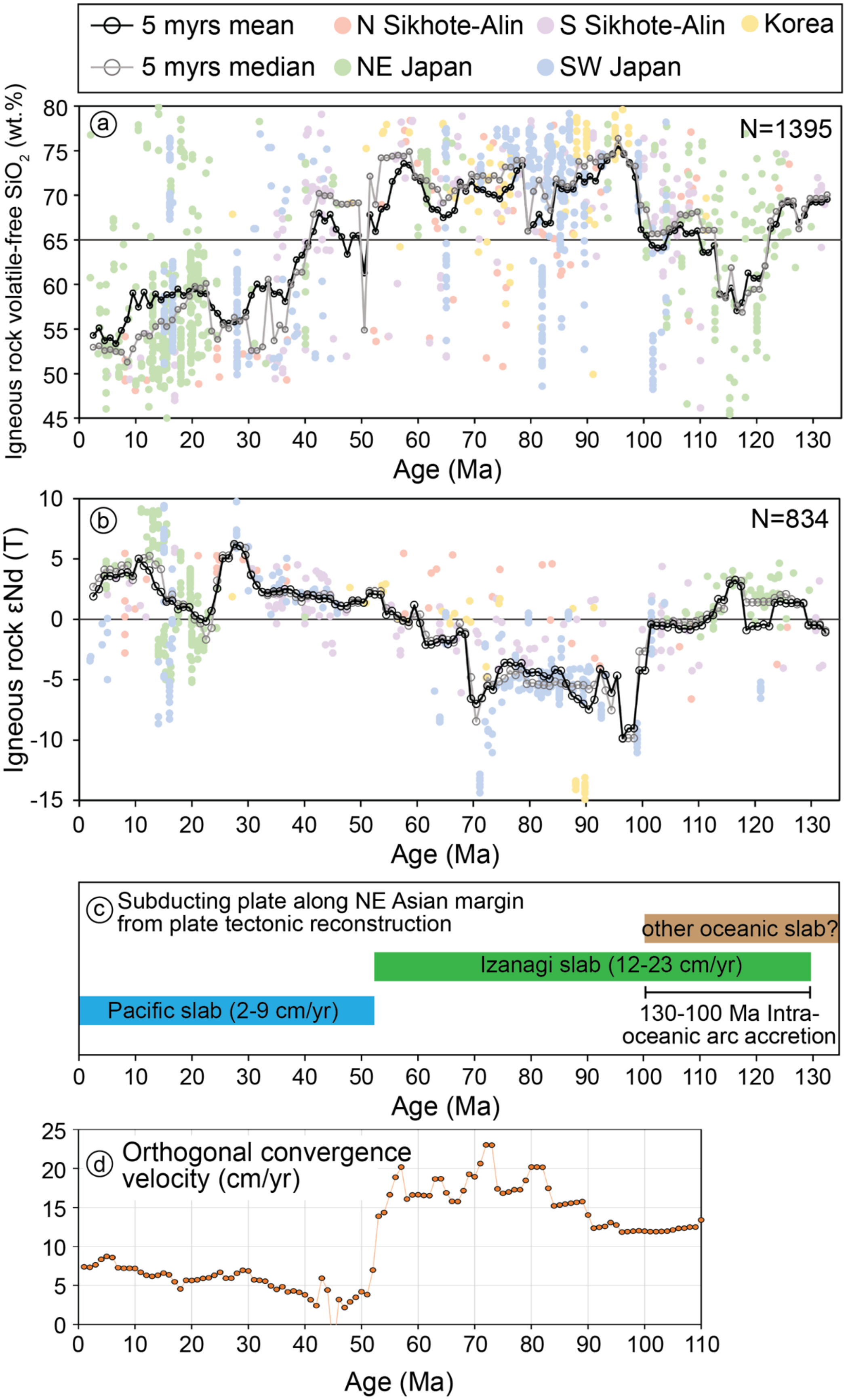

5 myrs mean
5 myrs median
N Sikhote-Alin
S Sikhote-Alin
Korea
NE Japan
SW Japan
a
N=1395
Igneous rock volatile-free SiO_2 (wt.%)
Age (Ma)
b
N=834
Igneous rock εNd (T)
Age (Ma)
c
Subducting plate along NE Asian margin from plate tectonic reconstruction
other oceanic slab?
Izanagi slab (12-23 cm/yr)
Pacific slab (2-9 cm/yr)
130-100 Ma Intra-oceanic arc accretion
Age (Ma)
d
Orthogonal convergence velocity (cm/yr)
Age (Ma)

5.4 Discussion

The NE Asia magmatism shows distinct chemistry (Fig. 5.4) corresponding to two distinct plate-tectonic periods along NW Pacific margin (Fig. 5.5): 100-52 Ma magmatism had larger flux (~1090 km^2/Ma) (Fig. 2.4c), higher silica content and enriched whole-rock Nd isotopic composition (5 Myrs-average SiO_2 from 65 to 75 wt.% and εNd(t) from -10 to 1) (Fig. 5.4a, b). In contrast, 52-0 Ma magmatism had smaller flux (~390 km^2/Ma) (Fig. 2.4c), lower silica content and depleted whole-rock Nd isotopic composition (5 Myrs-average SiO_2 from 54 to 67 wt.% and εNd(t) from 0 to 6) (Fig. 5.4).

The silica content (i.e. SiO_2 in whole-rock major element analysis) of intermediate to felsic magma was generally controlled by magma evolution (e.g. crystallization, assimilation, and magma mixing) within the overriding arc crust (Bachmann and Huber, 2016; Lee and Morton, 2015), which was one of the internal processes (Fig. 5.1). Particularly, high silica granites (SiO_2 > 70%) have been interpreted as the residual melt from an extensive crystallization differentiation during storage in crustal magma chamber (Bonin, 1999; Lee and Morton, 2015; Wu et al., 2017a). Following the discussion in section 4.5.1.2 in Chapter 4, the late Cretaceous (95 to 52 Ma) high silica magmatism was generated from extensive crystallization differentiation corresponding to higher magmatic flux, which may be linked to the high volatile flux from the dehydrating ultrafast-subducting Izanagi slab, in contrast to the 52 to 0 Ma low magmatic flux and slow Pacific subduction. The observation is supported with a positive correlation coefficient (0.45, dashed red line in Fig. 5.6a) between igneous rock SiO_2 and subduction velocity shown in a simple coefficient model. However, the TVLM shows a

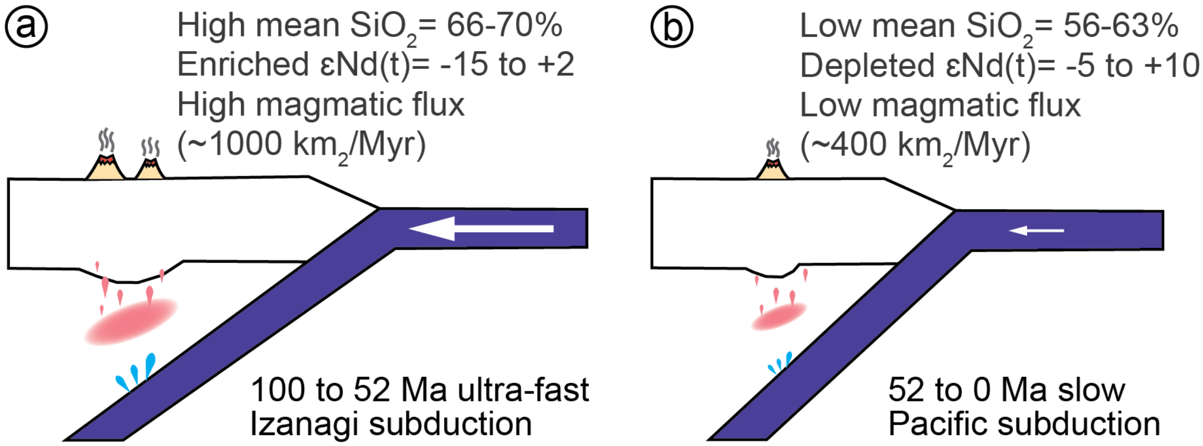

Figure 5. 5 NE Asia continental arc tempos corresponding to the 100 to 52 Ma Izanagi fast subduction and 52 to 0 Ma Pacific slow subduction periods.

general negative correlation (β_1= -3.8 to 0.2) (solid black line in Fig. 5.6a) that contradicts the result from the simple coefficient model. This may suggest that although external factors (i.e. subduction velocity) may control the arc magmatism on a longer time scale, other processes may be more dominated in shorter (<30 m.y.) time scales.

The Nd isotopic composition of magmatism is affected by mixing between juvenile mantle (depleted Nd isotopic composition) and recycled crust (usually having enriched Nd isotopic composition) components (White, 2015). In a continental arc setting, the crustal component could come from the assimilation of ascending magma with the wall rock within the overriding continental crust. This would result in the Nd composition varying with evolving magma (e.g., more enriched εNd(t) in igneous rock with higher SiO_2). This is not the case for the NE Asia magmatism because it does not show significant εNd(t) variations among the 60-80 SiO_2% igneous rocks (Fig. 5.7). Instead, the crustal component within the 135 to 0 Ma NE Asia magmatism likely comes from the subducting sediments. During the 100-52 Ma Izanagi fast subduction, the εNd(t) and subduction velocity have a generally negative, statistically significant coefficient (β_1= -0.3 to 0.1) (Fig. 5.6b), which is consistent with a higher subducting sedimentary flux that had more recycled sedimentary component with a low εNd(t) mixing with the juvenile mantle-derived magma. On the contrary, the 52 to 0 Ma slow Pacific subduction has a positive coefficient (β_1= 0 to 3) (Fig. 5.6b) that suggests the subducting sedimentary flux was not significantly controlling the Nd isotopic composition of the arc magma.

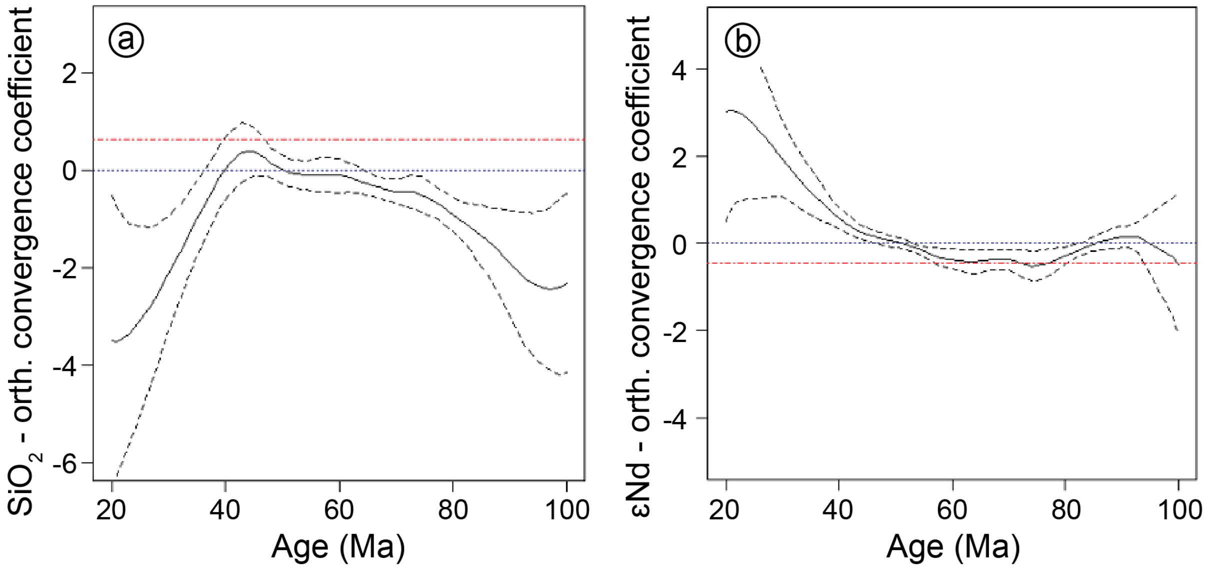

Figure 5. 6 Time-varying coefficient linear regression model (TVLM) for NE Asian arc tempos and subduction dynamics.

The TVLM of orthogonal convergence velocity (Fig. 5.3c) correlates to (a) silica content and (b) Nd isotopic composition of magmatism between 100 to 20 Ma along the NE Asian margin (Fig. 5.4 a, b). Bandwidth = 40. Solid black line: estimated coefficient (β), Dashed black line: 90 % confidence interval, Dashed red line: estimated coefficient from the simple linear regression model.

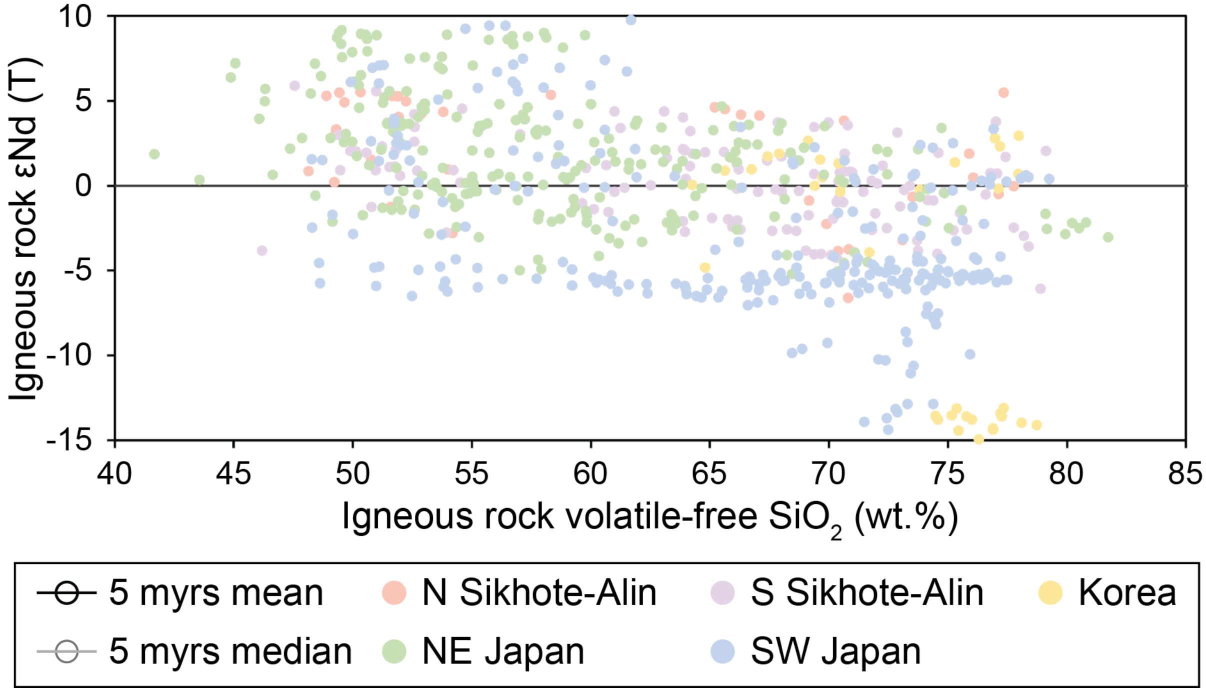

Figure 5. 7 Nd isotopic composition vs. SiO_2 plot.

5.5 Conclusion

Multivariate analysis reveals that NE Asia arc magmatism contains a statistically-significant, first-order correlation to the reconstructed subduction zone dynamics from the plate model. The Cretaceous to present orthogonal convergence velocity shows a positive correlation with magmatic silica content (correlation coefficient= 0.45), and a negative correlation to the Nd isotopic composition (-0.61). Future work is needed to further investigate NE Asia arc tempos, for example, to quantify the NE Asian magma flux by <20 Myrs timescale, invoking fluid-mobile elements into the multivariate analysis for correlation between subduction zone dynamics and fluid flux, and to explore internal factors such as crustal thickness from La/Yb and Sr/Y of intermediate rocks.

CHAPTER 6: SUMMARY AND CONCLUDING REMARKS

Active continental margins are locations where the oceanic lithosphere is subducted, accretionary orogens are formed, and arc magmatism is generated from subduction. This study has resulted in new constraints for the highly controversial regional plate tectonic history of NE Asia using magmatic constraints from the NE Asian continental arc (e.g. the upper plate). In particular, this thesis has shown:

(1) In the first study, our synthesis reveals a near-synchronous 56 to 46 Ma magmatic gap occurred across ~1500 km of the Eurasian continental margin between Japan and Sikhote-Alin. The magmatic gap separated two distinct phases of igneous activity: (1) an older Cretaceous to Paleocene pre-56 Ma episode that had relatively lower εNd(t) (-15 to +2), elevated $(^{87}Sr/^{86}Sr)_0$ (0.704 to 0.714), and relatively higher magmatic fluxes ~1090 km2/Ma; and, (2) a younger late Eocene to Miocene post-46 Ma phase that had relatively elevated εNd (-2 to +10), lower $(^{87}Sr/^{86}Sr)_0$ (0.702 to 0.707), and a lower 390 km^2/Ma magmatic flux. The 56 to 46 Ma magmatic gap links other geological evidence across NE Asia to constrain an early Cenozoic, low-angle ridge-trench intersection that had profound consequences for the Eurasian continental margin.

(2) In the second study, we show the early Cretaceous NE Asia igneous activity derived from multiple sources that include: (1) arc-related igneous rocks, (2) 132 to 99 Ma adakites in Japan and Sikhote-Alin derived from subducting oceanic crust, and (3) 145 to 120 Ma K-rich adakites derived from North China Craton (NCC) lower crust. Roughly co-eval to these periods (130 to 100 Ma), intra-oceanic arcs accreted diachronously along

the east Asian margin. Thus, eastern Eurasia-NW Panthalassan plate tectonics during the Early Cretaceous was more complex than generally recognized, involving intra-oceanic subduction zones and multiple oceanic plates. This model provides a more geologically plausible plate tectonic context for North China craton peak destruction and thinning ~125 Ma, which was explained within the context of a simple Andean-type margin in most previous studies.

(3) In the third study, we examine the continental arc evolution in Sikhote-Alin (Russian Fareast) with an igneous activity database including our new zircon U-Pb chronology/ whole-rock geochemistry results and published data. The database reveals four subduction-related magmatic episodes: (1) 134 to 120 Ma S-type magmatism, (2) 110 to 100 Ma I-type magmatism, (3) 95 to 52 Ma highly evolved I-type magmatism, and (4) <46 Ma I-type magmatism. The 95 to 52 Ma episode has a significant silica-enriched composition (average SiO_2= 70.0 wt.%) that resulted from extensive crystallization differentiation. In terms of spatiotemporal evolution, Jurassic to Cenozoic magmatism in northeast China, Sikhote-Alin, and Sakhalin shows an outboard (eastward) migration that followed accretion to the margin.

(4) In the fourth study, we compare a tomographic NE Asian plate model (Wu et al., in revision) that indicates the Cretaceous to Cenozoic northeast Asia subduction realm has two episodes: (1) 100 to 52 Ma ultrafast subduction (12 to 24 cm/yr) of the Izanagi plate in contrast to (2) 52 to 0 Ma slower Pacific subduction (2 to 8 cm/yr). Comparison to the NE Asia magmatic record compiled in this study (n> 800) reveals the igneous rocks generated during the 100-52 Ma ultrafast subduction show a statistical correlation to high

% SiO_2 (mean 66-70 %), and enriched εNd(t) isotopic ratios (-15 to +2). In comparison, igneous rocks generated during the slower 52 to 0 Ma subduction were characterized by SiO_2 (mean 56~63 %), and more depleted εNd(t) isotopic ratios (-5 to +10). Multivariate analysis shows that NE Asia Cretaceous to Cenozoic arc magmatism contains a statistically-significant, first-order correlation to subduction zone dynamics (i.e external factors on arc tempos) that can be further explored by future studies.

In summary, the evolutionary history of the Mesozoic to Cenozoic NE Asian continental margin can be summarized as follows: at least three oceanic plates likely subducted beneath the NE Asian margin: (1) one or multiple marginal sea plate(s) before 100 Ma, (2) the Izanagi plate between ~100 to 50 Ma, and (3) the Pacific Plate since ~50 Ma. The episodic subduction of these oceanic plates drives the tectonic accretion of oceanic material along the continental margin, and the evolution of the magmatic arc. Other events include an early Cretaceous (130 to 100 Ma) intra-oceanic arc accretion, early Eocene (~50 Ma) Pacific-Izanagi spreading ridge subduction, and the late Cenozoic Japan sea basin opening.

The Mesozoic to Cenozoic northeast Asian continental margin is growing through a process of terrane accretion, followed by outboard migration of the magmatic arc onto the earlier-accreted terranes. The evolution of the northeast Asian arc magmatism appears to have a first-order correlation to the subduction zone dynamics. Specifically, we link higher magmatic fluxes (up to 1000 km^2 /Myr), high % SiO_2 (mean 66 to 70 %), and enriched εNd(t) isotopic ratios (-15 to +2) to ultrafast subduction (12 to 24 cm/yr) Izanagi subduction between ~100-

50 Ma; and, lower magmatic flux (~400 km^2 /Myr), SiO_2 (mean 56-63 %), and more depleted εNd(t) isotopic ratios (-5 to +10) to slower (2 to 8 cm/yr) Pacific Plate subduction between 50 to 0 Ma.

BIBLIOGRAPHY

Abrajevitch, A., Zyabrev, S., Didenko, A. N., and Kodama, K., 2012, Palaeomagnetism of the West Sakhalin Basin: evidence for northward displacement during the Cretaceous: Geophysical Journal International, v. 190, no. 3, p. 1439-1454.

Agar, S., Cliff, R., Duddy, I., and Rex, D., 1989, Short paper: Accretion and uplift in the Shimanto Belt, SW Japan: Journal of the Geological Society, v. 146, no. 6, p. 893-896.

Allègre, C. J., 2008, Isotope geology, Cambridge University Press, p. 512.

Ando, H., 2003, Stratigraphic correlation of Upper Cretaceous to Paleocene forearc basin sediments in Northeast Japan: cyclic sedimentation and basin evolution: Journal of Asian Earth Sciences, v. 21, no. 8, p. 921-935.

Aoki, K., Kitajima, K., Masago, H., Nishizawa, M., Terabayashi, M., Omori, S., Yokoyama, T., Takahata, N., Sano, Y., and Maruyama, S., 2009, Metamorphic P-T-time history of the Sanbagawa belt in central Shikoku, Japan and implications for retrograde metamorphism during exhumation: Lithos, v. 113, no. 3-4, p. 393-407.

Aoki, S., Aoki, K., Chiba, K., Sakata, S., Tsuchiya, Y., and Kato, D., 2020a, Origin of the Tonaru body in the Sanbagawa metamorphic belt, SW Japan: Island Arc, v. 29, no. 1, p. e12332.

Aoki, S., Aoki, K., Tsuchiya, Y., and Kato, D., 2019, Constraint on the eclogite age of the Sanbagawa metamorphic rocks in central Shikoku, Japan: International Geology Review, v. 61, no. 18, p. 2211-2226.

Aoki, S., Aoki, K., Tsujimori, T., Sakata, S., and Tsuchiya, Y., 2020b, Oceanic-arc subduction, stagnation, and exhumation: zircon U-Pb geochronology and trace-element geochemistry of the Sanbagawa eclogites in central Shikoku, SW Japan: Lithos, v. 358, p. 105378.

Ardila, A. M. M., Paterson, S. R., Memeti, V., Parada, M. A., and Molina, P. G., 2019, Mantle driven cretaceous flare-ups in Cordilleran arcs: Lithos, v. 326, p. 19-27.

Arkhipov, M. V., Voinova, I. P., Kudymov, A. V., Peskov, A. Y., Otoh, S., Nagata, M., Golozubov, V. V., and Didenko, A. N., 2019, Comparative Analysis of Aptian-Albian Rocks of the Kema and Kiselevka-Manoma Terranes: Geochemistry, Geochronology, and Paleomagnetism: Russian Journal of Pacific Geology, v. 13, no. 3, p. 239-264.

Armstrong, R. L., Clark, S., Burchfiel, B., and Suppe, J., 1988, Mesozoic and early Cenozoic magmatic evolution of the Canadian Cordillera: Geological Society of America Special Paper, v. 218, p. 55-91.

Bachmann, O., Dungan, M., and Bussy, F., 2005, Insights into shallow magmatic processes in large silicic magma bodies: the trace element record in the Fish Canyon magma body, Colorado: Contributions to Mineralogy and Petrology, v. 149, no. 3, p. 338-349.

Bachmann, O., and Huber, C., 2016, Silicic magma reservoirs in the Earth’s crust: American Mineralogist, v. 101, no. 11, p. 2377-2404.

Bau, M., 1996, Controls on the fractionation of isovalent trace elements in magmatic and aqueous systems: evidence from Y/Ho, Zr/Hf, and lanthanide tetrad effect: Contributions to Mineralogy and Petrology, v. 123, no. 3, p. 323-333.

Belyansky, G., Rybalko, V., Syasko, A., Bazhanov, V., Uglova, N., Abramova, V., Oleinikov, A., Kovalenko, S., Kashtaev, B., and Alenicheva, A., 2011, Explanatory notes to the geological map of Russia, L-52/53, and K-52/53 map sheets, 1: 1,000,000 scale, 3rd generation: VSEGEI, St-Petersburg., p. 699.
Blichert-Toft, J., and Albarède, F., 1997, The Lu-Hf isotope geochemistry of chondrites and the evolution of the mantle-crust system: Earth and Planetary Science Letters, v. 148, no. 1-2, p. 243-258.
Bonin, B., 1999, Alkaline rocks and geodynamics: Turkish Journal of Earth Sciences, v. 7, no. 3, p. 105-118.
Bonin, B., 2007, A-type granites and related rocks: evolution of a concept, problems and prospects: Lithos, v. 97, no. 1-2, p. 1-29.
Boyd, F., 1989, Compositional distinction between oceanic and cratonic lithosphere: Earth and Planetary Science Letters, v. 96, no. 1-2, p. 15-26.
Boyden, J. A., Müller, R. D., Gurnis, M., Torsvik, T. H., Clark, J. A., Turner, M., Ivey-Law, H., Watson, R. J., and Cannon, J. S., 2011, Next-generation plate-tectonic reconstructions using GPlates. In: Keller, G.R., Baru, C. (Eds.), Geoinformatics: Cyberinfrastructure for the Solid Earth Sciences. Cambridge University Press, p. 95-114.
Cagnioncle, A. M., Parmentier, E., and Elkins-Tanton, L. T., 2007, Effect of solid flow above a subducting slab on water distribution and melting at convergent plate boundaries: Journal of Geophysical Research: Solid Earth, v. 112, no. B9.
Casas, I., and Fernandez-Casal, R., 2019, tvReg: Time-varying Coefficient Linear Regression for Single and Multi-Equations in R: Available at SSRN 3363526.
Castillo, P. R., 2012, Adakite petrogenesis: Lithos, v. 134, p. 304-316.
Cawood, P.A., Kröner,A., Collins, W.J., Kusky, T.M., Mooney, W.D., Windley, B.F., 2009. Earth Accretionary orogens through Earth history. In: Cawood, P.A., Kröner, A. (Eds.), Earth Accretionary Systems in Space and Time: The Geological Society, London Special Publications, 318, p. 1-36.
Chapman, J. B., Shields, J. E., Ducea, M. N., Paterson, S. R., Attia, S., and Ardill, K. E., 2021, The causes of continental arc flare ups and drivers of episodic magmatic activity in Cordilleran orogenic systems: Lithos, p. 106307.
Chappell, B., 1999, Aluminium saturation in I- and S-type granites and the characterization of fractionated haplogranites: Lithos, v. 46, no. 3, p. 535-551.
Chappell, B. W., and White, A., 1992, I- and S-type granites in the Lachlan Fold Belt: Earth and Environmental Science Transactions of the Royal Society of Edinburgh, v. 83, no. 1-2, p. 1-26.
Chappell, B. W., and White, A. J., 2001, Two contrasting granite types: 25 years later: Australian journal of earth sciences, v. 48, no. 4, p. 489-499.
Chashchin, A., Nechaev, V., Nechaeva, E., and Blokhin, M., 2011, Discovery of Eocene adakites in Primor'e: Doklady Earth Sciences 2011, v. 438, no. 2, p. 744-749.
Chekryzhov, I. Y., Popov, V., Panichev, A., Seredin, V., and Smirnova, E., 2010, New data on the stratigraphy, volcanism, and zeolite mineralization of the Cenozoic Vanchinskaya Depression in Primorye: Russian Journal of Pacific Geology, v. 4, no. 4, p. 314-330.

Chen, B., Jahn, B. M., Arakawa, Y., and Zhai, M., 2004, Petrogenesis of the Mesozoic intrusive complexes from the southern Taihang Orogen, North China Craton: elemental and Sr-Nd-Pb isotopic constraints: Contributions to Mineralogy and Petrology, v. 148, no. 4, p. 489-501.

Cheong, A. C. S., and Jo, H. J., 2017, Crustal evolution in the Gyeongsang Arc, southeastern Korea: Geochronological, geochemical and Sr-Nd-Hf isotopic constraints from granitoid rocks: American Journal of Science, v. 317, no. 3, p. 369-410.

Collins, W., Beams, S., White, A., and Chappell, B., 1982, Nature and origin of A-type granites with particular reference to southeastern Australia: Contributions to mineralogy and petrology, v. 80, no. 2, p. 189-200.

Condie, K.C., 2007. Accretionary orogens inspace and time. In: Hatcher Jr., R.D.,Carlson, M.P.,McBride, J.H., Martínez Catalán, J.R. (Eds.), 4-D Framework of Continental Crust:Geological Society of America Memoir, 200, p. 145-158.

Creaser, R. A., Price, R. C., and Wormald, R. J., 1991, A-type granites revisited: assessment of a residual-source model: Geology, v. 19, no. 2, p. 163-166.

Dai, L. Q., Zheng, Y. F., and Zhao, Z. F., 2016, Termination time of peak decratonization in North China: Geochemical evidence from mafic igneous rocks: Lithos, v. 240, p. 327-336.

De Silva, S. L., Riggs, N. R., and Barth, A. P., 2015, Quickening the pulse: fractal tempos in continental arc magmatism: Elements, v. 11, no. 2, p. 113-118.

Debon, F., and Le Fort, P., 1988, A cationic classification of common plutonic rocks and their magmatic associations: principles, method, applications: Bulletin de Minéralogie, v. 111, no. 5, p. 493-510.

DeCelles, P. G., Ducea, M. N., Kapp, P., and Zandt, G., 2009, Cyclicity in Cordilleran orogenic systems: Nature Geoscience, v. 2, no. 4, p. 251.

DeCelles, P. G., Zandt, G., Beck, S., Currie, C., Ducea, M. N., Kapp, P., Gehrels, G. E., Carrapa, B., Quade, J., and Schoenbohm, L., 2014, Cyclical orogenic processes in the Cenozoic central Andes: Geological Society of America Memoirs, v. 212, p. MWR212-222.

Defant, M. J., and Drummond, M. S., 1990, Derivation of some modern arc magmas by melting of young subducted lithosphere: Nature, v. 347, no. 6294, p. 662-665.

DePaolo, D. J., and Wasserburg, G., 1976, Nd isotopic variations and petrogenetic models: Geophysical Research Letters, v. 3, no. 5, p. 249-252.

Dickinson, W. R., and Snyder, W. S., 1979, Geometry of triple junctions related to San Andreas transform: Journal of Geophysical Research: Solid Earth, v. 84, no. B2, p. 561-572.

Didenko, A., Khanchuk, A., Tikhomirova, A., and Voinova, I., 2014, Eastern segment of the Kiselevka-Manoma terrane (Northern Sikhote Alin): Paleomagnetism and geodynamic implications: Russian Journal of Pacific Geology, v. 8, no. 1, p. 18-37.

Domeier, M., Shephard, G. E., Jakob, J., Gaina, C., Doubrovine, P. V., and Torsvik, T. H., 2017, Intraoceanic subduction spanned the Pacific in the Late Cretaceous-Paleocene: Science Advances, v. 3, no. 11, p. eaao2303.

Dostal, J., and Chatterjee, A., 2000, Contrasting behaviour of Nb/Ta and Zr/Hf ratios in a peraluminous granitic pluton (Nova Scotia, Canada): Chemical Geology, v. 163, no. 1-4, p. 207-218.
Ducea, M., 2001, The California arc: Thick granitic batholiths, eclogitic residues, lithospheric-scale thrusting, and magmatic flare-ups: GSA today, v. 11, no. 11, p. 4-10.
Ducea, M. N., Saleeby, J. B., and Bergantz, G., 2015, The architecture, chemistry, and evolution of continental magmatic arcs: Annual Review of Earth and Planetary Sciences, v. 43, p. 299-331.
Eby, G. N., 1992, Chemical subdivision of the A-type granitoids: petrogenetic and tectonic implications: Geology, v. 20, no. 7, p. 641-644.
Endo, S., Miyazaki, K., Danhara, T., Iwano, H., and Hirata, T., 2018, Progressive changes in lithological association of the Sanbagawa metamorphic complex, Southwest Japan: Relict clinopyroxene and detrital zircon perspectives: Island Arc, v. 27, no. 5, p. e12261.
Engebretson, D. C., Cox, A., Gordon, R. G., 1985. Relative motions between oceanic and continental plates in the Pacific Basin. Geological Society of America Special Paper 206, p. 59.
Frost, B. R., Barnes, C. G., Collins, W. J., Arculus, R. J., Ellis, D. J., and Frost, C. D., 2001, A geochemical classification for granitic rocks: Journal of petrology, v. 42, no. 11, p. 2033-2048.
Frost, B. R., and Frost, C. D., 2008, A geochemical classification for feldspathic igneous rocks: Journal of Petrology, v. 49, no. 11, p. 1955-1969.
Gao, Y., Hou, Z., Kamber, B. S., Wei, R., Meng, X., and Zhao, R., 2007, Adakite-like porphyries from the southern Tibetan continental collision zones: evidence for slab melt metasomatism: Contributions to Mineralogy and Petrology, v. 153, no. 1, p. 105-120.
Gelman, S. E., Deering, C. D., Bachmann, O., Huber, C., and Gutierrez, F. J., 2014, Identifying the crystal graveyards remaining after large silicic eruptions: Earth and Planetary Science Letters, v. 403, p. 299-306.
Gonevchuk, V., Gonevchuk, G., Lebedev, V., and Orekhov, A., 2011, Monzonitoid association of the Kavalerovo ore district (Primorye): geochronology and some genetic problems: Russian Journal of Pacific Geology, v. 5, no. 3, p. 199-209.
Gonevchuk, V., Khanchuk, A., Gonevchuk, G., and Lebedev, V., 2015, New K-Ar biotite and amphibole ages of granitoids of Sikhote-Alin (Russian Far East): criteria of reliability and interpretation: Russian Journal of Pacific Geology, v. 9, no. 6, p. 411-427.
Gorton, M. P., and Schandl, E. S., 2000, From continents to island arcs: a geochemical index of tectonic setting for arc-related and within-plate felsic to intermediate volcanic rocks: The Canadian Mineralogist, v. 38, no. 5, p. 1065-1073.
Gou, J., Sun, D. Y., and Qin, Z., 2019, Late Jurassic-Early Cretaceous tectonic evolution of the Great Xing'an Range: geochronological and geochemical evidence from granitoids and volcanic rocks in the Erguna Block, NE China: International Geology Review, v. 61, no. 15, p. 1842-1863.

Grebennikov, A., and Maksimov, S., 2021, Causes of the Occurrence of A-Type Volcanic Rocks in Active Continental Margins (Southern Sikhote-Alin, Russian Far East): Russian Geology and Geophysics, v. 62, no. 2, p. 207-222.
Grebennikov, A., and Popov, V., 2014, Petrogeochemical aspects of the Late Cretaceous and Paleogene ignimbrite volcanism of East Sikhote-Alin: Russian Journal of Pacific Geology, v. 8, no. 1, p. 38-55.
Grebennikov, A. V., Khanchuk, A. I., Gonevchuk, V. G., and Kovalenko, S. V., 2016, Cretaceous and Paleogene granitoid suites of the Sikhote-Alin area (Far East Russia): Geochemistry and tectonic implications: Lithos, v. 261, p. 250-261.
Griffin, B., Andi, Z., O'Reilly, S., and Ryan, C., 1998, Phanerozoic evolution of the lithosphere beneath the Sino-Korean Craton: Mantle Dynamics and Plate Interactions in East Asia, v. 27, p. 107-126.
Gu, H. O., Xiao, Y., Santosh, M., Li, W. Y., Yang, X., Pack, A., and Hou, Z., 2013, Spatial and temporal distribution of Mesozoic adakitic rocks along the Tan-Lu fault, Eastern China: constraints on the initiation of lithospheric thinning: Lithos, v. 177, p. 352-365.
Guan, Q., Liu, Z., Liu, Y., Li, S., Wang, S., Chen, Z., and Zhang, C., 2020, A tectonic transition from closure of the Paleo-Asian ocean to subduction of the Paleo-Pacific Plate: Insights from early Mesozoic igneous rocks in eastern Jilin Province, NE China: Gondwana Research.
Gutiérrez, F., Gioncada, A., Ferran, O. G., Lahsen, A., and Mazzuoli, R., 2005, The Hudson Volcano and surrounding monogenetic centres (Chilean Patagonia): an example of volcanism associated with ridge-trench collision environment: Journal of Volcanology and Geothermal Research, v. 145, no. 3-4, p. 207-233.
Gvozdev, V., 2010, Ore-Magmatic Systems of Skarn Scheelite-Sulfide Deposits of East Russia, Dal’nauka, Vladivostok. (in Russian)
Hall, R., 2012, Late Jurassic-Cenozoic reconstructions of the Indonesian region and the Indian Ocean: Tectonophysics, v. 570, p. 1-41.
Hara, H., and Kimura, K., 2008, Metamorphic and cooling history of the Shimanto accretionary complex, Kyushu, Southwest Japan: Implications for the timing of out-of-sequence thrusting: Island Arc, v. 17, no. 4, p. 546-559.
Harrison, T. M., Watson, E. B., and Aikman, A. B., 2007, Temperature spectra of zircon crystallization in plutonic rocks: Geology, v. 35, no. 7, p. 635-638.
Hastie, T., and Tibshirani, R., 1993, Varying-coefficient models: Journal of the Royal Statistical Society: Series B (Methodological), v. 55, no. 4, p. 757-779.
He, L., 2014, Numerical modeling of convective erosion and peridotite-melt interaction in big mantle wedge: Implications for the destruction of the North China Craton: Journal of Geophysical Research: Solid Earth, v. 119, no. 4, p. 3662-3677.
Holt, A., Royden, L., and Becker, T., 2017, The dynamics of double slab subduction: Geophysical Journal International, v. 209, no. 1, p. 250-265.
Huang, J. Z., Wu, C. O., and Zhou, L., 2002, Varying-coefficient models and basis function approximations for the analysis of repeated measurements: Biometrika, v. 89, no. 1, p. 111-128.
Hughes, G. R., and Mahood, G. A., 2008, Tectonic controls on the nature of large silicic calderas in volcanic arcs: Geology, v. 36, no. 8, p. 627-630.

Iida, K., Iwamori, H., Orihashi, Y., Park, T., Jwa, Y. J., Kwon, S. T., Danhara, T., and Iwano, H., 2015, Tectonic reconstruction of batholith formation based on the spatiotemporal distribution of Cretaceous-Paleogene granitic rocks in southwestern J apan: Island Arc, v. 24, no. 2, p. 205-220.

Imaoka, T., Kiminami, K., Nishida, K., Takemoto, M., Ikawa, T., Itaya, T., Kagami, H., and Iizumi, S., 2011, K-Ar age and geochemistry of the SW Japan Paleogene cauldron cluster: Implications for Eocene-Oligocene thermo-tectonic reactivation: Journal of Asian Earth Sciences, v. 40, no. 2, p. 509-533.

Imaoka, T., Nakashima, K., Kamei, A., Itaya, T., Ohira, T., Nagashima, M., Kono, N., and Kiji, M., 2014, Episodic magmatism at 105 Ma in the Kinki district, SW Japan: Petrogenesis of Nb-rich lamprophyres and adakites, and geodynamic implications: Lithos, v. 184, p. 105-131.

Isozaki, Y., Aoki, K., Nakama, T., and Yanai, S., 2010, New insight into a subduction-related orogen: a reappraisal of the geotectonic framework and evolution of the Japanese Islands: Gondwana Research, v. 18, no. 1, p. 82-105.

Isozaki, Y., and Itaya, T., 1990, Chronology of Sanbagawa metamorphism: Journal of Metamorphic Geology, v. 8, no. 4, p. 401-411.

Ito, H., Tamura, A., Morishita, T., and Arai, S., 2010, Zircon U-Pb and fission-track ages of granitic rocks from the Npjima Fault and its vicinity: A new horizon for the LA-ICP-MS U-Pb dating method: Jour. Geol. Soc. Japan, v. 116, no. 10, p. 544-551.

Itoh, Y., Takano, O., and Takashima, R., 2017, Tectonic synthesis: a plate reconstruction model of the NW Pacific region since 100 Ma. In Itoh, Y., Takano, O., Takashima, R., Nishi, H., and Yoshida, T., eds., Dynamics of Arc Migration and Amalgamation-Architectural Examples from the NW Pacific Margin, InTech, Rijeka, p. 93-111.

Jacobsen, S. B., and Wasserburg, G., 1980, Sm-Nd isotopic evolution of chondrites: Earth and Planetary Science Letters, v. 50, no. 1, p. 139-155.

Jahn, B. M., Usuki, M., Usuki, T., and Chung, S. L., 2014, Generation of Cenozoic granitoids in Hokkaido (Japan): Constraints from zircon geochronology, Sr-Nd-Hf isotopic and geochemical analyses, and implications for crustal growth: American Journal of Science, v. 314, no. 2, p. 704-750.

Jahn, B. M., Valui, G., Kruk, N., Gonevchuk, V., Usuki, M., and Wu, J. T. J., 2015, Emplacement ages, geochemical and Sr-Nd-Hf isotopic characterization of Mesozoic to early Cenozoic granitoids of the Sikhote-Alin Orogenic Belt, Russian Far East: Crustal growth and regional tectonic evolution: Journal of Asian Earth Sciences, v. 111, p. 872-918.

Jiang, N., Zhang, S., Zhou, W., and Liu, Y., 2009, Origin of a Mesozoic granite with A-type characteristics from the North China craton: highly fractionated from I-type magmas?: Contributions to Mineralogy and Petrology, v. 158, no. 1, p. 113-130.

Jing, J. H., Yang, H., Ge, W. C., Dong, Y., Ji, Z., Jing, Y., Bi, J. H., and Zhou, H. Y., 2021, Early Cretaceous crust-mantle interaction linked to rollback of the Palaeo-Pacific flat-subducting slab: constraints from the intermediate-felsic volcanic rocks of the northern Great Xing'an Range, NE China: Geological Magazine, p. 1-22.

Jolivet, L., Tamaki, K., and Fournier, M., 1994, Japan Sea, opening history and mechanism: A synthesis: Journal of Geophysical Research: Solid Earth, v. 99, no. B11, p. 22237-22259.

Kamei, A., 2004, An adakitic pluton on Kyushu Island, southwest Japan arc: Journal of Asian Earth Sciences, v. 24, no. 1, p. 43-58.

Kamei, A., and Takagi, T., 2003, Geology and petrography of the Abukuma granites in the Funehiki area, Fukushima Prefecture, NE Japan: The Journal of the Geological Society of Japan, v. 109, p. 234-251.

Kawakami, G., Ohira, H., Arita, K., Itaya, T., and Kawamura, M., 2006, Uplift history of the Hidaka Mountains, Hokkaido, Japan: a thermochronologic view: Journal Geological Society of Japan, v. 112, no. 11, p. 684.

Kemkin, I. V., 2008, Structure of terranes in a Jurassic accretionary prism in the Sikhote-Alin-Amur area: implications for the Jurassic geodynamic history of the Asian eastern margin: Russian Geology and Geophysics, v. 49, no. 10, p. 759-770.

Khanchuk, A., Grebennikov, A., and Ivanov, V., 2019, Albian-Cenomanian Orogenic Belt and Igneous Province of Pacific Asia: Russian Journal of Pacific Geology, v. 13, no. 3, p. 187-219.

Khanchuk, A., Kemkin, I., and Kruk, N., 2016, The Sikhote-Alin orogenic belt, Russian South East: Terranes and the formation of continental lithosphere based on geological and isotopic data: Journal of Asian Earth Sciences, v. 120, p. 117-138.

Khanchuk, A., Kruk, N., Golozubov, V., Kovach, V., Serov, P., Kholodnov, V., Gvozdev, V., and Kasatkin, S., 2013, The nature of the continental crust of Sikhote-Alin as evidenced from the Nb isotopy of Rocks of Southern Primorie: Doklady Earth Sciences, v. 451, no. 2, p. 809-813.

Khanchuk, A., Kruk, N., Valui, G., Nevolin, P., Moskalenko, E. Y., Fugzan, M., Kirnozova, T., and Travin, A., 2008, The Uspensk intrusion in South Primorye as a reference petrotype for granitoids of the transform continental margins; Doklady Earth Sciences, v. 421, no. 1, p. 734-737.

Khanchuk, A., Didenko, A. N., Tikhomirova, A. I., and Voinova, I. P., 2015, Paleomagnetism and geochemistry of the Kiselevka block of the Kiselevka-Manoma terrane (northern Sikhote-Alin): Geodynamic significance: Special Paper of Geological Society of America, v. 513, p. 483-508.

Kim, C. B., Chang, H. W., and Turek, A., 2003, U-Pb zircon ages and Sr-Nd-Pb isotopic compositions for Permian-Jurassic plutons in the Ogcheon belt and Ryeongnam massif, Korea: Tectonic implications and correlation with the China Qinling-Dabie belt and the Japan Hida belt: Island Arc, v. 12, no. 4, p. 366-382.

Kim, H. J., Lee, G. H., Jou, H. T., Cho, H. M., Yoo, H. S., Park, G. T., and Kim, J. S., 2007, Evolution of the eastern margin of Korea: Constraints on the opening of the East Sea (Japan Sea): Tectonophysics, v. 436, no. 1-4, p. 37-55.

Kim, S. W., Kwon, S., Park, S. I., Lee, C., Cho, D. L., Lee, H. J., Ko, K., and Kim, S. J., 2016, SHRIMP U-Pb dating and geochemistry of the Cretaceous plutonic rocks in the Korean Peninsula: A new tectonic model of the Cretaceous Korean Peninsula: Lithos, v. 262, p. 88-106.

Kiminami, K., 1986, Tectonic divisions and stratigraphy of the Mesozoic rocks of Hokkaido, Japan: Monogr. Assoc. Geol. Collab. Japan, no. 31, p. 1-15.
Kimura, G., Kitamura, Y., Yamaguchi, A., Kameda, J., Hashimoto, Y., and Hamahashi, M., 2019, Origin of the early Cenozoic belt boundary thrust and Izanagi-Pacific ridge subduction in the western Pacific margin: Island Arc, v. 28, no. 5, p. e12320.
Kincaid, C., and Griffiths, R., 2003, Laboratory models of the thermal evolution of the mantle during rollback subduction: Nature, v. 425, no. 6953, p. 58-62.
King, P., Chappell, B., Allen, C. M., and White, A., 2001, Are A-type granites the high-temperature felsic granites? Evidence from fractionated granites of the Wangrah Suite: Australian Journal of Earth Sciences, v. 48, no. 4, p. 501-514.
King, P., White, A., Chappell, B., and Allen, C., 1997, Characterization and origin of aluminous A-type granites from the Lachlan Fold Belt, southeastern Australia: Journal of petrology, v. 38, no. 3, p. 371-391.
Kirkland, C., Smithies, R., Taylor, R., Evans, N., and McDonald, B., 2015, Zircon Th/U ratios in magmatic environs: Lithos, v. 212, p. 397-414.
Kirsch, M., Paterson, S. R., Wobbe, F., Ardila, A. M. M., Clausen, B. L., and Alasino, P. H., 2016, Temporal histories of Cordilleran continental arcs: Testing models for magmatic episodicity: American Mineralogist, v. 101, no. 10, p. 2133-2154.
Kiyokawa, S., 1992, Geology of the Idonnappu belt, central Hokkaido, Japan: Evolution of a Cretaceous accretionary complex: Tectonics, v. 11, no. 6, p. 1180-1206.
Koike, W., and Tsutsumi, Y., 2018, Zircon U-Pb dating of plutonic rocks at the Tsukuba area, central Japan: Bull. Natl. Mus. Nat. Sci., v. C, no. 44, p. 1-11.
Kon, Y., Ejima, T., Morita, S., and Takagi, T., 2015, Spatial U-Pb age distribution of plutonic rocks in the central Abukuma Plateau, northeastern Japan Arc: Journal of Mineralogical and Petrological Sciences, v. 110, no. 3, p. 145-149.
Kon, Y., and Takagi, T., 2012, U-Pb zircon ages of Abukuma granitic rocks in the western Abukuma plateau, northeastern Japan Arc: Journal of Mineralogical and Petrological Sciences, v. 107, no. 5, p. 183-191.
König, S., Schuth, S., Münker, C., and Qopoto, C., 2007, The role of slab melting in the petrogenesis of high-Mg andesites: evidence from Simbo Volcano, Solomon Islands: Contributions to Mineralogy and Petrology, v. 153, no. 1, p. 85.
Kruk, N., Simanenko, V., Gvozdev, V., Golozubov, V., Kovach, V., Serov, P., Kholodnov, V., Moskalenko, E. Y., and Kuibida, M., 2014, Early Cretaceous granitoids of the Samarka terrane (Sikhote-Alin): geochemistry and sources of melts: Russian Geology and Geophysics, v. 55, no. 2, p. 216-236.
Kusky, T.M., Windley, B.F., Zhai, M.G., 2007, Tectonic evolution of the North ChinaBlock: from orogen to craton to orogen. In: Zhai, M.G., Windley, B.F., Kusky, T.,Meng, Q.R. (Eds.), Mesozoic Sub-continental Thinning Beneath Eastern North China: Geological Society Special Publication London, 280, p. 1-34.
Lagabrielle, Y., Moigne, J. L., Maury, R., Cotten, J., and Bourgois, J., 1994, Volcanic record of the subduction of an active spreading ridge, Taitao Peninsula (southern Chile): Geology, v. 22, no. 6, p. 515-518.
Le Maitre, R. W., Streckeisen, A., Zanettin, B., Le Bas, M., Bonin, B., and Bateman, P., 2005, Igneous rocks: a classification and glossary of terms: recommendations of the

International Union of Geological Sciences Subcommission on the Systematics of Igneous Rocks, Cambridge University Press, p. 235.
Lee, C. T. A., Luffi, P., and Chin, E. J., 2011, Building and destroying continental mantle: Annual Review of Earth and Planetary Sciences, v. 39, p. 59-90.
Lee, C. T. A., and Morton, D. M., 2015, High silica granites: Terminal porosity and crystal settling in shallow magma chambers: Earth and Planetary Science Letters, v. 409, p. 23-31.
Lee, T. H., Park, K. H., and Yi, K., 2018, SHRIMP U-Pb ages of detrital zircons from the Early Cretaceous Nakdong Formation, South East Korea: Timing of initiation of the Gyeongsang Basin and its provenance: Island Arc, v. 27, no. 5, p. e12258.
Lesher, C. E., and Spera, F. J., 2015, Thermodynamic and transport properties of silicate melts and magma. In: The encyclopedia of volcanoes, Academic Press, p. 113-141.
Li, S., Suo, Y., Li, X., Zhou, J., Santosh, M., Wang, P., Wang, G., Guo, L., Yu, S., and Lan, H., 2019, Mesozoic tectono-magmatic response in the East Asian ocean-continent connection zone to subduction of the Paleo-Pacific Plate: Earth-science Reviews, v. 192, p. 91-137.
Li, S., and Wang, Y., 2018, Formation time of the big mantle wedge beneath eastern China and a new lithospheric thinning mechanism of the North China craton-Geodynamic effects of deep recycled carbon: Science China Earth Sciences, v. 61, no. 7, p. 853-868.
Li, X. H., 2000, Cretaceous magmatism and lithospheric extension in Southeast China: Journal of Asian Earth Sciences, v. 18, no. 3, p. 293-305.
Liao, J. P., Jahn, B. M., Alexandrov, I., Chung, S. L., Zhao, P., Ivin, V., and Usuki, T., 2018, Petrogenesis of Mid-Eocene granites in South Sakhalin, Russian Far East: Juvenile crustal growth and comparison with granitic magmatism in Hokkaido and Sikhote-Alin: Journal of Asian Earth Sciences. Journal of Asian Earth Sciences, v. 167, p. 103-129.
Ling, M. X., Li, Y., Ding, X., Teng, F. Z., Yang, X. Y., Fan, W. M., Xu, Y. G., and Sun, W., 2013, Destruction of the North China Craton induced by ridge subductions: The Journal of Geology, v. 121, no. 2, p. 197-213.
Liu, J., Cai, R., Pearson, D. G., and Scott, J. M., 2019, Thinning and destruction of the lithospheric mantle root beneath the North China Craton: A review: Earth-Science Reviews, v. 196, p. 102873.
Liu, S. A., Li, S., Guo, S., Hou, Z., and He, Y., 2012, The Cretaceous adakitic-basaltic-granitic magma sequence on south-eastern margin of the North China Craton: implications for lithospheric thinning mechanism: Lithos, v. 134, p. 163-178.
Liu, S. A., Li, S., He, Y., and Huang, F., 2010, Geochemical contrasts between early Cretaceous ore-bearing and ore-barren high-Mg adakites in central-eastern China: implications for petrogenesis and Cu-Au mineralization: Geochimica et Cosmochimica Acta, v. 74, no. 24, p. 7160-7178.
Loiselle, M. C. and Wones, D. R., 1979, Characteristics of Anorogenic Granites: Geological Society of America, Abstracts with Programs, 11, 468.
Ludwig, K., 2012, User's manual for Isoplot 3.75: A geochronological toolkit for Microsoft Excel, 75 pp: Berkeley Geochronology Center, Special Publication, no. 5., p. 71.

Ma, L., Jiang, S. Y., Hofmann, A. W., Xu, Y. G., Dai, B. Z., and Hou, M. L., 2016a, Rapid lithospheric thinning of the North China Craton: New evidence from cretaceous mafic dikes in the Jiaodong Peninsula: Chemical Geology, v. 432, p. 1-15.

Ma, Q., Xu, Y. G., Zheng, J. P., Griffin, W. L., Hong, L. B., and Ma, L., 2016b, Coexisting early Cretaceous high-Mg andesites and adakitic rocks in the North China Craton: The role of water in intraplate magmatism and cratonic destruction: Journal of Petrology, v. 57, no. 7, p. 1279-1308.

Mackenzie, J. S., Taguchi, S., and Itaya, T., 1990, Cleavage dating by K-Ar isotopic analysis in the Paleogene Shimanto Belt of eastern Kyushu, SW Japan: Journal of Mineralogy, Petrology and Economic Geology, v. 85, no. 4, p. 161-167.

Macpherson, C. G., Dreher, S. T., and Thirlwall, M. F., 2006, Adakites without slab melting: high pressure differentiation of island arc magma, Mindanao, the Philippines: Earth and Planetary Science Letters, v. 243, no. 3, p. 581-593.

Maeda, J. I., and Kagami, H., 1996, Interaction of a spreading ridge and an accretionary prism: Implications from MORB magmatism in the Hidaka magmatic zone, Hokkaido, Japan: Geology, v. 24, no. 1, p. 31-34.

Malinovsky, A., 2010, Lithological composition of island-arc complexes in the Russian Far East: Lithology and Mineral Resources, v. 45, no. 1, p. 24-38.

Malinovsky, A., Golozoubov, V., and Simanenko, V., The Kema island-arc terrane, eastern Sikhote Alin: Formation settings and geodynamics, *in* Proceedings Doklady earth sciences2006, Volume 410, Springer, p. 1026-1029.

Malinovsky, A., and Markevich, P., 2007, Heavy clastic minerals from the Far East island-arc complexes: Russian Journal of Pacific Geology, v. 1, no. 1, p. 71-81.

Malinovsky, A. I., Golozoubov, V. V., Simanenko, V. P., and Simanenko, L. F., 2008, Kema terrane: A fragment of a back-arc basin of the early Cretaceous Moneron-Samarga island-arc system, East Sikhote-Alin range, Russian Far East: Island Arc, v. 17, no. 3, p. 285-304.

Maniar, P. D., and Piccoli, P. M., 1989, Tectonic discrimination of granitoids: Geological society of America bulletin, v. 101, no. 5, p. 635-643.

Martin, R. F., 2006, A-type granites of crustal origin ultimately result from open-system fenitization-type reactions in an extensional environment: Lithos, v. 91, no. 1-4, p. 125-136.

Maruyama, S., Isozaki, Y., Kimura, G., and Terabayashi, M., 1997, Paleogeographic maps of the Japanese Islands: plate tectonic synthesis from 750 Ma to the present: Island arc, v. 6, no. 1, p. 121-142.

Matsubara, M., Sato, H., Ishiyama, T., and Van Horne, A., 2017, Configuration of the Moho discontinuity beneath the Japanese Islands derived from three-dimensional seismic tomography: Tectonophysics, v. 710, p. 97-107.

Matsuda, T., and Isozaki, Y., 1991, Well-documented travel history of Mesozoic pelagic chert in Japan: From remote ocean to subduction zone: Tectonics, v. 10, no. 2, p. 475-499.

Matsuoka, A., 1996, Late Jurassic tropical Radiolaria: Vallupus and its related forms: Palaeogeography, Palaeoclimatology, Palaeoecology, v. 119, no. 3-4, p. 359-369.

Matthews, K. J., Maloney, K. T., Zahirovic, S., Williams, S. E., Seton, M., and Mueller, R. D., 2016, Global plate boundary evolution and kinematics since the late Paleozoic: Global and Planetary Change, v. 146, p. 226-250.

Menzies, M. A., Fan, W., and Zhang, M., 1993, Palaeozoic and Cenozoic lithoprobes and the loss of >120 km of Archaean lithosphere, Sino-Korean craton, China: Geological Society of London, Special Publications, v. 76, no. 1, p. 71-81.

Miyashiro, A., and Shido, F., 1975, Tholeiitic and calc-alkalic series in relation to the behaviors of titanium, vanadium, chromium, and nickel: American Journal of Science, v. 275, no. 3, p. 265-277.

Miyashita, S., and Katsushima, T., 1986, The Tomuraushi greenstone complex of the central Hidaka zone: Contemporaneous occurrence of abyssal tholeiite and terrigenous sediments: Journal of the Geological Society of Japan, v. 92, no. 8, p. 535-557.

Morioka, K., Tainosho, Y., and Kagami, H., 2000, Rb-Sr isochron ages of the Cretaceous granitoids in the Ryoke belt, Kinki district, Southwest Japan: Island Arc, v. 9, no. 1, p. 46-54.

Moyen, J. F., 2009, High Sr/Y and La/Yb ratios: the meaning of the "adakitic signature": Lithos, v. 112, no. 3, p. 556-574.

Mukoyoshi, H., Hirono, T., Hara, H., Sekine, K., Tsuchiya, N., Sakaguchi, A., and Soh, W., 2009, Style of fluid flow and deformation in and around an ancient out-of-sequence thrust: An example from the Nobeoka Tectonic Line in the Shimanto accretionary complex, Southwest Japan: Island Arc, v. 18, no. 2, p. 333-351.

Müller, R. D., Seton, M., Zahirovic, S., Williams, S. E., Matthews, K. J., Wright, N. M., Shephard, G. E., Maloney, K. T., Barnett-Moore, N., and Hosseinpour, M., 2016, Ocean basin evolution and global-scale plate reorganization events since Pangea breakup: Annual Review of Earth and Planetary Sciences, v. 44, p. 107-138.

Nakajima, T., Kamiyama, H., Williams, I. S., and Tani, K., 2004, Mafic rocks from the Ryoke Belt, southwest Japan: implications for Cretaceous Ryoke/San-yo granitic magma genesis: Earth and Environmental Science Transactions of The Royal Society of Edinburgh, v. 95, no. 1-2, p. 249-263.

Nakamura, H., Iwamori, H., and Kimura, J. I., 2008, Geochemical evidence for enhanced fluid flux due to overlapping subducting plates: Nature Geoscience, v. 1, no. 6, p. 380-384.

Nakamura, H., Iwamori, H., Nakagawa, M., Shibata, T., Kimura, J. I., Miyazaki, T., Chang, Q., Vaglarov, B. S., Takahashi, T., and Hirahara, Y., 2019, Geochemical mapping of slab-derived fluid and source mantle along Japan arcs: Gondwana Research, v. 70, p. 36-49.

Nanayama, F., Takahashi, Y., Yamasaki, T., Nakagawa, M., Iwano, H., Danhara, T., and Hirata, T., 2018, U-Pb zircon ages of the Nakanogawa Group in the Hidaka Belt, northern Japan: Implications for its provenance and the protolith of the Hidaka metamorphic rocks: Island Arc, v. 27, no. 2, p. e12234.

Nevstruyev, V., and Kozlova, O., 2018, Geodynamic and structural factors of porphyritic objects localization in Sikhote-Alin: Proceedings E3S Web of Conferences, v. 56, p. 04020.

Niu, Y., 2005, Generation and evolution of basaltic magmas: some basic concepts and a new view on the origin of Mesozoic-Cenozoic basaltic volcanism in eastern China: Geological Journal of China Universities, v. 11, no. 1, p. 9-46.
Nozaki, T., Nakamura, K., Awaji, S., and Kato, Y., 2006, Whole-rock geochemistry of basic schists from the Besshi area, Central Shikoku: Implications for the tectonic setting of the Besshi sulfide deposit: Resource Geology, v. 56, no. 4, p. 423-432.
Nur, A., 1981, Volcanic gaps and the consumption of aseismic ridges in South America: Memoir of the Geological Society of America, v. 154, p. 729-740.
O'Connor, J. M., Steinberger, B., Regelous, M., Koppers, A. A., Wijbrans, J. R., Haase, K. M., Stoffers, P., Jokat, W., and Garbe-Schönberg, D., 2013, Constraints on past plate and mantle motion from new ages for the Hawaiian-Emperor Seamount Chain: Geochemistry, Geophysics, Geosystems, v. 14, no. 10, p. 4564-4584.
Okamoto, K., Maruyama, S., and Isozaki, Y., 2000, Accretionary complex origin of the Sanbagawa, high P/T metamorphic rocks, Central Shikoku, Japan. Layer-parallel shortening structure and greenstone geochemistry: Jour. Geol. Soc. Japan, v. 106, no. 1, p. 70-86.
Okamoto, K., Shinjoe, H., Katayama, I., Terada, K., Sano, Y., and Johnson, S., 2004, SHRIMP U-Pb zircon dating of quartz-bearing eclogite from the Sanbagawa Belt, south-west Japan: implications for metamorphic evolution of subducted protolith: Terra Nova, v. 16, no. 2, p. 81-89.
Okamura, S., Arculus, R. J., and Martynov, Y. A., 2004, Cenozoic magmatism of the North-Eastern Eurasian margin: the role of lithosphere versus asthenosphere: Journal of Petrology, v. 46, no. 2, p. 221-253.
Okamura, S., Inaba, M., Adachi, Y., and Shinjo, R., 2016, Miocene-Pliocene mantle depletion event in the northern Fossa Magna, western NE Japan: Journal of Geodynamics, v. 97, p. 42-61.
Okamura, S., Martynov, Y. A., Furuyama, K., and Nagao, K., 1998, K-Ar ages of the basaltic rocks from Far East Russia: Constraints on the tectono-magmatism associated with the Japan Sea opening: Island Arc, v. 7, no. 1-2, p. 271-282.
Osozawa, S., Usuki, T., Usuki, M., Wakabayashi, J., and Jahn, B. M., 2019, Trace elemental and Sr-Nd-Hf isotopic compositions, and U-Pb ages for the Kitakami adakitic plutons: Insights into interactions with the early Cretaceous TRT triple junction offshore Japan: Journal of Asian Earth Sciences, p. 103968.
Otofuji, Y. I., Matsuda, T., Enami, R., Uno, K., Nishihama, K., Su, L., Kulinich, R. G., Zimin, P. S., Matunin, A. P., and Sakhno, V. G., 2002, Internal deformation of Sikhote Alin volcanic belt, far eastern Russia: Paleocene paleomagnetic results: Tectonophysics, v. 350, no. 3, p. 181-192.
Otofuji, Y. I., Matsuda, T., Itaya, T., Shibata, T., Matsumoto, M., Yamamoto, T., Morimoto, C., Kulinich, R. G., Zimin, P. S., and Matunin, A. P., 1995, Late Cretaceous to early Paleogene paleomagnetic results from Sikhote Alin, far eastern Russia: implications for deformation of East Asia: Earth and Planetary Science Letters, v. 130, no. 1, p. 95-108.

Otofuji, Y. I., Matsuda, T., and Nohda, S., 1985, Paleomagnetic evidence for the Miocene counter-clockwise rotation of Northeast Japan—rifting process of the Japan Arc: Earth and Planetary Science Letters, v. 75, no. 2-3, p. 265-277.
Otofuji, Y. I., 1996, Large tectonic movement of the Japan Arc in late Cenozoic times inferred from paleomagnetism: Review and synthesis: Island Arc, v. 5, no. 3, p. 229-249.
Otsuki, K., 1990, Westward migration of the Izu-Bonin Trench, northward motion of the Philippine Sea Plate, and their relationships to the Cenozoic tectonics of Japanese island arcs: Tectonophysics, v. 180, no. 2-4, p. 351-367.
Pan, Y., Sha, J., Zhou, Z., and Fürsich, F. T., 2013, The Jehol Biota: definition and distribution of exceptionally preserved relicts of a continental Early Cretaceous ecosystem: Cretaceous Research, v. 44, p. 30-38.
Pastor-Galán, D., Spencer, C. J., Furukawa, T., and Tsujimori, T., 2021, Evidence for crustal removal, tectonic erosion and flare-ups from the Japanese evolving forearc sediment provenance: Earth and Planetary Science Letters, v. 564, p. 116893.
Paterson, S. R., and Ducea, M. N., 2015, Arc magmatic tempos: Gathering the evidence: Elements, v. 11, no. 2, p. 91-98.
Paton, C., Hellstrom, J., Paul, B., Woodhead, J., and Hergt, J., 2011, Iolite: Freeware for the visualisation and processing of mass spectrometric data: Journal of Analytical Atomic Spectrometry, v. 26, no. 12, p. 2508-2518.
Pearce, J., 1996, Sources and settings of granitic rocks: Episodes, v. 19, p. 120-125.
Pearce, J. A., 2003, Supra-subduction zone ophiolites: The search for modern analogues: Special Papers-Geological Society of America, p. 269-294.
Pearce, J. A., Alabaster, T., Shelton, A., and Searle, M. P., 1981, The Oman ophiolite as a Cretaceous arc-basin complex: evidence and implications: Philosophical Transactions of the Royal Society of London. Series A, Mathematical and Physical Sciences, v. 300, no. 1454, p. 299-317.
Pearce, J. A., Harris, N. B., and Tindle, A. G., 1984, Trace element discrimination diagrams for the tectonic interpretation of granitic rocks: Journal of petrology, v. 25, no. 4, p. 956-983.
Pearson, D., 1999, The age of continental roots, Developments in Geotectonics, Volume 24, Elsevier, p. 171-194.
PérEz-SobA, C., and Villaseca, C., 2010, Petrogenesis of highly fractionated I-type peraluminous granites: La Pedriza pluton (Spanish Central System): Geologica Acta: an international earth science journal, v. 8, no. 2, p. 131-149.
PérEz-SobA, C., and Villaseca, C., 2019, Li-Na-metasomatism related to I-type granite magmatism: A case study of the highly fractionated La Pedriza pluton (Iberian Variscan belt): Lithos, v. 344, p. 159-174.
Pubellier, M., Monnier, C., Maury, R., and Tamayo, R., 2004, Plate kinematics, origin and tectonic emplacement of supra-subduction ophiolites in SE Asia: Tectonophysics, v. 392, no. 1-4, p. 9-36.
Qiu, Z., Yan, Q., Li, S., Wang, H., Tong, L., Zhang, R., Wei, X., Li, P., Wang, L., and Bu, A., 2017, Highly fractionated Early Cretaceous I-type granites and related Sn polymetallic mineralization in the Jinkeng deposit, eastern Guangdong, SE China: Constraints from

geochronology, geochemistry, and Hf isotopes: Ore Geology Reviews, v. 88, p. 718-738.
Raimbourg, H., Augier, R., Famin, V., Gadenne, L., Palazzin, G., Yamaguchi, A., and Kimura, G., 2014, Long-term evolution of an accretionary prism: The case study of the Shimanto Belt, Kyushu, Japan: Tectonics, v. 33, no. 6, p. 936-959.
Ren, J. S., Niu, B. G., Wang, J., He, Z. J., Jin, X. C., Xie, L. Z., Zhao, L., Liu, R. Y., Jiang, X. J., and Li, S., 2013, 1: 5 million international geological map of Asia: Diqiu Xuebao (Acta Geoscientica Sinica), v. 34, no. 1, p. 24-30.
Reymer, A., and Schubert, G., 1986, Rapid growth of some major segments of continental crust: Geology, v. 14, no. 4, p. 299-302.
Ribeiro, J. M., Maury, R. C., and Grégoire, M., 2016, Are adakites slab melts or high-pressure fractionated mantle melts?: Journal of Petrology, v. 57, no. 5, p. 839-862.
Robinson, P. M., 1989, Nonparametric estimation of time-varying parameters. In: Statistical analysis and forecasting of economic structural change, Springer, p. 253-264.
Russell, J. K., 2014, Sticky issues arising from high-viscosity magma: Settling arguments on magmatic structures: Geology, v. 42, no. 11, p. 1023-1024.
Sagong, H., Kwon, S. T., and Ree, J. H., 2005, Mesozoic episodic magmatism in South Korea and its tectonic implication: Tectonics, v. 24, no. 5.
Sajona, F. G., Maury, R. C., Bellon, H., Cotten, J., and Defant, M., 1996, High Field Strength Element Enrichment of Pliocene—Pleistocene Island Arc Basalts, Zamboanga Peninsula, Western Mindanao (Philippines): Journal of Petrology, v. 37, no. 3, p. 693-726.
Sajona, F. G., Maury, R. C., Pubellier, M., Leterrier, J., Bellon, H., and Cotten, J., 2000, Magmatic source enrichment by slab-derived melts in a young post-collision setting, central Mindanao (Philippines): Lithos, v. 54, no. 3-4, p. 173-206.
Sakashima, T., Terada, K., Takeshita, T., and Sano, Y., 2003, Large-scale displacement along the Median Tectonic Line, Japan: evidence from SHRIMP zircon U-Pb dating of granites and gneisses from the South Kitakami and paleo-Ryoke belts: Journal of Asian Earth Sciences, v. 21, no. 9, p. 1019-1039.
Sato, D., Matsuura, H., and Yamamoto, T., 2016, Timing of the Late Cretaceous ignimbrite flare-up at the eastern margin of the Eurasian Plate: New zircon U-Pb ages from the Aioi-Arima-Koto region of SW Japan: Journal of Volcanology and Geothermal Research, v. 310, p. 89-97.
Sato, K., Rodionov, S. M., and Brublevsky, A. A., 2006, Lermontovskoe Tungsten Skarn Deposit: the Oldest Mineralization in the Sikhote-Alin Orogen, Far East Russia: Resource Geology, v. 56, no. 3, p. 257-266.
Sengör, A. C., and Natal'In, B. A., 1996, Turkic-type orogeny and its role in the making of the continental crust: Annual Review of Earth and Planetary Sciences, v. 24, no. 1, p. 263-337.
Seton, M., Flament, N., Whittaker, J., Müller, R. D., Gurnis, M., and Bower, D. J., 2015, Ridge subduction sparked reorganization of the Pacific plate-mantle system 60-50 million years ago: Geophysical Research Letters, v. 42, no. 6, p. 1732-1740.
Shanmugam, G., 2016, Submarine fans: a critical retrospective (1950-2015): Journal of Palaeogeography, v. 5, no. 2, p. 110-184.

Shibata, K., and Ishihara, S., 1979, Initial 87Sr/86Sr ratios of plutonic rocks from Japan: Contributions to Mineralogy and Petrology, v. 70, no. 4, p. 381-390.
Simanenko, V., Rasskazov, S., Yasnygina, T., Simanenko, L., and Chashchin, A., 2011, Cretaceous complexes of the frontal zone of the Moneron-Samarga Island arc: Geochemical data on the basalts from the deep borehole on Moneron Island, the Sea of Japan: Russian Journal of Pacific Geology, v. 5, no. 1, p. 26-46.
Sisson, V. B., Pavlis, T. L., Roeske, S. M., and Thorkelson, D. J., 2003, Introduction: An overview of ridge-trench interactions in modern and ancient settings: Geological Society of America Special Papers, v. 371, p. 1-18.
Skrzypek, E., Kawakami, T., Hirajima, T., Sakata, S., Hirata, T., and Ikeda, T., 2016, Revisiting the high temperature metamorphic field gradient of the Ryoke Belt (SW Japan): New constraints from the Iwakuni-Yanai area: Lithos, v. 260, p. 9-27.
Söderlund, U., Patchett, P. J., Vervoort, J. D., and Isachsen, C. E., 2004, The 176Lu decay constant determined by Lu-Hf and U-Pb isotope systematics of Precambrian mafic intrusions: Earth and Planetary Science Letters, v. 219, no. 3-4, p. 311-324.
Song, Y., Ren, J., Liu, K., Shen, C., and Stepashko, A., 2018, Post-rift anomalous thermal flux in the Songliao Basin, NE China, as revealed from fission track thermochronology and tectonic analysis: Palaeogeography, palaeoclimatology, palaeoecology, v. 508, p. 148-165.
Song, Y., Ren, J., Stepashko, A. A., and Li, J., 2014, Post-rift geodynamics of the Songliao Basin, NE China: Origin and significance of T11 (Coniacian) unconformity: Tectonophysics, v. 634, p. 1-18.
Stern, C. R., 2011, Subduction erosion: rates, mechanisms, and its role in arc magmatism and the evolution of the continental crust and mantle: Gondwana Research, v. 20, no. 2-3, p. 284-308.
Sueoka, S., Shimada, K., Ishimaru, T., Danhara, T., Iwano, H., and Yagi, K., 2018, Formation Age and Cooling History of Kojaku Granite: Journal of Geography, v. 127, no. 6, p. 795-803.
Sun, S. S., and McDonough, W. F., 1989, Chemical and isotopic systematics of oceanic basalts: implications for mantle composition and processes: Geological Society, London, Special Publications, v. 42, no. 1, p. 313-345.
Suzuki, K., and Adachi, M., 1998, Denudation history of the high T/P Ryoke metamorphic belt, southwest Japan: constraints from CHIME monazite ages of gneisses and granitoids: Journal of Metamorphic Geology, v. 16, no. 1, p. 23-37.
Taira, A., 1988, The Shimanto Belt in Shikoku, Japan. Evolution of Cretaceous to Miocene accretionary prism: Modern Geology, v. 12, p. 5-46.
Taira, A., Ohara, Y., Wallis, S., Ishiwatari, A., and Iryu, Y., 2016, Geological evolution of Japan: an overview. In: Moreno, T., Wallis, S., Kojima, T., Gibbons, W. (Eds.), The geology of Japan. Geological Society of London, London, p. 1-24.
Takahashi, Y., Cho, D. L., and Kee, W. S., 2010, Timing of mylonitization in the Funatsu Shear Zone within Hida Belt of southwest Japan: Implications for correlation with the shear zones around the Ogcheon Belt in the Korean Peninsula: Gondwana Research, v. 17, no. 1, p. 102-115.

Takahashi, Y., Mao, J., and Zhao, X., 2012, Timing of mylonitization in the Nihonkoku Mylonite Zone of north Central Japan: Implications for Cretaceous to Paleogene sinistral ductile deformation in the Japanese Islands: Journal of Asian Earth Sciences, v. 47, p. 265-280.

Takahashi, Y., Mikoshiba, M., Kubo, K., Iwano, H., Danhara, T., and Hirata, T., 2016, Zircon U-Pb ages of plutonic rocks in the southern Abukuma Mountains: Implications for Cretaceous geotectonic evolution of the Abukuma Belt: Island Arc, v. 25, no. 2, p. 154-188.

Takashima, R., Nishi, H., and Yoshida, T., 2002, Geology, petrology and tectonic setting of the Late Jurassic ophiolite in Hokkaido, Japan: Journal of Asian Earth Sciences, v. 21, no. 2, p. 197-215.

Takashima, R., Nishi, H., and Yoshida, T., 2006, Late Jurassic-Early Cretaceous intra-arc sedimentation and volcanism linked to plate motion change in northern Japan: Geological Magazine, v. 143, no. 6, p. 753-770.

Tamura, Y., Ishizuka, O., Aoike, K., Kawate, S., Kawabata, H., Chang, Q., Saito, S., Tatsumi, Y., Arima, M., and Takahashi, M., 2010, Missing Oligocene crust of the Izu-Bonin arc: consumed or rejuvenated during collision?: Journal of Petrology, v. 51, no. 4, p. 823-846.

Tanaka, S., 1987, Rb-Sr isotopic ages of the granitic rocks in the Tsurugidake-Kekachiyama area, northern Japan Alps: Journal of the Geological Society of Japan, v. 93, p. 368-376.

Tang, J., Xu, W., Niu, Y., Wang, F., Ge, W., Sorokin, A., and Chekryzhov, I., 2016, Geochronology and geochemistry of Late Cretaceous-Paleocene granitoids in the Sikhote-Alin Orogenic Belt: Petrogenesis and implications for the oblique subduction of the paleo-Pacific plate: Lithos, v. 266, p. 202-212.

Tani, K., Tsutsumi, Y., Shigeoka, M., and Yokoyama, K., 2016, Zircon U-Pb Dating of the Akashima Formation, Oga Peninsula, Akita Prefecture, Japan: Mem. Natl. Mus. Nat. Sci., Tokyo, v. 51, p. 45-51.

QGIS, D. T. (2015). QGIS geographic information system. Open source geospatial Foundation project, 1(2), 1-10.

Terakado, Y., and Nohda, S., 1993, Rb-Sr dating of acidic rocks from the middle part of the Inner Zone of southwest Japan: tectonic implications for the migration of the Cretaceous to Paleogene igneous activity: Chemical Geology, v. 109, no. 1-4, p. 69-87.

Thorkelson, D. J., 1996, Subduction of diverging plates and the principles of slab window formation: Tectonophysics, v. 255, no. 1-2, p. 47-63.

Torsvik, T. H., Steinberger, B., Shephard, G. E., Doubrovine, P. V., Gaina, C., Domeier, M., Conrad, C. P., and Sager, W. W., 2019, Pacific-Panthalassic reconstructions: Overview, errata and the way forward: Geochemistry, Geophysics, Geosystems, v. 20, no. 7, p. 3659-3689.

Tsuchiya, N., and Kanisawa, S., 1994, Early Cretaceous Sr-rich silicic magmatism by slab melting in the Kitakami Mountains, northeast Japan: Journal of Geophysical Research: Solid Earth, v. 99, no. B11, p. 22205-22220.

Tsuchiya, N., Kimura, J. I., and Kagami, H., 2007, Petrogenesis of Early Cretaceous adakitic granites from the Kitakami mountains, Japan: Journal of Volcanology and Geothermal Research, v. 167, no. 1, p. 134-159.

Tsuchiya, N., Suzuki, S., Kimura, J. I., and Kagami, H., 2005, Evidence for slab melt/mantle reaction: petrogenesis of Early Cretaceous and Eocene high-Mg andesites from the Kitakami Mountains, Japan: Lithos, v. 79, no. 1, p. 179-206.

Tsuchiya, N., Takeda, T., Tani, K., Adachi, T., Nakano, N., and Osanai, Y., 2012, Zircon U-Pb geochoronology and petrochemistry of Early Cretaceous adakitic granites in the Kitakami Mountains, Japan, Annual Meeting of Japan Association of Mineralogical Sciences, Volume 2012, Japan Association of Mineralogical Sciences, p. 190.

Tsutsumi, Y., Yokoyama, K., Kasatkin, S. A., and Golozubov, V. V., 2016, Age of igneous rocks in southern part of Primorye, Far East Russia: Memoirs of the National Museum of Nature and Science, no. 51, p. 71-78.

Turner, S., Foden, J., and Morrison, R., 1992, Derivation of some A-type magmas by fractionation of basaltic magma: an example from the Padthaway Ridge, South Australia: Lithos, v. 28, no. 2, p. 151-179.

Ueda, H., 2001, Tectonic evolution of Cretaceous accretionary complex in the Idonnappu Zone, Urakawa area, central Hokkaido, Northern Japan: with reference to radiolarian ages and thermal structure: Jour. Geol. Soc. Japan, v. 107, p. 81-98.

Ueda, H., 2016, Hokkaido, In: Moreno, T., Wallis, S. R., Kojima, T., and Gibbons, W., eds., The Geology of Japan: London, Geological Society, p. 201-221.

Ueda, H., and Miyashita, S., 2005, Tectonic accretion of a subducted intraoceanic remnant arc in Cretaceous Hokkaido, Japan, and implications for evolution of the Pacific northwest: Island Arc, v. 14, no. 4, p. 582-598.

Uno, K., Furukawa, K., and Hada, S., 2011, Margin-parallel translation in the western Pacific: Paleomagnetic evidence from an allochthonous terrane in Japan: Earth and Planetary Science Letters, v. 303, no. 1-2, p. 153-161.

Utsunomiya, A., Jahn, B. M., Okamoto, K., Ota, T., and Shinjoe, H., 2011, Intra-oceanic island arc origin for Iratsu eclogites of the Sanbagawa belt, central Shikoku, southwest Japan: Chemical Geology, v. 280, no. 1-2, p. 97-114.

Valuy, G., 2014, Petrology of Granitoids and Differentiation of Melts under Shallowdepth Conditions (East-Sikhote-Alinsky Volcanic Belt): Dal'nauka, Vladivostok (in Russian).

Van der Meer, D., Torsvik, T., Spakman, W., Van Hinsbergen, D., and Amaru, M., 2012, Intra-Panthalassa Ocean subduction zones revealed by fossil arcs and mantle structure: Nature Geoscience, v. 5, no. 3, p. 215.

Van Horne, A., Sato, H., and Ishiyama, T., 2017, Evolution of the Sea of Japan back-arc and some unsolved issues: Tectonophysics, v. 710, p. 6-20.

Vervoort, J. D., and Blichert-Toft, J., 1999, Evolution of the depleted mantle: Hf isotope evidence from juvenile rocks through time: Geochimica et cosmochimica acta, v. 63, no. 3-4, p. 533-556.

Vervoort, J. D., Patchett, P. J., Albarède, F., Blichert-Toft, J., Rudnick, R., and Downes, H., 2000, Hf-Nd isotopic evolution of the lower crust: Earth and Planetary Science Letters, v. 181, no. 1-2, p. 115-129.

Wakita, K., 2013, Geology and tectonics of Japanese islands: a review-the key to understanding the geology of Asia: Journal of Asian Earth Sciences, v. 72, p. 75-87.
Wang, C., Feng, Z., Zhang, L., Huang, Y., Cao, K., Wang, P., and Zhao, B., 2013, Cretaceous paleogeography and paleoclimate and the setting of SKI borehole sites in Songliao Basin, northeast China: Palaeogeography, Palaeoclimatology, Palaeoecology, v. 385, p. 17-30.
Wang, F., Zhou, X. H., Zhang, L. C., Ying, J. F., Zhang, Y. T., Wu, F. Y., and Zhu, R. X., 2006, Late Mesozoic volcanism in the Great Xing'an Range (NE China): timing and implications for the dynamic setting of NE Asia: Earth and Planetary Science Letters, v. 251, no. 1-2, p. 179-198.
Wang, Q., Wyman, D. A., Xu, J., Jian, P., Zhao, Z., Li, C., Xu, W., Ma, J., and He, B., 2007, Early Cretaceous adakitic granites in the Northern Dabie Complex, central China: implications for partial melting and delamination of thickened lower crust: Geochimica et Cosmochimica Acta, v. 71, no. 10, p. 2609-2636.
Watanabe, T., Ireland, T., Tainosho, Y., and Nakai, Y., 2000, Zircon U-Pb sensitive high mass-resolution ion microprobe dating of granitoids in the Ryoke metamorphic belt, Kinki District, Southwest Japan: Island Arc, v. 9, no. 1, p. 55-63.
Whalen, J. B., Currie, K. L., and Chappell, B. W., 1987, A-type granites: geochemical characteristics, discrimination and petrogenesis: Contributions to mineralogy and petrology, v. 95, no. 4, p. 407-419.
White, A. J., and Chappell, B. W., 1977, Ultrametamorphism and granitoid genesis: Tectonophysics, v. 43, no. 1-2, p. 7-22.
White, W. M., 2015, Isotope geochemistry, John Wiley & Sons., p. 496 .
Whittaker, J., Müller, R., Leitchenkov, G., Stagg, H., Sdrolias, M., Gaina, C., and Goncharov, A., 2007, Major Australian-Antarctic plate reorganization at Hawaiian-Emperor bend time: Science, v. 318, no. 5847, p. 83-86.
Wilde, S. A., 2015, Final amalgamation of the Central Asian Orogenic Belt in NE China: Paleo-Asian Ocean closure versus Paleo-Pacific plate subduction—A review of the evidence: Tectonophysics, v. 662, p. 345-362.
Wood, D. A., 1980, The application of a Th-Hf-Ta diagram to problems of tectonomagmatic classification and to establishing the nature of crustal contamination of basaltic lavas of the British Tertiary Volcanic Province: Earth and Planetary Science Letters, v. 50, no. 1, p. 11-30.
Wu, C. O., Chiang, C. T., and Hoover, D. R., 1998, Asymptotic confidence regions for kernel smoothing of a varying-coefficient model with longitudinal data: Journal of the American statistical Association, v. 93, no. 444, p. 1388-1402.
Wu, F. Y., Liu, X., Ji, W., Wang, J., and Yang, L., 2017a, Highly fractionated granites: Recognition and research: Science China Earth Sciences, v. 60, no. 7, p. 1201-1219.
Wu, F. Y., Han, R. H., Yang, J. H., Wilde, S. A., Zhai, M. G., and Park, S. C., 2007, Initial constraints on the timing of granitic magmatism in North Korea using U-Pb zircon geochronology: Chemical Geology, v. 238, no. 3-4, p. 232-248.
Wu, F. Y., Jahn, B. M., Wilde, S. A., Lo, C. H., Yui, T. F., Lin, Q., Ge, W. C., and Sun, D. Y., 2003, Highly fractionated I-type granites in NE China (I): geochronology and petrogenesis: Lithos, v. 66, no. 3-4, p. 241-273.

Wu, F. Y., Lin, J. Q., Wilde, S. A., Zhang, X. O., and Yang, J. H., 2005, Nature and significance of the Early Cretaceous giant igneous event in eastern China: Earth and Planetary Science Letters, v. 233, no. 1-2, p. 103-119.
Wu, F. Y., Yang, J. H., Xu, Y. G., Wilde, S. A., and Walker, R. J., 2019, Destruction of the North China Craton in the Mesozoic: Annual Review of Earth and Planetary Sciences.
Wu, J., Suppe, J., Lu, R., and Kanda, R., 2016, Philippine Sea and East Asian plate tectonics since 52 Ma constrained by new subducted slab reconstruction methods: Journal of Geophysical Research: Solid Earth, v. 121, no. 6, p. 4670-4741.
Wu, J., Lin, Y. A., Flament, N., Wu, J. T. J., Liu, Y., in revision. Northwest Pacific-Izanagi plate tectonics since Cretaceous times from western Pacific mantle structure: Earth Science Reviews.
Wu, J. T. J., Jahn, B. M., Nechaev, V., Chashchin, A., Popov, V., Yokoyama, K., and Tsutsumi, Y., 2017b, Geochemical characteristics and petrogenesis of adakites in the Sikhote-Alin area, Russian Far East: Journal of Asian Earth Sciences, v. 145, p. 512-529.
Wu, J. T. J., and Wu, J., 2019, Izanagi-Pacific ridge subduction revealed by a 56 to 46 Ma magmatic gap along the northeast Asian margin: Geology, v. 47, no. 10, p. 953-957.
Xia, Q. K., Liu, J., Kovács, I., Hao, Y. T., Li, P., Yang, X. Z., Chen, H., and Sheng, Y. M., 2019, Water in the upper mantle and deep crust of eastern China: concentration, distribution and implications: National Science Review, v. 6, no. 1, p. 125-144.
Xia, Q. K., Liu, J., Liu, S. C., Kovacs, I., Feng, M., and Dang, L., 2013, High water content in Mesozoic primitive basalts of the North China Craton and implications on the destruction of cratonic mantle lithosphere: Earth and Planetary Science Letters, v. 361, p. 85-97.
Xu, W. L., Wang, Q. H., Wang, D. Y., Guo, J. H., and Pei, F. P., 2006, Mesozoic adakitic rocks from the Xuzhou-Suzhou area, eastern China: evidence for partial melting of delaminated lower continental crust: Journal of Asian Earth Sciences, v. 27, no. 2, p. 230-240.
Yamakita, S., and Otoh, S., 2000, Cretaceous rearrangement processes of pre-Cretaceous geologic units of the Japanese Islands by MTL-Kurosegawa left-lateral strike-slip fault system: The Memoirs of the Geological Society of Japan, v. 56, p. 23-38.
Yan, J., Liu, J., Li, Q., Xing, G., Liu, X., Xie, J., Chu, X., and Chen, Z., 2015, In situ zircon Hf-O isotopic analyses of late Mesozoic magmatic rocks in the Lower Yangtze River Belt, central eastern China: Implications for petrogenesis and geodynamic evolution: Lithos, v. 227, p. 57-76.
Yuhara, M., 1998, Rb-Sr whole rock isochron ages and source materials of granitic rocks in Awaji Island, Southwest Japan Arc: Bulletin of the Geological Survey of Japan, v. 49, p. 477-491.
Zellmer, G. F., 2008, Some first-order observations on magma transfer from mantle wedge to upper crust at volcanic arcs: Geological Society, London, Special Publications, v. 304, no. 1, p. 15-31.
Zhai, M., Zhang, Y., Zhang, X., Wu, F., Peng, P., Li, Q., Hou, Q., Li, T., and Zhao, L., 2016, Renewed profile of the Mesozoic magmatism in Korean Peninsula: Regional

correlation and broader implication for cratonic destruction in the North China Craton: Science China Earth Sciences, v. 59, no. 12, p. 2355-2388.
Zhang, Q., Guo, F., Zhao, L., and Wu, Y., 2017, Geodynamics of divergent double subduction: 3-D numerical modeling of a Cenozoic example in the Molucca Sea region, Indonesia: Journal of Geophysical Research: Solid Earth, v. 122, no. 5, p. 3977-3998.
Zhang, S. H., Zhao, Y., Davis, G. A., Ye, H., and Wu, F., 2014, Temporal and spatial variations of Mesozoic magmatism and deformation in the North China Craton: Implications for lithospheric thinning and decratonization: Earth-Science Reviews, v. 131, p. 49-87.
Zhang, Y. B., Zhai, M., Hou, Q. L., Li, T. S., Liu, F., and Hu, B., 2012, Late Cretaceous volcanic rocks and associated granites in Gyeongsang Basin, SE Korea: Their chronological ages and tectonic implications for cratonic destruction of the North China Craton: Journal of Asian Earth Sciences, v. 47, p. 252-264.
Zhao, P., Jahn, B. M., and Xu, B., 2017, Elemental and Sr-Nd isotopic geochemistry of Cretaceous to Early Paleogene granites and volcanic rocks in the Sikhote-Alin Orogenic Belt (Russian Far East): implications for the regional tectonic evolution: Journal of Asian Earth Sciences, v. 146, p. 383-401.
Zharov, A., 2005, South Sakhalin tectonics and geodynamics: A model for the Cretaceous-Paleogene accretion of the East Asian continental margin: Russian Journal of Earth Sciences, v. 7, no. 5.
Zheng, J., and Dai, H., 2018, Subduction and retreating of the western Pacific plate resulted in lithospheric mantle replacement and coupled basin-mountain respond in the North China Craton: Science China Earth Sciences, v. 61, no. 4, p. 406-424.
Zheng, Y., Xu, Z., Zhao, Z., and Dai, L., 2018, Mesozoic mafic magmatism in North China: Implications for thinning and destruction of cratonic lithosphere: Science China Earth Sciences, v. 61, no. 4, p. 353-385.
Zhou, B. X., Sun, T., Shen, W., Shu, L., and Niu, Y., 2006, Petrogenesis of Mesozoic granitoids and volcanic rocks in South China: a response to tectonic evolution: Episodes, v. 29, no. 1, p. 26.
Zhou, J. B., Wilde, S. A., Zhang, X. Z., Zhao, G. C., Zheng, C. Q., Wang, Y. J., and Zhang, X. H., 2009, The onset of Pacific margin accretion in NE China: evidence from the Heilongjiang high-pressure metamorphic belt: Tectonophysics, v. 478, no. 3-4, p. 230-246.
Zhu, G., Jiang, D., Zhang, B., and Chen, Y., 2012a, Destruction of the eastern North China Craton in a backarc setting: Evidence from crustal deformation kinematics: Gondwana Research, v. 22, no. 1, p. 86-103.
Zhu, R., and Xu, Y., 2019, The subduction of the west Pacific plate and the destruction of the North China Craton: Science China Earth Sciences, p. 1-11.
Zhu, R. X., Yang, J. H., and Wu, F. Y., 2012b, Timing of destruction of the North China Craton: Lithos, v. 149, p. 51-60.
Zyabrev, S., 2011, Stratigraphy and structure of the central East Sakhalin accretionary wedge (Eastern Russia): Russian Journal of Pacific Geology, v. 5, no. 4, p. 313.

Appendix A: Compiled published age and Nd-Sr isotopic composition of late Cretaceous to Cenozoic NE Asia igneous rock

The data is placed in the UH Cougar ROAR data repository.

Link: https://dataverse.tdl.org/file.xhtml?fileId=124815&version=1.0

Appendix B: Data and reference of the early Cretaceous adakitic rocks in NE Asia

The data is placed in the UH Cougar ROAR data repository.

Link: https://dataverse.tdl.org/file.xhtml?fileId=124816&version=1.0

Appendix C New zircon U-Pb age result of Sikhote-Alin igneous rocks

The data is placed in the UH Cougar ROAR data repository.

Link: https://dataverse.tdl.org/file.xhtml?fileId=124812&version=1.0

Appendix D Whole-rock geochemical result of Sikhote-Alin igneous rocks

The data is placed in the UH Cougar ROAR data repository.

Link: https://dataverse.tdl.org/file.xhtml?fileId=124813&version=1.0